

**THE NEURAL MECHANISMS OF PERSISTENT
INHIBITION IN THE DNLL OF THE GERBIL
(*Meriones unguiculatus*)**

Dissertation
zur Erlangung des Grades eines Doktors
der Naturwissenschaften

der Fakultät für Biologie
der Ludwig-Maximilians-Universität München

vorgelegt von
Bernadette T. Saunier Rebori
München, February 2008

Erstgutachter : Prof. Dr. Benedikt Grothe

Zweitgutachter : Prof. Dr. Axel Borst

Tag d. mündl. Prüfung : 31. März 2008

ERKLÄRUNG

Ich versichere, daß ich meine Dissertation selbstständig, ohne unerlaubte Hilfe angefertigt, und mich dabei keiner anderen als der von mir ausdrücklich bezeichneten Hilfen und Quellen bedient habe.

Die Dissertation wurde in der jetzigen oder ähnlichen Form bei keiner anderen

Hochschule eingereicht und hat noch keinen sonstigen Prüfungszwecken gedient.

(Ort, Datum)

(BernadetteT. Saunier Rebori)

(...) antes de descubrir, en descubrirnos; antes de modelar la Naturaleza, en modelarnos. Forjarnos un cerebro fuerte, un cerebro original, exclusivamente nuestro: he aquí la labor preliminar absolutamente inexcusable.

Reglas y consejos sobre la investigación científica. Los tónicos de la voluntad.

Santiago Ramón y Cajal.

TABLE OF CONTENTS

ACKNOWLEDGMENTS	1
1. ABSTRACT	3
2. INTRODUCTION	5
2.1 Sound localization in the mammalian brain.....	5
2.2 Binaural processing in the DNLL.....	7
2.3 The precedence effect and echo suppression	10
2.4 Synaptic transmission.....	13
2.5 The Mongolian gerbil as an animal model	17
2.6 Scope of the study.....	18
3. MATERIALS AND METHODS	21
3.1 In vivo recordings	21
3.1.1 Animal preparation.....	21
3.1.2 Stereotatic procedure.....	21
3.1.3 Recording procedure	22
3.1.4 Acoustic stimuli	23
3.1.5 Data analysis.....	24
3.1.6 Histology	25
3.2 In vitro recordings	27
3.2.1 Brain slice preparation	27
3.2.2 Whole cell recordings.....	31
3.2.3 Stimulation of synaptic inputs	32
3.2.4 Data analysis.....	32
3.2.5 Statistical analysis.....	33
3.3 Appendix.....	34
3.3.1 Histology	34
3.3.1.1. Ringer solution containing heparin (for animal perfusion)	34
3.3.1.2. Nissl staining.....	34

3.3.2 Data analysis.....	35
3.3.2.1. Convert.pl.....	35
3.3.2.2. Last peak.....	36
3.3.2.3. All peaks.....	37
3.3.2.4. bpc_Mini.xop.....	38
4. RESULTS	39
4.1 Binaural response properties of DNLL neurons.....	39
4.2 In vitro physiology.....	42
4.2.1 The contralateral DNLL provides the long lasting GABAergic inhibition	42
4.2.2 The decay time constant of GABAergic IPSCs can explain the PI found in vivo and in vitro	45
4.2.3 The stimulation strength increase in the IPSC kinetics suggest a possible role of spillover in DNLL long lasting inhibition	46
4.2.4 Pre-synaptic mechanisms might be involved in extending synaptic inhibition in DNLL neurons	51
4.2.5 The application of a low affinity GABA _A receptor antagonist suggest the involvement of extrasynaptic receptors in prolonging synaptic inhibition in DNLL	56
4.2.6 Blocking GABA clearance prolonged the IPSC kinetics.....	63
4.2.7 Reducing release probability decreased the IPSCs kinetics.....	68
4.2.8 Glycinergic inputs onto DNLL neurons	74
5. DISCUSSION	83
5.1 Persistent inhibition in the DNLL of the Mongolian gerbil.....	83
5.2 DNLL cell types and their physiological properties in vitro.....	85
5.3 The source of PI in the DNLL	87
5.4 Spillover prolongs synaptic inhibition in the DNLL	89
5.5 Asynchronous release in DNLL principal neurons contributes to PI at high frequency activity levels.....	97
5.6 Glycinergic inputs onto DNLL neurons.....	99

6. CONCLUSIONS.....	101
7. REFERENCES.....	105
LIST OF ABBREVIATIONS	117
CURRICULUM VITAE	121

INDEX OF TABLES AND FIGURES

Fig. 2.1. The DNLL circuitry.....	8
Fig. 2.2. The precedence effect.....	11
Fig. 3.2.1. Schematic illustration of DNLL location in the mammalian brain	27
Table 3.2.1. Extracellular solutions for slicing and recording DNLL	28
Table 3.2.2. Internal solutions for voltage and current clamp recordings.....	29
Table 3.2.3. Drugs and concentrations used during the experiments.....	30
Fig. 4.1. PI evoked in vivo by ipsilateral stimulation.....	40
Fig. 4.2. PI evoked in vitro by stimulation of the Commissure of Probst.....	44
Fig. 4.3. Decay time of evoked IPSCs in vitro mimics PI in vivo.....	46
Fig. 4.4. GABAergic IPSCs kinetics dependency on stimulation strength.....	49
Fig. 4.5. Depression curves of GABAergic IPSCs after a stimulation train.....	53
Fig. 4.6. Frequency dependency of GABAergic IPSCs after a stimulation train	54
Fig. 4.7. Effect of 100 μ M TPMPA on the IPSCs kinetics.....	57
Fig. 4.8. Effect of 200 μ M TPMPA on the kinetics of the last IPSC after stimulation train	59
Fig. 4.9. Effect of 200 μ M TPMPA on the kinetics of a single evoked IPSC.....	61
Fig. 4.10..Effect of a low concentration of a high affinity GABA _A antagonist on the IPSCs kinetics	63
Fig. 4.11. Effect of NO711 on the IPSCs decay	64
Fig. 4.12. Low concentrations of NNC711 prolongs IPSCs kinetics	66
Fig. 4.13. Reducing the extracellular calcium reduces the IPSCs kinetics	69
Fig. 4.14. The reduction on extracellular calcium reduces GABA spillover.....	71
Fig. 4.15. Cadmium induces a reduction of GABA spillover	73
Fig. 4.16. DNLL neurons receive both GABA and glycinergic inputs	76
Fig. 4.17. Dependency of glycinergic IPSCs kinetics on stimulation strength...	79
Fig. 4.18. Frequency dependency of glycinergic IPSCs.....	81

ACKNOWLEDGMENTS

I would like to thank my supervisor Prof. Dr. Benedikt Grothe for giving me the opportunity to join his lab and for his guidance during my PhD.

I also want to thank Dr. Felix Felmy for his contagious enthusiasms for science and for his permanent interest in discussing experiments and give advice. Many thanks to Dr. Achim Klug for their support and advice.

Thanks to all present and past members of the Grothe group. Many thanks to Teresa Kindermann, Ben Haßfurth and Gabi Schebesch for their constant support, their friendship and because my time in the lab would have been less enjoyable without them. I would also like to thank Dr. Ursula Koch for fruitful discussions and advice throughout all these years. I also thank Claudia Schulte and Olga Alexandrova for their incalculable assistance and to Nick Lesica for proofreading the thesis!

Quiero agradecer enormemente a todos mis amigos de acá y allá que me brindaron su apoyo y su cariño durante todos estos años: Nico Plachta y Steffi Bissiere, Mati Okawa y Eva Wertheimer, Gabi Pirk, Nataly O'Leary, Mira Kuisle, Ariel Méndez y Caro Haupt, Ianna Bechten, Lule Kargiemann, Barbara Mulinacci, Stefano Pegoraro, José Álvarez-Castro y muchos otros que seguramente olvido mencionar en este momento. GRACIAS por estar ahí siempre!!!

Finalmente, mi mayor gratitud es para toda mi familia (incluidos Luli, tíos y primos) por cuidarme y quererme tanto y hacerme sentir que la distancia no era tan grande. Quiero agradecer especialmente a mis viejos porque gracias a ellos hoy termino mi doctorado. A mi mamá por creer en mí más de lo que yo misma creo y por siempre darme el coraje para seguir adelante y llevar acabo mis sueños. Gracias GIGANTES a mis hermanos por apoyarme en mi decisión de irme tan lejos, por ser mis amigos más queridos y por estar siempre cerca. Gracias a mis cuñados por su apoyo incondicional y a mis hermosos sobrinos, Sofi y Tobi por su enorme amor y por la paciencia infinita de tener una tía del otro lado del océano.

1. ABSTRACT

One function of the auditory system is sound localization. However, when a sound is produced in a reverberant environment, it propagates in multiple directions and is subsequently reflected from nearby surfaces, potentially compromising accurate localization. Therefore, repeated wave fronts of the same sound are suppressed by the auditory system, an effect termed *precedence effect* (Blauert, 1997; Litovsky et al., 1999). Several lines of evidence suggest that this effect is mediated by persistent inhibition (PI) in the dorsal nucleus of the lateral lemniscus (DNLL) (Yang and Pollak, 1994; Burger and Pollak, 2001; Pollak et al., 2003); however, the underlying neural mechanism remains unknown.

One possibility suggests that the PI might be the result of network properties within the auditory nuclei (Kelly and Kidd, 2000). In this scenario, auditory cells in some nucleus yet to be determined would fire for a prolonged period of time after the offset of the stimulus, providing neural inhibition to the DNLL. But this has not been observed. Alternatively, synaptic or membrane properties in the DNLL might cause the PI.

The results described here provide strong evidence of the role of the DNLL in echo suppression. Furthermore, the interplay of two synaptic mechanisms is suggested as the cellular mechanisms underlying PI. On one hand, spillover of GABA is described as the mechanisms responsible for extending the inhibitory signal after one pulse stimulation. Spillover of the transmitter might also be involved in amplifying the inhibition as large amounts of neurotransmitter seem to be released as response to stimulation trains. On the other hand, the results

described here suggest an additional mechanism that is also involved: asynchronous release of the neurotransmitter. This modality has an important role in prolonging the decay of synaptic inhibition in DNLL neurons after high activity levels induced by trains of high frequency stimulation to their input fibers.

Interestingly, both mechanisms occur at physiological temperature *in vitro*, suggesting that these pre- and post-synaptic mechanisms for generating long lasting inhibition may also occur *in vivo*. Together these two mechanisms seem to be crucial to allow the inferior colliculus (IC) to detect trailing sounds in echoic environments.

Part of the results presented in chapters 4.1, 4.2.1 and 4.2.2 has been published in Pecka et al., JNeurosci. 27 (7), 1782-90 (2007).

2. INTRODUCTION

Every action of an animal depends on the reception and correct interpretation of the information coming from its surroundings. Sensory organs provide the nervous system with the ability to sense dynamic changes occurring in their environment. In particular, the processing of auditory information is extremely relevant for an animal to detect and identify the location of a sound. The ability to determine whether a sound originates from one side or the other allows the animal to localize a possible prey or predator and thus, may also determine its survival.

2.1 Sound localization in the mammalian brain

The binaural localization of a sound source relies on the comparison of auditory inputs arriving at the two ears. Two sounds can be discriminated from another by the different physical parameters that characterize them, based on the sound pressure, spectrum and phase. Moreover, the task of localizing a sound source can be accomplished by means of these characteristics. Two major binaural cues for localizing acoustic stimuli in the horizontal plane have been proposed based on the differences perceived by the two ears: the interaural time differences (ITDs) and the interaural intensity differences (IIDs) (Thompson, 1882; Rayleigh, 1907).

The ITDs are the differences in the arrival time of a sound at the two ears and are the main cue for localizing low frequency sounds (Rayleigh, 1907). A sound

traveling from its source will reach first the ear of the listener that is on the hemisphere closer to the source and only after traveling a certain distance it will reach the other ear. The magnitude of the ITD depends on the separation distance between the two ears of the listener (Heffner and Heffner, 1992; Erulkar, 1972).

The IIDs are differences in the sound pressure level (SPL) at the two ears and provide the major cue for localizing high frequency sounds (Rayleigh, 1877; Erulkar, 1972). The generation of IIDs is related to the loss of energy by the sound wave as it propagates from the source to the detection organ. The head of the animal reduces the intensity of the sound even further (acoustic shadow). Therefore, the difference on the intensity at which the sound reaches both ears can bring information about the location of a sound source.

The neuronal circuitry underlying ITDs and IIDs are essentially different, involving different nuclei in the auditory brainstem. The two pathways originate in the superior olivary complex (SOC) and their properties depend on the specific connections they receive from the cochlear nucleus (CN). ITDs are first processed by neurons in the medial superior olive (MSO) (Moushegian et al., 1964; Goldberg and Brown, 1968; Watanabe et al., 1968; Grothe and Park, 1998; Brand et al., 2002), whereas IIDs are encoded by neurons in the lateral superior olive (LSO) (Boudreau and Tsuchitani, 1968; Caird and Klinke, 1983; Cant and Casseday, 1986; Moore and Caspary 1983; Sanes and Rubel, 1988).

It has been shown that most of the neurons exhibiting sensitivity to IIDs are those that receive excitatory inputs from one ear and inhibitory inputs from the other

one, the so called excitatory/inhibitory (EI) neurons (Rose et al., 1966; Goldberg and Brown, 1969).

The LSO receives excitatory inputs from the ipsilateral anteroventral cochlear nucleus (AVCN) and glycinergic inhibitory inputs from the ipsilateral medial nucleus of the trapezoid body (MNTB) (Moore and Caspary, 1983; Tsuchitani, 1988a,b; Sanes and Rubel, 1988; Covey et al., 1991) which receives strong excitatory inputs from the contralateral AVCN (Fig. 2.1; Glendenning et al., 1985; Cant and Casseday, 1986). Accordingly, most studies in the LSO have found that the majority of its neurons are EI neurons (Park et al., 1996, Joris and Yin, 1998) and code IIDs by subtracting the activity of the inhibitory input from the excitatory one.

The LSO projects bilaterally to the dorsal nucleus of the lateral lemniscus (DNLL) and the inferior colliculus (IC) (Henkel and Brunso-Bechtold, 1993; Kelly et al., 1998) and transfers the IID sensitivity to these two nuclei.

2.2 Binaural processing in the DNLL

The lateral lemniscus consists of three nuclei: the DNLL, the intermediate nucleus of the lateral lemniscus (INLL) and the ventral nucleus of the lateral lemniscus (VNLL). Even though, it has often been regarded a relay station for the information transferred from the CN and the SOC to the IC, recent studies have shown that significant auditory processing occurs in this structure. In particular, the contribution of the DNLL to binaural processing has been extensively

examined. Several studies have shown that most of its neurons are sensitive to binaural stimulation.

The DNLL receives excitatory inputs from the ipsilateral MSO and the contralateral LSO as well as inhibitory inputs from the ipsilateral LSO (glycinergic) and the contralateral DNLL (GABAergic) (Fig. 2.1; Glendenning et al., 1981; Oliver, 2000; Shneiderman et al., 1988; Adams, 1979; Brunso-Bechtold et al., 1981; Kudo, 1981).

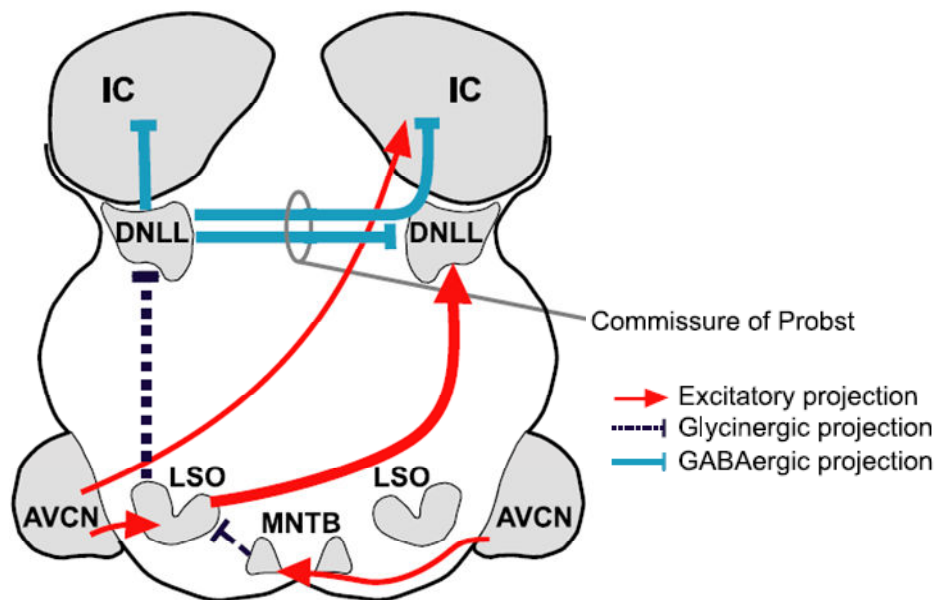


Fig. 2.1. The DNLL circuitry. DNLL neurons receive excitatory input from the contralateral LSO and two inhibitory inputs driven by ipsilateral sound stimulation, one from the ipsilateral LSO (glycinergic) and one from the contralateral DNLL (GABAergic). DNLL sends projections to its contralateral counterpart and to the IC in both sides. LSO neurons are excited by ipsilateral sounds via the AVCN and inhibited via a glycinergic projection of the contralateral MNTB. (From Pecka et al. 2007)

Due to the inputs that DNLL neurons receive they can exhibit sensitivity to both IIDs and ITDs (Brugge et al., 1970; Fitzpatrick and Kuwada, 2001; Kelly et al.,

1998, Kuwada et al., 2005; Markovitz and Pollak, 1994). In particular, this nucleus contains a large amount of EI cells a condition that favors the processing of IID (Brugge et al., 1970; Kelly et al., 1998; Yang et al., 1996; Markovitz and Pollak, 1994). The processing of these binaural cues in the DNLL of bats has been shown to be more complex than in the LSO. This complexity arises as a result of the binaural projections that this nucleus receives from the LSO in addition to the inhibitory projection from its contralateral counterpart.

Different types of neurons have been identified in the DNLL based on their morphology and physiology in the rat (Bajo et al., 1993; Wu and Kelly, 1995; Tanaka et al., 1985), mouse (Iwahori, 1986), cat (Adams 1979, Shneiderman et al. 1988) and the big brown bat (Covey, 1993). It has been observed in different species that DNLL neurons exhibit a frequency distribution that represents the entire audiogram of an animal (Markovitz and Pollak, 1993; Covey, 1993; Burger and Pollak, 2001; Bajo et al., 1998; Bajo et al., 1999). A heterogeneous population of neurons has been described in relation to their physiological properties and their responses to auditory stimulation. In general, two main response categories have been identified within the nucleus: onset neurons, responding only at the beginning of the signal, and sustained neurons, responding throughout the duration of the stimulus (Markowitz and Pollak, 1993; Siveke et al., 2006; Yang and Pollak, 1997; Brugge et al., 1970; Kelly et al., 1998).

Anatomical data showed that the vast majority of DNLL neurons is GABA or GAD immunopositive (Adams and Mugnaini, 1984; Moore and Moore, 1987) and is thought to provide a strong inhibition to its targets, mainly the IC and the

contralateral DNLL (Oliver and Shneiderman, 1989; Shneiderman and Oliver, 1989; Adams, 1979; Bajo et al., 1993; Kudo, 1981; Henkel et al., 2003; Merchán et al., 1994). The role of this GABAergic inhibition has been studied in both the DNLL (Yang and Pollak, 1994, Burger and Pollak, 2001) and the IC (Li and Kelly, 1992; Kidd and Kelly, 1996; Bauer et al., 2000). Kidd and Kelly (1997) have shown that injections of kynurenic acid, a non-specific glutamate receptor blocker, into the DNLL block the inhibition in the contralateral nucleus at least partially. Moreover, the reversible inactivation of the DNLL showed that some EI cells in the IC exhibited properties that were not present before suppressing the inhibitory source (Burger and Pollak, 2001), revealing an important role of the GABAergic inhibition in the IC.

2.3 The precedence effect and echo suppression

The precedence effect (PE), also known as the *law of the first wave-front* or the *Haas effect*, is a perceptual phenomenon that is thought to enhance our ability to localize sounds in a reverberant environment. The PE is experienced when two sounds are presented from different locations with a brief delay between them (in the range of 2 to 10-20 ms). If the delay is short enough (<2 ms), instead of localizing each sound at its respective position, the listener perceives one “fused” sound and localizes it at a virtual location which is dominated by the leading source. If the two sounds are separated by >10-20 ms, exceeding the “*echo threshold*”, they are perceived as independent entities and both sounds can be localized (Fig. 2.2; Blauert, 1997; Litovsky et al., 1999; Yin 1994).

The *echo suppression* is the range of interstimulus delays (ISDs) at which the PE is active and only one sound is localized. Echo suppression is a prerequisite for localizing a sound source in natural environments, but it can break down depending on the behavioral context. The range of ISDs at which *echo suppression* breaks down and the lagging sound is localized at its respective position is called *echo threshold* (Litovsky & Yin, 1998).

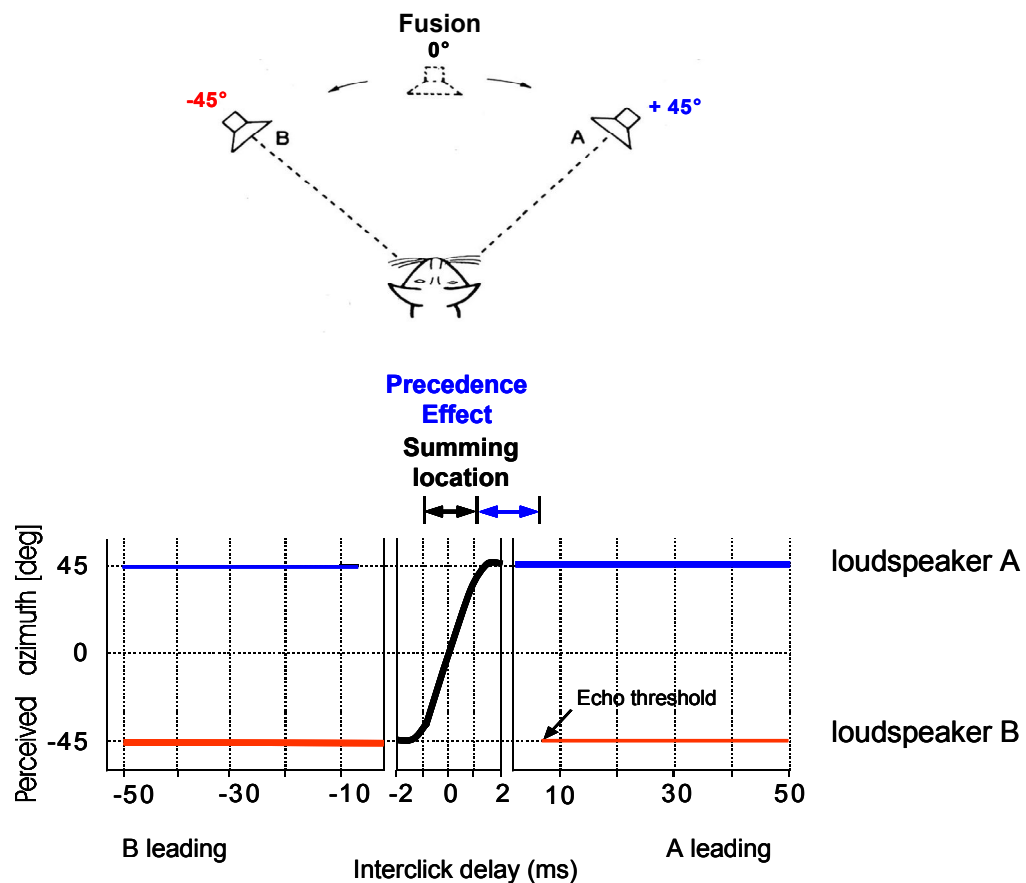


Fig. 2.2. The precedence effect.

A cat is positioned midway between two speakers that are located at 0° elevation and -45° azimuth. Two clicks, one from each speaker, are delivered with variable interclick delay. By convention negative interclick delays correspond to delays of the click to speaker A in the contralateral sound field. In the lower panel, the perceived location of the clicks, as derived from results of psychophysical experiments in humans. Three time periods have been identified: summing localization, precedence effect, and interclick delays greater than echo threshold (from Yin 1994).

The precedence effect has been already described in psychoacoustical experiments in rats, barn owls and bats (Litovsky and Yin, 1998; Keller and Takahashi, 1996; Kelly, 1974; Litovsky et al., 1999; Fitzpatrick et al., 1995). However, most of the studies addressing the issue have focused on low frequency sensitive cells of the IC (Yin, 1994; Fitzpatrick et al., 1995; Litovski and Delgutte, 2002; Tollin et al., 2004) which are mostly EE neurons and involve a different pathway in the binaural circuitry.

The mechanisms that produce the PE are thought to be responsible for enhancing the ability to localize sounds in reverberant environments (Pollak et al., 2002; Pollak, 1997). Although the physiological bases for the PE have been studied, little is known about how these sounds are localized. The innervation from the contralateral DNLL to the IC has been suggested to contribute to the precedence effect in bats (Pollak et al., 2002). It has been shown in bats that DNLL neurons exhibit a specific response feature when stimulated with IIDs that favor the inhibitory ear. Such stimuli can persistently suppress the neuron's response to trailing sounds for tens of milliseconds (Yang and Pollak, 1994). Pollak and his colleagues proposed that this suppression is mediated by a persistent inhibition (PI) driven by the contralateral DNLL and that it might be relevant in echo suppression (Yang and Pollak, 1994; Burger and Pollak, 2001). It has been suggested that the DNLL may mediate the change in responsiveness to trailing sounds in IC neurons. During the period of PI in the DNLL, some IC neurons are deprived of their strong inhibitory innervation and therefore, can respond to auditory stimulation. This is an important feature because IC cells are then able to process signals coming from moving sound sources or those

generated by echoes (Pollak et al., 2002; Burger et al., 2001; Yang et al., 1994). This observation suggests that the circuitry involving the DNLL may contribute to the precedence effect.

It has been speculated that the kinetics of glutamate receptors in the LSO may account for the long lasting inhibition observed in DNLL (Kelly and Kidd, 2000). This would imply the presence of persistently active neurons in the LSO and therefore in the contralateral DNLL. However, no persistent firing has been observed (Covey, 1993; Bajo et al., 1998; Siveke et al., 2006). Another possibility is that this long lasting inhibition may be generated by the intrinsic properties of neurons in the DNLL.

2.4 Synaptic transmission

The response pattern of auditory neurons and all neurons in general, is the result of several characteristics both morphological and physiological. The number and location of the synapses and the dynamics of the transmitter release may determine the amplitude and the kinetics of the postsynaptic response, together with the intrinsic properties of the neurotransmitter receptors and the type of ion channels that are present in the postsynaptic cell.

The major inhibitory neurotransmitters in the central nervous system and, in particular, the auditory brainstem, are GABA and glycine. Among other differences, in the auditory system the inhibition generated by these two transmitters can be distinguished by the duration of the inhibitory postsynaptic potentials (IPSPs) that they evoke. Glycinergic inhibition has been shown to be of

short duration, whereas GABAergic inhibition often exhibits a slower decay time (Magnusson et al., 2005, Smith et al., 2000).

Most of the inhibitory neurons in the brain release GABA, which can bind to two classes of receptors, the ionotropic receptors (GABA_A and GABA_C receptors) and the G-protein-linked metabotropic GABA_B receptors. GABA_A receptors are associated with chloride conductances (Allen et al., 1977) (fast neurotransmission), whereas activation of GABA_B receptors is mainly associated to potassium conductances which activate G protein-regulated inwardly rectifying K⁺ channels (GIRK channels) (Gähwiler and Brown, 1985; Newberry and Nicoll, 1985).

GABA_A receptors are known to be pentameric assemblies of multiple subunits (α_{1-6} , β_{1-4} , γ_{1-3} , δ , ϵ , ρ and π_{1-3}) (Whiting et al., 1999; Barnard et al., 1998) that are closely related genetically, as GABA can bind to any of them (Olsen and Tobin, 1990). This multiplicity of subunits confers the potential of a large diversity of receptors with different affinities for GABA and desensitization rates (for review see Smith and Simpson, 2003). Some GABA_A receptors that exhibit a high affinity for GABA are also characterized by a slow desensitization (Banks and Pearce, 2000). Moreover, the location of the receptors can also be determined by the presence or absence of certain subunits in the pentamer. For example, it has been shown that the expression of the δ subunit in cerebellar granule cells results in the expression of the receptor in the perisynaptic membrane (Nusser et al., 1998; Wei et al., 2003).

Synaptic transmission is initiated in a presynaptic neuron when it releases vesicles containing the neurotransmitter into the synaptic cleft. The release of neurotransmitter is coupled to the entrance of calcium through voltage gated channels (del Castillo and Katz, 1954; Llinás, 1982). In most synapses, calcium enters through P/Q-(Ca_v2.1) or N-type Ca²⁺ channels (Ca_v2.2) whereas the R-(Ca_v2.3) and L-type Ca²⁺ channels (Ca_v1 series) are rarely involved in vesicle release (Llinás, 1982).

This Ca²⁺-triggered release of the transmitter can be achieved through two modes: fast synchronous release and slower asynchronous release (del Castillo and Katz, 1954; Dodge and Rahamimoff, 1967; Barret and Stevens, 1972; Schneggenburger and Neher, 2005; Meinrenken et al., 2003; Atluri and Regehr, 1998; Lu and Trussell, 2000). In most synapses, when action potentials (APs) fire at low frequency, most release is synchronous. On the other hand, when APs fire at high frequency, the release of transmitter becomes largely asynchronous (Lu and Trussell, 2000; Jensen et al., 2000; Maximov and Südhof, 2005).

Synchronous release is triggered by brief localized Ca²⁺ signals induced by APs, while asynchronous release is due to increased residual calcium in the presynaptic terminal (Lu and Trussell, 2000; Llinás et al., 1995; Atluri and Regehr, 1998). Südhof and collaborators (2007) recently showed that synchronous and asynchronous release act on the same vesicle pools but that they are caused by different mechanisms involving different calcium sensors.

Asynchronous release of transmitter after high frequency activity has been described in glutamatergic (Goda and Stevens, 1994; Atluri and Regehr, 1998;

Diamond and Jahr 1995) as well as in GABAergic synapses (Lu and Trussell, 2000; Heft and Jonas, 2005). At the auditory Calyx of Held synapse, asynchronous release of glutamate has been observed in immature animals (Chuhma et al., 2001; Awatramani et al., 2005; Sun et al., 2007; Scheuss et al., 2007). Nevertheless, during development the calcium dynamics in the calyx changes (along with the buffering capacities and the expression of some Ca^{2+} binding proteins (Lohmann and Friauf, 1996)), leading to an important decrease in the decay time constant of the excitatory postsynaptic currents (EPSCs) after a stimulation train (Chuhma et al., 2001). This reduction of the asynchronous release component during maturation is an important step to ensure precise transmission of the auditory signal.

In addition to a good control of the release machinery to maintain faithful neurotransmission, a quick transmitter clearance is also important to ensure synaptic independence, and thus a tight information transfer.

During intense synaptic activity large amounts of neurotransmitter are being released and this can induce the transmitter to spill out of the synaptic cleft. Spillover of the transmitter can activate not only extrasynaptic receptors but also receptors located further away from the release site, generating crosstalk between synapses (Semyanov et al., 2003; Isaacson et al., 1993; Scanziani, 2000). Even though spillover can reduce synaptic independence, it has also been shown that it might be important for amplifying the signal (Trussell et al., 1993; DiGregorio et al., 2002) and ensuring transmission reliability (Takahashi et al., 1995; Barbour et al., 1994; Roepstorff and Lambert, 1994).

Neurotransmitter spillover has been described both at GABAergic (Semyanov et al., 2003; Isaacson et al., 1993; Overstreet and Westbrook, 2003; Alle and Geiger, 2007) and glutamatergic (Mitchel and Silver, 2000; Scanziani, 2000; Vogt and Nicoll, 1999) synapses. In the cerebellum mossy fiber synapses (Mitchel and Silver, 2000) as well as in pyramidal neurons of the CA3 of the hippocampus (Scanziani, 2000; Vogt and Nicoll, 1999) the degree of glutamate spillover was found to be dependent on the frequency and duration of stimulation of the input fibers. This suggests that during intense activity more neurotransmitter is released, permitting the activation of receptors located extrasynaptically and possibly receptors at neighboring synapses as well.

2.5 The Mongolian gerbil as an animal model

The Mongolian gerbil (*Meriones unguiculatus*) was chosen for this study because it has a well developed brainstem auditory nuclei and they possess a broad hearing range. Even though they are specialized in low frequency hearing, they also hear well in the high frequency range up to 60 kHz (Ryan, 1976). Moreover, humans and gerbils exhibit quite similar audiograms and have the lowest auditory thresholds (at 2 to 5 kHz) (Ryan 1976).

The gerbil has served as a good experimental model for both anatomical (Roberts and Ribak, 1987; Kapfer et al., 2002) and physiological (Siveke et al., 2006; Brand et al. 2002; Heffner and Heffner, 1988, Ryan, 1976; Grothe and Sanes, 1994) studies.

2.6 Scope of the study

The physiological circuitry by which the echoes can be suppressed is not fully understood, but current experimental results suggest a significant role of the DNLL. This nucleus is mainly populated by inhibitory neurons (Adams and Mugnaini, 1984; Moore and Moore, 1987), with some of them showing EI response properties (Kelly et al., 1998; Covey, 1993; Siveke et al., 2006). Moreover, DNLL neurons exhibit a particular feature which is the ability to remain inhibited for a period of time that outlasts the duration of the auditory stimulus. This persistent inhibition has been shown to enhance the ability of IC cells to perceive trailing sounds, suggesting its role in echo suppression (Yang and Pollak, 1994; Burger and Pollak, 2001; Pollak et al., 2003).

The aim of this study is to provide information that would help to identify the neural mechanisms responsible for mediating the suppressive effects observed in the DNLL. In particular, the questions that will be addressed are:

I. Does the DNLL of the gerbil exhibit the long lasting inhibition that has been described in bats? PI in the DNLL has been suggested to play an important role for the suppression of echoes in bats (Pollak, 1997) and thus this nucleus might have a key role in precedence. Determining the presence of PI in the DNLL of the gerbil might suggest that it is a common feature in mammals.

II. What is the source of this long lasting inhibition? It has been suggested that persistent inhibition is derived from the opposite DNLL through the Commissure of Probst (Yang and Pollak 1998). On the other hand, another hypothesis suggests that network properties might underlie the observed long lasting

inhibition (Kelly and Kidd, 2000). Even though no persistently firing neurons have been observed in vivo, the effect of anesthetics in suppressing the response can not be ruled out. Therefore, an in vitro approach would help us to understand if this feature (PI) is the result of network properties or if it is due to synaptic or cellular properties of DNLL neurons.

III. What are the mechanisms that underlie PI? The mechanisms that promote this long lasting inhibition in an otherwise temporally very precise binaural circuit are unknown. Thus, the third aim of this study is to identify the presynaptic and/or postsynaptic neuronal properties that underlie persistent inhibition in the DNLL.

3. MATERIALS AND METHODS

Animals were maintained in a 12 hr light/dark schedule with food and water *ad libitum*. All efforts were made to minimize animal suffering and to reduce the number of animals used. All experiments were performed according to the German Tierschutzgesetz (AZ 211-2531-40/01).

3.1 In vivo recordings

3.1.1 Animal preparation

Four Mongolian gerbils (*Meriones unguiculatus*) of two to three months of age were anaesthetized by an initial intraperitoneal injection (0.5 ml per 100 g body weight) of a physiological NaCl solution containing ketamine (20%) and xylazine (2%), with supplementary doses of 0.05 ml of the same mixture given subcutaneously every 30 minutes through out the experiment. The body temperature was maintained constant at 37-39 °C by using a thermostatically controlled heating blanket. After recordings (10-12 hours) animals were sacrificed without awakening by injection of 0.2 ml T61 (BGA-Reg No T331, Intervet, Germany).

3.1.2 Stereotatic procedure

The skin and tissue covering the upper part of the skull were dissected and removed. In order to fix the head of the animal to the stereotaxic frame, a metal rod was mounted on the skull rostral to Bregma using an UV-sensitive dental

material (Charisma, Heraeus Kulzer, Germany). The rod was used to reproducibly secure the head of the animal in a custom made stereotaxic device during recordings. The animal was then transferred to a sound attenuated chamber mounted in the stereotaxic instrument (Schuller et al., 1986). Its position in the chamber was standardized by stereotaxic landmarks on the surface of the skull (intersections of the bregmoid and lamboid sutures with the sagittal suture in horizontal alignment). For electrode penetrations to the DNLL, a small craniotomy (approximately 1 mm²) was performed on the left side of the skull, 0.7 cm caudal and 2 cm lateral to Bregma following the stereotaxic coordinates (Loskota et al., 1974). The duramatter was then removed and ringer solution was frequently applied to the opening to prevent dehydration of the brain.

3.1.3 Recording procedure

Single units were recorded extracellularly using glass electrodes (Harvard Instruments, USA) pulled in a custom-made puller and filled with 1M NaCl with resistances between 5-10 MΩ. The recording electrode was advanced under remote control, using a motorized micromanipulator (Digimatic, Mitutoyo, Neuss, Germany) and a piezodriven (Inchworm controller 8200, EXFO Burleigh Products Group Inc., USA). Spikes were recorded via an electrometer (npi electronics, Germany), a noise eliminator (Humbug, Quest Scientific, Canada) removing residual line noise picked up by the electrode, a band-pass filter (VBF/3, Kemo, Italy) and an additional amplifier (Toellner 7607, Germany) and fed into a computer via an A/D converter (RP2-1, TDT). Signals were displayed through the Brainware application (Brainware, Jan Schnupp, TDT).

3.1.4 Acoustic stimuli

Acoustic stimuli were digitally generated at a sampling rate of 50 kHz by TDT System III (Tucker Davis Technologies, USA), converted to analogue signals (DA3-2/RP2-1, TDT), attenuated (PA5, TDT) and delivered to the ear-phone tubes (EC1, Tucker Davis Technologies, USA). Stimuli were delivered via customized commercial software (Brainware – for sensory Electrophysiology, Version 7.0.2 with support for TDT System, Jan Schnupp, Department of Physiology University of Oxford, UK).

The standard setting for the stimulus was duration of 200 ms plus squared-cosine rise-fall times of 5 ms, presented at a repetition rate of 4 Hz. For all recordings, the presentation of the stimulus was randomized.

To search for acoustic responses, uncorrelated noise bursts were delivered monaurally favoring the excitatory ear (contralateral to the recording site). When a neuron was found, its best frequency (BF) and absolute threshold were determined using binaurally identical sinus tone stimulation (ITD/IID=0). The frequency that elicited responses at the lowest sound intensity was defined as BF and the lowest sound intensity that evoked a noticeable response at the neuron's BF was defined as threshold. Additionally, monaural and binaural pure tones were presented to determine the binaural properties of the neurons. These properties were determined online by audio-visual inspection and confirmed afterwards by offline analysis of the response areas for the frequencies and intensities used. These parameters were used to set stimulus parameters subsequently controlled by the computer.

The IID sensitivity was evaluated by stimulating binaurally, holding the intensity at the excitatory ear constant at 20 dB above threshold while varying the sound level at the inhibitory ear in 10 dB steps between 10 dB below and 50 dB above threshold. The resulting IIDs of -30 dB (negative IIDs indicate higher intensities at the inhibitory ear) to +30 dB were presented for 5 to 7 different frequencies centered on the BF.

To test an IID-sensitive neuron for PI, a steady response was evoked by presenting a tone burst (200 ms at BF) at 20 dB above threshold on the excitatory ear. Additionally, shorter tone bursts (20 ms at BF) were presented with several different intensities (from 30 dB below (-30 dB) to 30 dB above (+30 dB) threshold) on the inhibitory ear midway through the excitatory stimulus. Stimuli were cos²-function gated with rise-fall times of 5 ms for the contralateral and 2 ms for the ipsilateral side (if not stated otherwise). A DNLL neuron was defined as persistently inhibited if the duration of total suppression of responses to contralateral stimulation exceeded ipsilateral stimulus duration by at least 5 ms.

3.1.5 Data analysis

All quantifications in this study are based on offline analysis. Brainware was used to calculate firing frequencies and spikes timing and all data was then transferred to Excel MS Excel 2004 (Microsoft, USA) to calculate averages. All errors are expressed as standard error of the mean (SEM).

Neurons were defined as IID-sensitive when ipsilateral (inhibitory) stimulation reduced the maximal response elicited by contralateral (excitatory) stimulation by more than 50%. The IID of maximal inhibition was defined as the smallest IID

(lowest intensity at the inhibitory ear) that caused the maximal suppression of the response to contralateral stimulation.

The duration of PI was evaluated from peristimulus-time histograms of 1 ms bin width. The period of inhibition measured was the interval between the last discharge evoked by the excitatory stimulation right before the inhibitory stimulus was presented and the next discharge after the inhibitory stimulus ended. The period of inhibition that occurred during the inhibitory stimulation and the period of inhibition that outlasted the inhibitory stimulation were measured. From the duration of the total evoked response, the portion corresponding to the duration of the inhibitory stimulus (20 ms) was subtracted. The period of the inhibition remaining after this subtraction was defined as the persistent inhibition.

3.1.6 Histology

After some recording sessions, current induced lesions using metal 5 M Ω electrodes (2 nA for 80-120 seconds) were made to mark the position of the last recording site. Animals were deeply anesthetized with 0.1ml chloral hydrate 5% every 10 g animal mass and then perfused. The perfusion through the aorta was reached by opening the chest cavity after removal of skin and muscles. A needle was inserted through the left side of the heart and the atrium was cut, allowing the flow of a heparinized Ringer solution through out the whole animal's body. When the blood was washed out, 2% PFA was perfused until the tail of the animal hardened.

The heads of these animals were dissected out and then fixed in 4 % PFA for 24 hours. The brains were then removed and transferred successively to sucrose 20 % until they sank and then sucrose 30 % before they were sliced in a cryostat in 40 μ m thickness slices and Nissl-stained by standard methods (see appendix).

3.2 *In vitro* recordings

3.2.1 Brain slice preparation

14 to 19 days-old Mongolian gerbils were anesthetized by isoflurane inhalation (Isofluran Curamed, Curamed Pharma, Karlsruhe, Germany) and decapitated. The head was immediately immersed in an ice-cold slicing solution (see Table 2.1) carbogen saturated (5% CO₂, 95% O₂). The low calcium concentration (0.1 mM) and the low temperature were chosen to minimize metabolic processes. The brain was then dissected out and with an angle of ~30° the caudal part containing DNLL was cut out (Fig. 2.1). The cerebellum was then removed and the stack of isolated tissue containing most of the brainstem was fixed with superglue to the plate of the vibratome chamber (VT1000S, Leica, Nussloch, Germany).

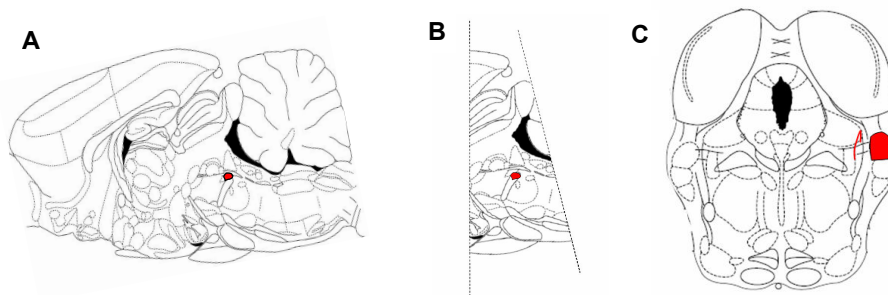


Fig. 3.2.1 Schematic illustration of the location of the DNLL in the mammalian brain.

Schematic representation of slice preparation. A) Sagittal plane of the whole brain 2 cm lateral to midline. B) Illustration of DNLL containing stack after a 30° angle posterior cut. C) Illustration of a typical slice containing DNLL. The DNLL is marked in red in all figures as well as the stimulation artefact placed in the Commissure of Probst in C). Note that the figures are schemes of the rat brain taken from The Rat Brain Atlas (Paxinos and Watson, 1998).

The tissue was then bathed with ice-cold slicing solution (Table 2.1) and the *duramater* was removed from the brainstem with forceps to facilitate slicing. The

plate was then placed in the vibratome and 200 μm thick slices were cut. DNLL was contained in two to three of the slices per animal. Each slice was transferred to an incubation chamber containing extracellular solution (recording solution, Table 3.2.1), bubbled with 5% CO_2 -95% O_2 and incubated for at least 30 minutes at 37°C. After incubation, slices were kept at room temperature until they were transferred to the recording chamber.

EXTRACELLULAR SOLUTIONS (in mM)		
	SLICING	RECORDING
NaCl	125	125
KCl	2.5	2.5
MgCl	1	1
CaCl ₂	0.1	2
glucose	25	25
NaH ₂ PO ₄	1.25	1.25
NaHCO ₃	25	25
ascorbic acid	0.4	0.4
myo-inositol	3	3
pyruvic acid	2	2

Table 3.2.1 Extracellular solutions for slicing and recording DNLL.

Two different internal solutions were used depending on whereas voltage or current clamp experiments were conducted (Table 3.2.2). For voltage clamp

recordings, 5 mM QX314 (lidocaine *N*-ethyl bromide, Alomone Labs, Jerusalem, Israel) was added to 1 ml CsCl internal solution prior each experiment to prevent sodium currents.

For some experiments, Alexa 568 or Alexa 468 (Invitrogen) was used in the internal solution to better visualize the morphology of the recorded cells.

INTERNAL SOLUTIONS (in mM)			
VOLTAGE CLAMP		CURRENT CLAMP	
CsCl	140	K-Gluconate	125
HEPES	10	HEPES	10
EGTA	10	EGTA	1
NaCl	2	KCl	5
CaCl ₂	1	Na ₂ -ATP	2
Mg-ATP	2	Mg-ATP	2
Na ₂ -GTP	0.3	Na ₂ -GTP	0.3
		Na-phosphocreatine	10

Table 3.2.2 Internal solutions for voltage and current clamp recordings.

The pH was adjusted to 7.25 with 1 M KOH for the K-gluconate based solution and to 7.3 with 1 M CsOH for the Cs containing solution. The osmolarity was adjusted to 280-290 mOsm.

During experiments, excitatory inputs were abolished by application of the glutamate receptor blockers DNQX and dAP-V to prevent NMDA and non-NMDA

receptor activation respectively or Kynurenic Acid as a general excitatory blocker. Strychnine was added to the bath to prevent glycinergic currents and SR95531 was used to block GABAergic IPSCs in some experiments.

DRUG	FINAL CONC.	COMPANY
SR95531	20 μ M / 50 nM	Tocris Biosc.
Strychnine	500 nM	Sigma
Kynurenic acid	5 mM	Sigma
d-AP-V	50 μ M	Tocris Biosc.
DNQX (in DMSO)	20 μ M	Tocris Biosc.
TPMPA	200 μ M / 100 μ M	Tocris Biosc.
alexa 488	50 μ M	Molecular Probes
alexa 568	50 μ M	Molecular Probes
EGTA-AM	100 μ M	Molecular Probes
NO711	10 μ M	Sigma
NNC711	2 μ M	Tocris Biosc.
CdCl₂	10 μ M	Sigma

Table 3.2.3 Drugs and concentrations used during the experiments.

All drugs were dissolved in water or DMSO (final concentration <0.01%) and prepared in advance. Stock solutions were kept frozen until the moment of use, except for Kynurenic acid which was dissolved directly before the experiment. Compounds were purchased as detailed in Table 3.2.3.

3.2.2 Whole cell recordings

Slices were fixed to a slice-chamber with an inner volume of about 1.5 ml with a custom made grid, made of stretched nylon strings glued onto a “U” shaped platinum wire. The slice was continuously perfused with a flow rate of about 1-1.5 ml/min through a gravity-fed perfusion system. A complete exchange of the extracellular solution was accomplished within two to three minutes. The bath was kept at 37 °C and the temperature was monitored through out the experiment with a dual automatic temperature controller (Warner Instruments Corporation, Hamden, CT, USA).

DNLL neurons were visually identified through a Zeiss Axioskop 2 FS microscope equipped with DIC and dot contrast optics and a 40x water-immersion objective (Zeiss, Germany).

The recording electrode was advanced with a Luigs & Neumann SM-5 micromanipulator (Germany).

Whole cell recordings were made with an EPC 10 double amplifier (HEKA Instruments, Germany). Signals were filtered at 5 - 10 kHz and subsequently digitized at 20 - 100 kHz using Patchmaster Version 2.02 software (HEKA Instruments, Germany). Uncompensated series resistance was between 5.5 and 15 M Ω and were compensated between 50 and 80 % with a lag time of 10 microseconds. Potential changes in series resistance were monitored throughout the recordings and data collection was discontinued whenever the residual uncompensated series resistance was larger than 4 M Ω .

Patch pipettes were pulled from 1.5 mm borosilicate glass (Harvard Instruments, United Kingdom) using a Sutter P-97 electrode puller (Sutter Instruments, USA) or a DMZ Universal Puller (Zeitz Instruments, Germany).

After some recordings, slices were then kept in 4% PFA overnight and then washed in PBS. The slices were mounted with Vector-Shield medium and maximal projections of the Alexa-stained neurons were obtained with a Leica TCS SP confocal microscope (25x 0.75 n.a.).

3.2.3 Stimulation of synaptic inputs

Synaptic currents were elicited by stimulation of the Commissure of Probst with a 5 M Ω bipolar stimulation electrode (matrix electrodes with 270 μ m distance, Frederic Haer Company, USA). Stimuli were 100 microsecond long square pulses of 5 to 100 Volts delivered with a STG 2004 computer controlled 4-channel stimulator (Multichannel Systems, Germany) and a stimulation isolation unit (Iso-flex, AMPI, Israel).

3.2.4 Data analysis

All voltage clamp data were analyzed in IGOR 5 (Wavemetrics, USA). Different macros were used to detect amplitudes, measure IPSC kinetics and for analyzing miniature IPSCs (see Appendix). Decay times were measured as from the 10% of the peak of the IPSCs and they were fitted with a single exponential function. Rise times were measured between the 20% and the 80% of the rising phase of the IPSCs.

Current clamp data was converted from ASCII to “abf” format through a custom made program in PEARL (see Appendix). These data was then analyzed in Clampfit (version 9.0.1.07, Axon Instruments Inc).

All data was then transferred to MS Excel 2004 (Microsoft, USA) for calculation of averages and statistics.

3.2.5 Statistical analysis

All errors are reported as the standard error of the mean (SEM). Statistical significance was tested with a student’s paired T-test, unless otherwise noted.

3.3 Appendix

3.3.1 Histology

3.3.1.1. Ringer solution containing heparin (for animal perfusion)

- 0.9% NaCl (4.5 g)
- 0.02% heparin
- 0.02% lidocain
- 500 ml PBS 0.1mol (pH7.4)

3.3.1.2. Nissl staining

- 2x 2 min EtOH 100%
- 1x 2 min EtOH 70%
- 1x 2 min EtOH 50%
- 1x 5-7 min Cresil Violet
- 3x 1min H₂O dest.
- 1x 2 min EtOH 70%
- 1x 2 min EtOH 96%
- 1x 2 min EtOH 96% + Acetic acid
- 1x 2 min EtOH 100%
- 3x 2 min xilol
- mount


```

        for($m=0; $m < @values-1; $m++) {
            print OUTPUT "\t".$values[$m][$n] * 1e3;
        }
        print OUTPUT "\n";
    }
close(DATA);
close(OUTPUT);

```

3.3.2.2. Last peak

For analyzing IPSCs amplitudes and kinetics for the last peak of a train with IGOR, by Felix Felmy

Macro Table_() → makes table

```

Make/N=40/D Amp_A, TToPeak_A, monoTauA, dbl1TauA, dbl2TauA, H_width, I_Charge,
VoltMake/N=40/T SweepNum, Obs
Edit SweepNum, Amp_A, TToPeak_A, monoTauA, dbl1TauA, dbl2TauA, H_width, I_Charge,
Volt, Obs

```

end

```

=====
=====

```

Macro IPSC_1PHz(wIPost, wIPostCorr, wIPostInt, wIPSC, RunNum) → A macro to analyse rise time, peak, and rate of rise

```

String wIPost="W270307_c3_1P_1_17_1_1"           → defines wave to analyze
String wIPostCorr="cW270307_c3_1P_1_17_1_1"
String wIPostInt="iW270307_c3_1P_1_17_1_1"
String wIPSC="W270307_c3_1P_1_17_1_1"
Variable RunNum
silent(1)

```

```

Duplicate/O $wIPost, $wIPostCorr                → duplicates waves to display
    display $wIPost
    ModifyGraph rgb($wIPost)=(0,0,0)
    SetAxis left -10e-10,1e-10
    ShowInfo

```

```

WaveStats/Q/R=(0.4,0.5) $wIPost                → defines baseline
$wIPost-=V_Avg                                  → introduces leak-correction in original
trace
Duplicate/O $wIPost, $wIPostInt
Integrate $wIPostInt                            → integrates leak corrected wave
$wIPostInt = $wIPostInt*(-1)                    → inverts sign of the integration
AppendToGraph/L=int $wIPostInt                 → appends integrated wave to graph

```

```

Variable AmpTime, background, TrueAmp, Amp     → defines variables
WaveStats/Q/R=(0.5,2) $wIPostInt

```

```

I_Charge[RunNum] = V_max
WaveStats/Q/R=[9920,9930] $wIPSC
background = V_avg
WaveStats/Q/R=[9970,12500] $wIPost           → determines FIRST peak amp and
time to peak
Amp=V_min
TrueAmp=Amp-background
Amp_A[RunNum]=TrueAmp
Amptime = V_minloc
TToPeak_A[RunNum]=(V_minloc - 0.497)*1000

Tag/C/N=text1/A=LB $wIPost, Amptime,"peak" → shows you where the peak is in the
graph

Variable Fitstart_X, Fitstart_Y, F_start       → defines variables
Fitstart_X = V_minloc
Fitstart_Y = Amp*0.95
FindLevel/Q/R=(Fitstart_X,1) $wIPost, Fitstart_Y → finds value at 80% rise of
peak amp   F_start = V_levelX
CurveFit/Q dblexp $wIPost[x2pnt($wIPost,F_start),16000] /D → fits double
exponential
dbl1TauA [RunNum] = (1/W_coef[2])*1000 // time in ms
dbl2TauA [RunNum] = (1/W_coef[4])*1000 // time in ms

CurveFit/Q exp_Xoffset $wIPost[x2pnt($wIPost,F_start),16000] /D → fits mono
exponential
monoTauA [RunNum] = (W_coef[2])*1000 // time in ms

Variable Half_Y, Half_X                       → defines Variables
Half_Y = Amp_A[RunNum] / 2
FindLevel/Q/R=(Fitstart_X,1) $wIPost, Half_Y → finds value for 80% rise of peak
amp
Half_X = V_levelX
H_width [RunNum] = (Half_X - 0.497)*1000 → determines Half width from stimulus
onset

End

```

3.3.2.3. All peaks

For analyzing IPSCs amplitudes and time to peak of all peaks on a train with IGOR, by Felix Felmy

Macro Tr10Hz_2P(wIPSC) (i.e. for a 2 pulse train at 10 Hz)

```

String wIPSC = "W060307_c2_10Hz_1_2_1_1" → wave name
silent(1)
Make/N=20/D/O wName → makes table
Variable background, Amp,TrueAmp, TtP → defines variables
// first peak
WaveStats/Q/R=[11880,11890] $wIPSC → defines baseline

```

```

background = V_avg
WaveStats/Q/R=[11980,13900] $wIPSC      → finds peak
Amp = V_min
TrueAmp = Amp - background             → defines real peak by subtracting
baseline
wName [0] = TrueAmp
TtP= (V_minloc - 0.595)*1000           → finds time to peak
wTiming[0]=TtP
// second peak
WaveStats/Q/R=[13880,13890] $wIPSC
background = V_avg
WaveStats/Q/R=[13980,15900] $wIPSC
Amp = V_min
TrueAmp = Amp - background
wName [1] = TrueAmp
TtP= (V_minloc-0.695)*1000
wTiming[1]=TtP

// Edit wName
wName*=-1                               → inverts sign of peak amplitude
End                                       → ends macro

```

3.3.2.4. bpc_Mini.xop

For analyzing mIPSCs with IGOR, gift by Holger Taschenberger

4. RESULTS

4.1 Binaural response properties of DNLL neurons

In vivo experiments were designed in order to determine whether EI neurons the DNLL of the gerbil exhibit the persistent inhibition (PI) as shown in bats.

A total of 13 neurons were recorded in the left DNLL, exhibiting best frequencies (BF) ranging from 2.7 to 18 kHz. All neurons responded to monaural tones (20 dB above threshold) presented at the right (excitatory) ear with a sustained firing of spikes (average firing rate 66.5 ± 20.9 Hz) that lasted as long as the stimulus was presented. When these neurons received binaural stimulation, the evoked responses were progressively diminished as the stimulus intensity at the left ear was increased. Thus, these neurons were considered IID sensitive. Eight of the 13 neurons recorded exhibited this feature (Fig. 4.1A); the other 5 neurons were excited monaurally. Figure 4.1B shows a representative IID curve for a neuron at its best frequency (BF). The dashed line represents the 50% reduction on the firing rate that for this particular neuron was at an IID of 22.4 dB. On average, this reduction was at an IID of 8.82 ± 2.56 dB ($n=8$), ranging from 1.65 to 22.4 dB.

Persistent inhibition (PI) was evaluated in all 8 IID-sensitive neurons by driving the cells with a 200 ms tone burst at the BF of the neuron presented to the excitatory ear while simultaneously presenting a 20 ms tone burst at the inhibitory ear, in the middle of the excitatory stimulus. The intensity of the excitatory stimulus was kept constant (at 20 dB above threshold) while varying the intensity at the inhibitory ear from 20 dB below (+20 dB) to 20 dB above (-20 dB) the intensity at the excitatory ear. Figure 4.1C shows the post-stimulus histogram

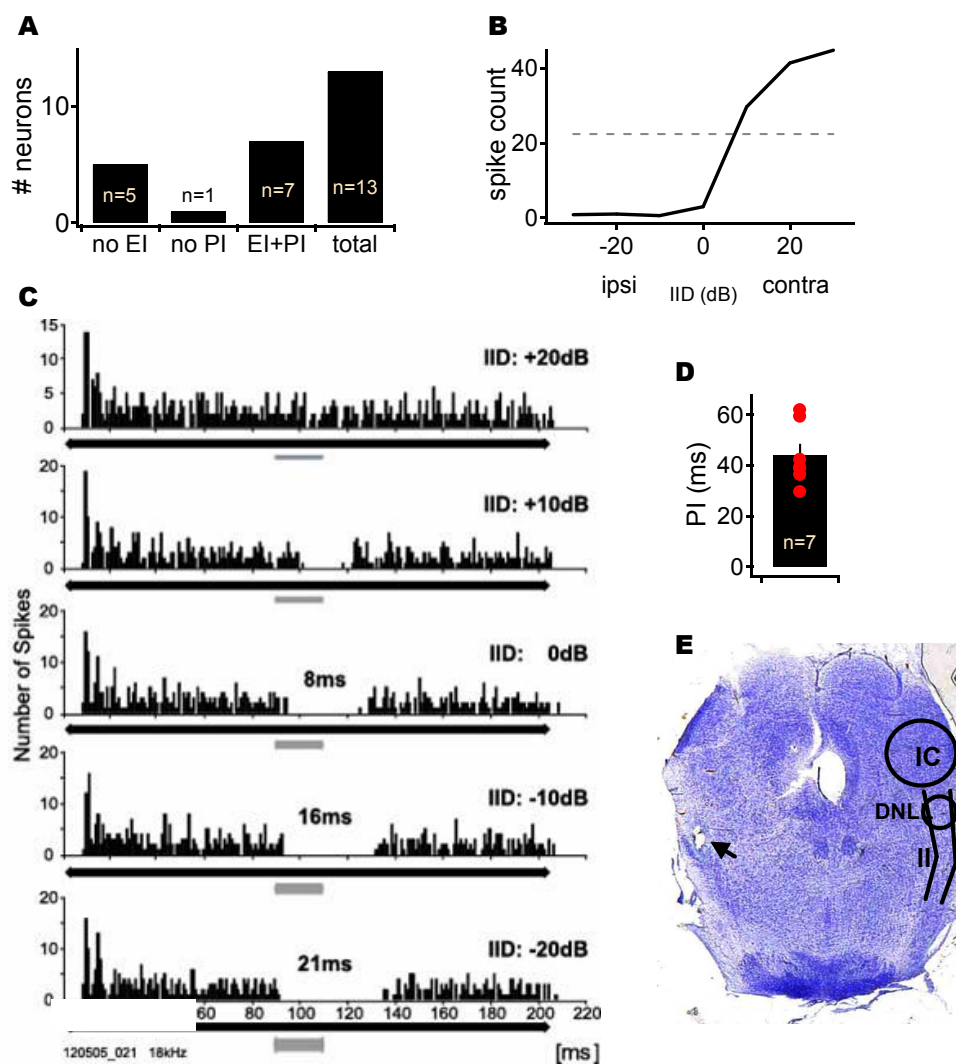


Fig. 4.1. PI evoked *in vivo* by ipsilateral stimulation. A) Response type distribution for high frequency neurons in DNLL. B) Response function of an IID sensitive neuron. C) Persistent inhibition evoked by ipsilateral stimulation. Peri-stimulus-time histograms (bin size 1 ms) showing the responses of a DNLL neuron to 200 ms contralateral pure tone stimulation (at BF= 18 kHz, 20 dB above threshold, black bar) plus a short, 20 ms long ipsilateral tone burst (at BF, gray bar) starting 90 ms after contralateral stimulation. The tone intensity at the ipsilateral ear was varied in 10 dB steps to create IIDs between +20dB (sound louder at the contralateral ear) and -20dB (louder at the ipsilateral ear). D) Quantitative analysis of PI evoked with the protocol showed in C for 7 neurons. E) Nissl-stained slice containing DNLL. The arrow head indicates the place of the last extracellular recording site (IC: inferior colliculus, DNLL: dorsal nucleus of the lateral lemniscus, II: lateral lemniscus).

(PSTH) for a representative neuron. Seven of these cells exhibited PI as a progressive suppression on the spike firing as the intensity at the right ear was increased. The period of inhibition was calculated as the interval between the last discharge evoked by the excitatory stimulation and the first discharge after the inhibitory stimulus had terminated.

For the neuron in Figure 4.1C, the maximal duration of suppression observed was 21 ms (bottom, IID=-20 dB). On average, the maximum PI duration at the most negative IID was 44.1 ± 4.6 ms, with values ranging from 29.6 to 62.1 ms (Fig. 4.1D, n=7).

Thus, these results suggest that binaural sounds that favor the inhibitory ear (negative IIDs) can create PI in the DNLL of the gerbil, suppressing the contralateral excitation for several tens of milliseconds.

Figure 4.1E shows a Nissl-stained section containing the DNLL in which the current-induced lesion made at the last recording site for a given experiment can be observed. The DNLL was visually identified as the nucleus sitting between the fibers of the lateral lemniscus (ll) and the Commissure of Probst. Typically, the lesion was observed as a small hole in the tissue (arrow head)

4.2 *In vitro* physiology

4.2.1 The contralateral DNLL provides the long lasting GABAergic inhibition

PI was then evaluated *in vitro* through stimulation of input fibers (the Commissure of Probst) to determine the source of this long lasting inhibition.

At least two different types of neurons were visually identified in the DNLL slices which also showed a different physiology. They exhibited a different firing pattern in response to supra-threshold depolarization (Fig. 4.2 A and B). Typically, one type had an elongated shape and fired action potentials (APs) as long as the depolarizing current was injected whereas the other type were smaller and rounded and fired only one AP (some neurons up to 3 AP). For simplification, the first type of neurons will be referred to as *sustained* type and the second type, as *onset* neurons. Differences were also observed between their voltage responses to hyperpolarizing constant current injections. The characteristic sag in the voltage observed for sustained cells (black filled circle in Fig. 4.2A) was nearly absent in onset neurons (black filled circle in Fig. 4.2B) which appeared to have higher leak conductance. A representative example of the sustained type morphology is depicted in Fig. 4.2G. These cells present an elongated somatic area and bipolar arrangement of its processes.

Figure 4.2C illustrates the membrane potential as a function of the current injection for both types of cells (sustained neurons in black (n=6) and onset neurons in red (n=4) at the beginning of the current step (filled circle) and at the

end of it (open circles). To test the effectiveness and duration of inhibition on the firing rate the sustained type is needed

Neurons were driven to fire AP by continuous current injections of 100 to 200 pA (Fig. 4.2D, top panel). Midway to these current injections, the fibers in the Commissure of Probst were electrically stimulated with a train of 3 pulses at a frequency of 500 Hz (Fig. 4.2D, middle panel). This elicited a suppression of the spikes that lasted, on average, 55.6 ± 9.4 ms ($n=11$). The mean firing frequency of these cells was 43.2 ± 10.3 Hz, resulting in interspike intervals of ~ 39 ms. The effective PI was in the range of 12 ms. When trains of a larger number of pulses were applied, the effective PI increased. A 10-pulse train elicited a PI of 19.2 ± 6.7 ms ($n=8$), whereas after stimulating with 20 pulses a PI of 31.9 ± 16.5 ms ($n=5$) was observed. The application of 20 μM of the GABA_A receptor blocker (2-(3-carboxyl)-3-amino-6-(4-methoxyphenyl)-pyridazinium bromide (SR95531)) caused the elimination of this PI (Fig. 4.2 D, lower panel) in a $77.5 \pm 8.8\%$ ($n=5$), indicating that all of the inhibition was transmitted by GABA_A synaptic current.

Simulation of phase-locked excitation was mimicked by injecting current pulses for 0.5 ms at 100 Hz. The amount of current injected (never exceeded 2 nA) was adjusted in order to elicit one spike per pulse (Fig 4.2E, top panel). The stimulation of the Commissure (3 pulses at 500 Hz) lead to a suppression of 2 spikes (Fig. 4.2E, lower panel). Consequently, the PI lasted for ~ 14 ms after the stimulus termination ($n=6$). On average, PI was calculated to last for 19.4 ± 3.2 ms at the 90% of recovery. Under the same conditions, a train stimulation of 10 pulses elicited an inhibition of 20.7 ± 7.8 ms ($n=4$). On the other hand, a 20 pulses train led to PI of 26.5 ± 10.4 ms ($n=4$) (Fig. 4.2F).

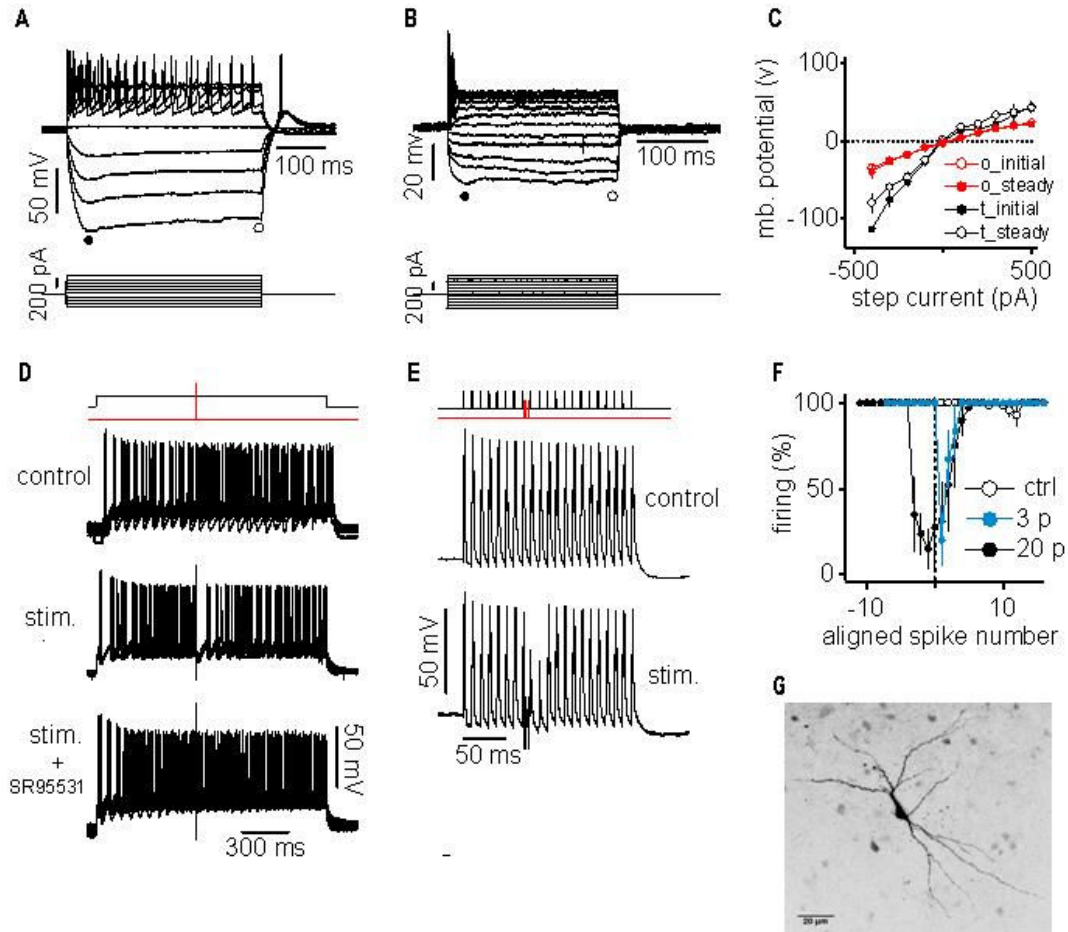


Fig. 4.2. PI evoked in vitro by stimulation of the Commissure of Probst. A) Sustained type response of a DNLL neuron to different current injections. B) Onset type response of a DNLL neuron to different current injections. C) Membrane potential as a function of the current injection for sustained (black) and onset (red) neurons. Filled circles represent the potential at the initiation of the current step whereas open circles indicate the recorded potential at the end of the current injection. D) Overlay of 10 traces of current clamp recording from a DNLL neuron. Spikes were elicited via a continuous current injection of 200 pA for 1000 ms (top, black line). The commissure of Probst was stimulated with a short train of 3 pulses at 500 Hz (top, red line) to elicit the GABAergic inhibitory input from the contralateral DNLL. E) Simulation of sound evoked excitatory inputs through brief repetitive injections of current (top, black line), which in each case elicited an action potential in the neuron. The injected current was 1-2 nA for 0.5 ms, followed by a 9.5 ms long pause, entraining the neuron at 100 Hz. The commissure was stimulated with the same protocol used in D (top, red line), leading to action potential suppression. F) Firing probability of 6 neurons before and after the recruitment of the GABAergic inhibition. Open circles: Control without fiber stimulation showing the high spiking fidelity of the neurons, blue circles: after a 3-pulses stimulation, black circles: after a 20-pulses stimulation. G) Maximal projection of a representative Alexa 468 filled sustained type neuron exhibiting an elongated soma

These results suggest that PI in the DNLL of the gerbil might be due to cellular properties rather than to network properties as the long lasting inhibition could be elicited by commissural stimulation.

4.2.2 The decay time constant of GABAergic IPSCs can explain the PI found *in vivo* and *in vitro*

If PI is due to GABAergic synaptic inhibition, then the kinetics of the inhibitory postsynaptic currents (IPSCs) should resemble the time course of PI at a cellular level. Therefore, voltage clamp recordings were performed and the decay times of the GABAergic IPSCs were measured.

GABAergic IPSCs were elicited by stimulating the Commissure of Probst with a train of 3 pulses at 500 Hz at 10-20 volts above threshold. The amplitude of the IPSC depicted in Fig. 4.3 A was 1.96 nA (black trace) and its decay time was 15 ms. The application of 2-(3-Carboxypropyl)-3-amino-6-(4 methoxyphenyl)-pyridazinium bromide (SR95531) led to a reduction of the IPSC amplitudes of $96.3 \pm 1.7\%$ ($n=5$, Fig 4.3A, red trace and Fig. 4.3B). On average, IPSC amplitude was 0.76 ± 0.32 nA (Fig. 4.3B).

No significant differences between the different groups of animal ages tested were found on IPSCs amplitudes and decay time constants for stimulation of the fibers with one pulse at 60 volts ($p>0.05$, paired t-test). Decay time values were 26.4 ± 1.8 ms, 29.5 ± 2.0 ms, 22.6 ± 2.2 ms and 27.7 ms at postnatal day 14 ($n=10$), 15 ($n=14$), 16 ($n=5$) and 17 ($n=1$) respectively (Fig. 4.3C).

The reversal potential of the evoked IPSCs for the neuron depicted in Fig. 4.3D was found to be between 0 and +10 mV. The calculated reversal potential with the Nernst equation was estimated to be +2 mV, whereas the potential at which the measured currents reversed was $\sim +10$ mV on average (Fig 4.3E, $n=6$).

These results indicate that in gerbils PI can be achieved by stimulation of the Commissure of Probst and that it is mediated by GABA_A receptors.

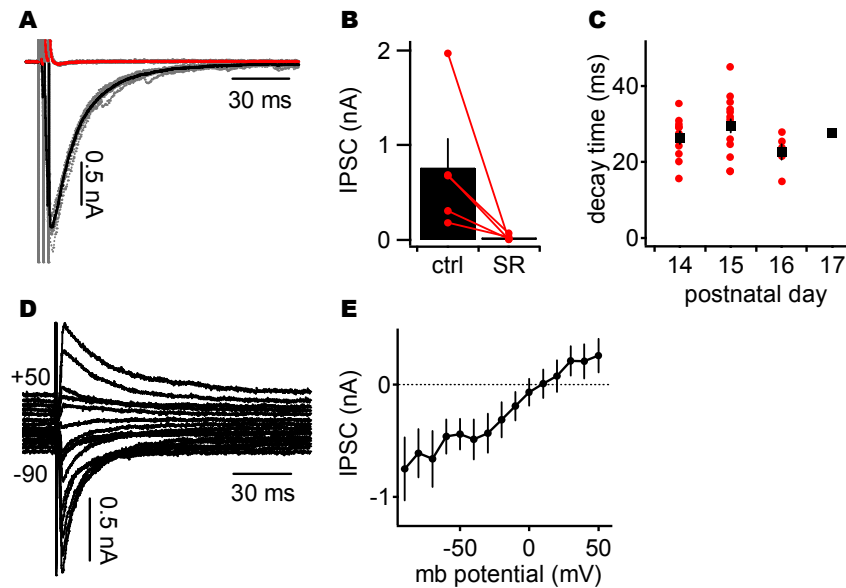


Fig. 4.3. Decay time of evoked IPSCs *in vitro* mimics PI *in vivo*. A) Voltage clamp recordings from a DNLL neuron showing inhibitory postsynaptic currents in response to the same 3-pulses fiber stimulation described above. Fiber stimulation recruited an IPSC of ~2 nA. SR95531 effectively blocked the evoked IPSCs. Solid black and red lines: average of 10 traces. B) Average IPSCs evoked and current elimination after application of SR95531 (black bars). Single cell responses are shown in red. C) Postnatal day dependency of evoked IPSCs decay time. D) Response of a representative neuron to fiber stimulation at different holding potentials. E) Average response to different holding potentials, showing a reversal potential around 0 mV.

4.2.3 The stimulation strength increase in the IPSC kinetics suggest a possible role of spillover in DNLL long lasting inhibition

In order to investigate the possible pre- and post-synaptic mechanisms underlying this long lasting inhibition, further voltage clamp experiments were performed. If the prolonged currents are due to spillover of the neurotransmitter,

then the IPSCs kinetics should become slower as the stimulus strength increases. At larger stimulation intensities more fibers are likely to be recruited. Thus, more GABA would be released into the cleft and receptors located further away from the release sites might be activated

This hypothesis was tested by stimulating the fibers with a 2 pulse protocol at a frequency of 10 Hz and different voltage strengths ranging from 0 to 100 volts in 5 volts steps (Fig 4.4A). In general, the step like increase of the IPSC amplitudes was masked, exhibiting a nearly linear increase in most of the cells tested (n=9). The inset shows the dependence of the amplitude on the stimulation strength for the first and the second peak (open and filled circles respectively) for this particular cell. In this case, the amplitudes ranged from ~ 30 to ~ 950 pA and the threshold for eliciting an IPSC was found to be at 10 volts.

On average, this threshold was at 20 volts, with 1st peak amplitudes of 110 ± 28 pA and 2nd peak amplitudes of 150 ± 42 pA. At 100 volts, the maximal strength tested, IPSC amplitudes were 770 ± 170 pA and 820 ± 180 pA, respectively. When the paired pulses were applied at different frequencies, the same stimulation strength dependency was met. At threshold, IPSC amplitudes were 124 ± 55 pA and 148 ± 70 pA for the 1st and 2nd peak at 20 Hz (n=9) and 150 ± 69 pA and 120 ± 48 pA at 100 Hz (n=6). At the maximal stimulation, these values were 850 ± 17 pA and 890 ± 28 pA at 20 Hz and 480 ± 30 pA and 490 ± 36 pA at 100 Hz, for the 1st and the 2nd peak in that order.

This linear increase was also observed after stimulating with a single pulse, leading to amplitudes of 145 ± 49 pA at threshold and 830 ± 120 pA at 100 volts (n=9).

The paired pulse ratio showed no obvious facilitation or depression of the 2nd peak at the 3 frequencies and all different voltages tested, showing values of 1.3 ± 0.4 , 1.2 ± 0.1 and 1.2 ± 0.2 at 10 Hz stimulation frequency at threshold, 60 and 100 volts, respectively ($p > 0.05$). Similar values were calculated at 20 Hz stimulation frequency (1.4 ± 0.2 , 1.0 ± 0.4 and 1.3 ± 0.3) and at 100 Hz (1.3 ± 0.6 , 1.7 ± 0.6 and 1.3 ± 0.5).

Figure 4.4B illustrates the stimulation strength dependency of the charge considered as the integral of the area below the IPSCs. Both single and double pulse stimulation (at 10 and 20 Hz) showed a linear rise over the voltage range. The increase reached through the 2 pulses protocol doubles the one with the single stimulation, for which values range from 53 ± 16 pC to 380 ± 53 pC (at threshold and 100 volts, in that order) in contrast to the 92 ± 30 pC to 780 ± 135 pC range for the 10 Hz, 102 ± 28 pC to 908 ± 175 pC for the 20 Hz condition and 148 ± 91 pC and 1.03 ± 0.35 nC at 100 Hz.

The half width and decay time also showed a clear dependence on the stimulation strength in all conditions tested (1 pulse and 2 pulses at the different frequencies tested). In figure 4.4C the average for both kinetic properties at the 10 Hz state is depicted, in which the values for the decay time constant ranged from 29.7 ± 10.7 ms and 34.5 ± 2.6 ms for the 1st peak at threshold and maximal stimulation strength respectively. Similarly, the values for the second peak were

28.8 ± 5.6 ms and 43.8 ± 2.1 ms (lower panel). These values did not differ much from those calculated for the second peak after a 20 Hz stimulation (28.8 ± 9.5 ms at threshold and 46.8 ± 3.3 ms at 100 volts) or after a 100 Hz stimulation (33.8 ± 4.5 ms and 44.2 ± 4.1 ms at minimal and maximal stimulation correspondingly).

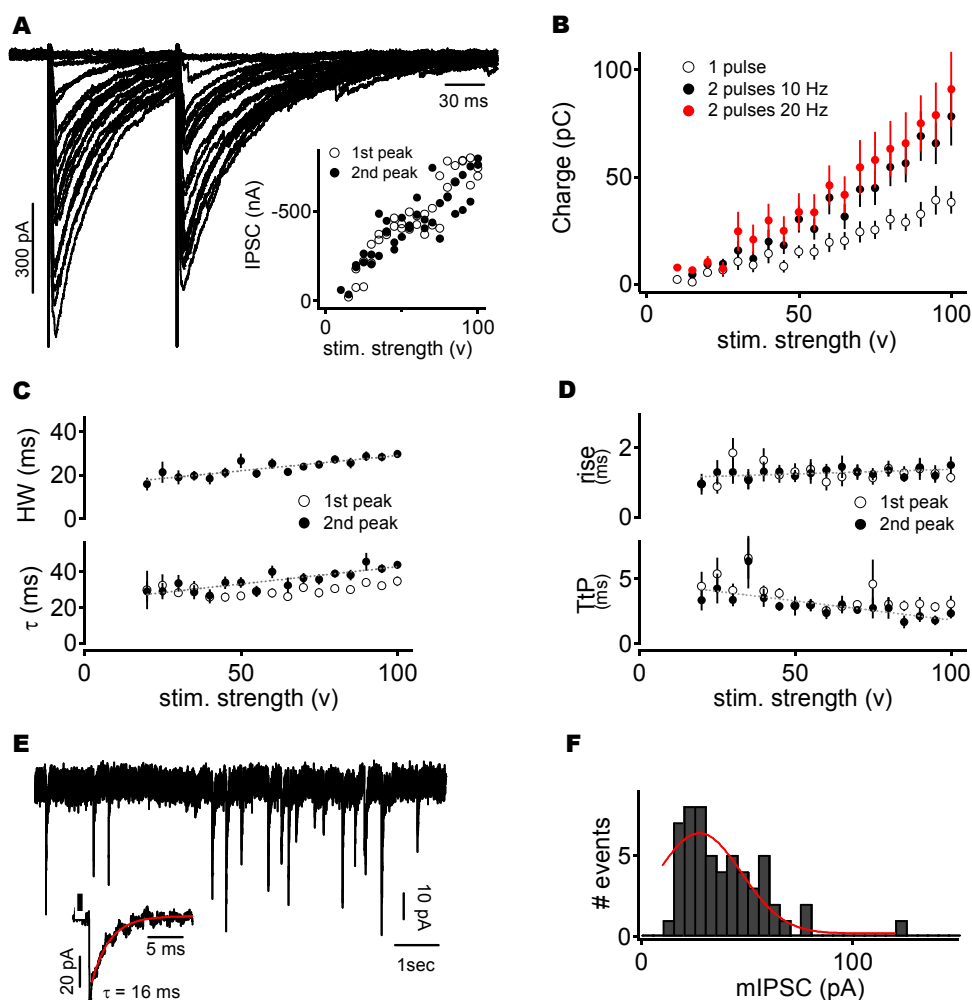


Fig. 4.4. GABAergic IPSCs kinetics dependency on stimulation strength.

A) Representative example of evoked GABAergic IPSCs after a 10 Hz paired stimulation. Each of the superimposed traces corresponds to a 5 volt increase, ranging from 0 to 100 volts. Inset: IPSCs amplitudes increase gradually with the voltage strength. B) Integral of the charge as a function of the stimulus strength after 1 and 2 pulses stimulation at different frequencies. C) Half width (top panel) and decay time (lower panel) of the 2nd IPSC of a pair depend on the stimulation strength. D) Rise time and Rise time (top panel) and time to peak (lower panel) show no dependency on the stimulus intensity. Open circles: 1st IPSC, filled circles: 2nd IPSC, red dashed lines: linear fit. E) mIPSCs recording for the cell depicted in A. Inset: distribution for the cell depicted in A). Typical GABAergic mIPSC recorded in the DNLL. Red line shows the exponential fit. F) Amplitudes distribution of the mIPSCs for the cell depicted in A. The red line shows the Gaussian fit for the distribution (see text for value of the mean).

Also, after a single pulse protocol, these values were 28.7 ± 3.8 ms and 37.8 ± 2.1 ms. Overall, there is an effective increase in the decay time of ~ 5 ms and ~ 15 ms at 10 Hz for each peak and ~ 18 ms and ~ 10 ms at 20 and 100 Hz respectively.

In the same way, the half width of the second peak ranged between 15.8 ± 2.9 ms and 29.6 ± 1.7 ms at 10 Hz (Fig. 4.4C, top panel). When stimulating at 20 Hz, these values were 19.9 ± 5.5 ms and 46.8 ± 2.4 ms, whereas at 100 Hz they were 21.4 ± 6.0 ms and 30.9 ± 3.2 ms. The single pulse stimulation showed results ranging from 21.9 ± 2.5 ms and 30.5 ± 1.5 ms.

Rise time and time to peak did not change over the range of stimulation strength evaluated, exhibiting values of 1 ± 0.2 ms and 1.3 ± 0.2 ms for the rise time of the 1st and 2nd peak, and 2.5 ± 0.4 ms and 2.3 ± 0.4 ms for the time to peak at 60 volts, correspondingly (Fig. 4.4D, top and lower panels). This was also observed for the one pulse condition as well as for all evaluated frequencies. This observation suggests that the slow decays are not due to the interaction of inputs with different latencies.

In Fig. 4.4E an example of the recorded mIPSCs is depicted. The inset zooms in on a typical GABAergic mIPSC of DNLL neuron, with a decay value of ~ 16 ms (exponential fit in red). Figure 4.4F illustrates the amplitude distribution for the miniature IPSC (mIPSC) for the same cell depicted in Fig. 4.4A (bin size of 5 pA). For the example depicted, 56 minis were found with amplitude values that ranged from 12.1 pA to 120 pA. The median value of the amplitude distribution was 29.86 pA (Gaussian fit in Fig 4.4F). On average, from a total of 3271 mIPSCs out

of 30 neurons, the amplitude ranged from 4.6 pA to 363 pA and the mean decay time was 19.5 ± 0.8 ms.

The dependency of the decay time constants on the stimulus strength suggest that spillover of GABA onto nearby synapses and/or extrasynaptic receptors might be involved in prolonging the inhibitory signal. Higher stimulation intensities seem to recruit more fibers generating GABA pooling and slowing down the decay time of the IPSCs. Since the rise time of the evoked currents did not change, these results suggest that activation of neighboring synapses might be occurring.

4.2.4 Pre-synaptic mechanisms might be involved in extending synaptic inhibition in DNLL neurons

Another possibility that might explain the long lasting inhibition observed in DNLL neurons relates to presynaptic mechanisms. A build-up of calcium in the presynaptic terminal might be achieved after repetitive stimulation of the fibers, leading to asynchronous release of the neurotransmitter and therefore, to a prolonged inhibitory signal. To test this hypothesis, IPSCs were recorded in response to stimulation trains of 2, 10 and 20 pulses were done at different frequencies.

Figure 4.5A illustrates a representative example of evoked IPSCs after stimulating the fibers at 60 volts with a 10-pulse train at different frequencies for a given cell. The top panel shows the superimposed traces of the evoked response after a 10 Hz train; the middle panel exhibits the response to 100 Hz whereas in the lower panel the response to 500 Hz stimulation is depicted. Note the

asynchronous release evoked at higher frequencies (indicated in the figure with stars). In particular, at 100 Hz this asynchronous release component seemed to induce to a prolongation of the IPSCs decay time.

The depression curves constructed for 10 pulse trains show no difference between the amplitudes of evoked IPSCs at 10 or 20 Hz (Fig. 4.5B, n=7). The depression reached at the last pulse was in both cases ~ 30% of the initial amplitude. On the other hand, at 50 Hz the amplitude of the second peak of the train exhibited a reduction of ~ 20% and at the end of the train of about 70%. In this case, depression was ~ 50% already after the 5th pulse. At higher frequencies a more significant depression was achieved earlier in the train. Typically, at 100 Hz the reduction was ~ 50% at the 2nd pulse of the train, reaching values of ~ 90% at the last peak evoked whereas trains of 200 Hz led to a reduction of ~ 95% for the last IPSC, being ~ 70% of the depression found at the 2nd peak.

Summarizing these findings, in Figure 4.5C the steady state of depression is plotted as a function of the train frequency. To construct this curve, the average of the last 3 points on the depression curve of each frequency was taken.

The decay time constant of the last peak of the same trains as in Fig. 4.5 was found to be frequency and pulse number dependent (Fig. 4.6A). For instance, with trains consisting of only 2 pulses (n=7) the decay constant was 21.17 ± 1.8 ms at 10 Hz, 24.6 ± 2.73 ms at 20 Hz, 30.7 ± 2.99 ms at 50 Hz, 31.83 ± 2.58 ms at 100 Hz, 31.24 ± 3.17 ms at 200 Hz and 30.28 ± 3.13 at 500 Hz. The kinetics of the last IPSC was also increasing while increasing the frequency after trains of 10

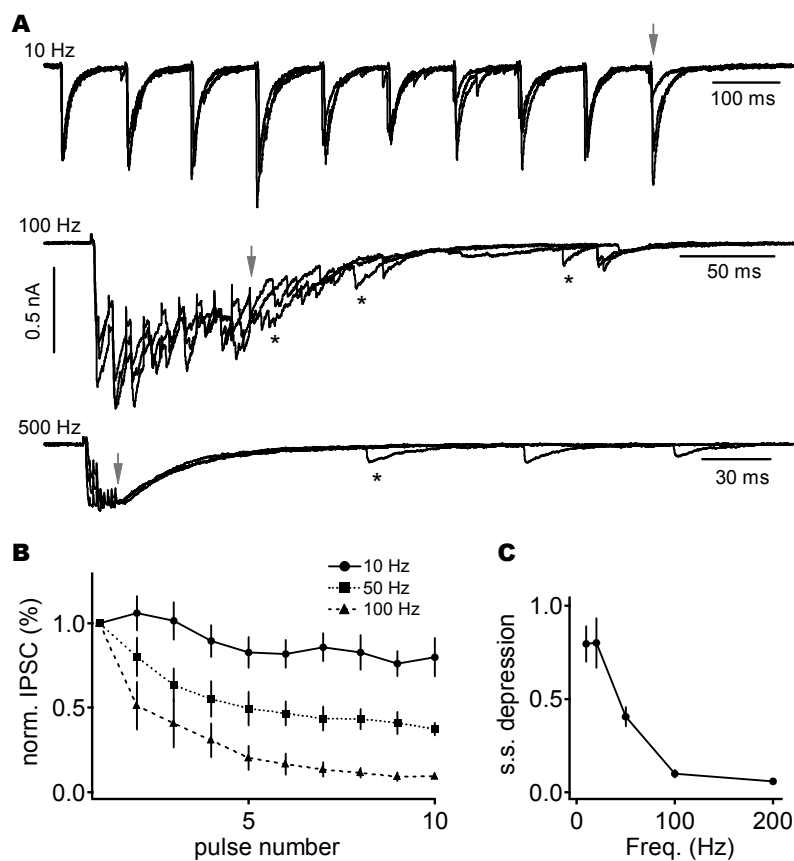
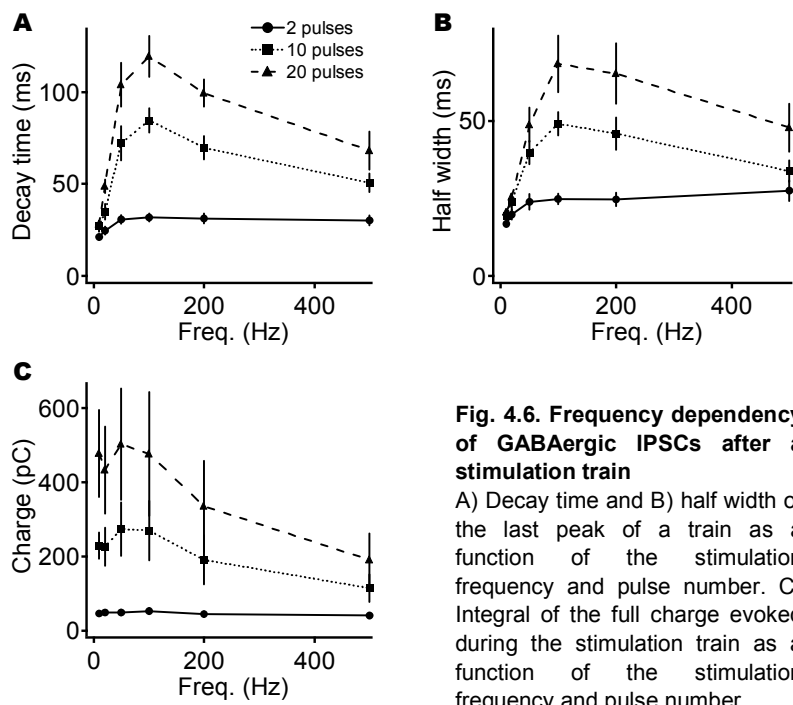


Fig. 4.5. Depression curves of GABAergic IPSCs after a stimulation train

Superimposed traces of GABAergic IPSCs after a 10-pulses stimulation at different frequencies for a given cell. Artifacts were deleted for better visualization. Grey arrows show the last stimulation artifact. Stars indicate non phasic events. B) Depression curve of evoked IPSCs after a 10-pulses train at 10, 100 and 500 Hz. C) Steady-state depression as a function of the stimulation frequency.

or 20 pulses ($n=7$). Higher values for the decay time constant were found at 100 Hz after stimulation with 10 or 20 pulses compared with those recorded at all other frequencies. Typically, with 10 pulses decays were 84.52 ± 7.1 ms whereas with 20 the values were 120.4 ± 11.6 ms. Nevertheless, long lasting decays were also found at 50 Hz and 200 Hz, being 72.05 ± 9.8 ms and 103.92 ± 12.6 ms at 50 Hz and 69.84 ± 6.8 ms and 99.44 ± 7.9 ms at 200 Hz, for the 10- and 20-pulse trains respectively. At 500 Hz these values were 50.74 ± 5.49 ms and $68.18 \pm$

10.93 ms. Long trains at low frequencies, gave decays of 27.14 ± 2.78 ms and 28.05 ± 2.78 ms at 10 Hz and 35.09 ± 4.7 ms and 48.68 ± 4.37 ms at 20 Hz, for 10 and 20 pulses trains correspondingly. In all cases, within one stimulus frequency the kinetics became slower as the number of pulses increased. The same trend was observed for the half width of the IPSCs (Fig. 4.6B). At 10 Hz the half width of the last peak of the train was 16.88 ± 1.27 ms, 19.47 ± 1.22 ms and 20.54 ± 1.15 ms for a 2-, 10- and 20-pulses train respectively. The corresponding recorded values after a 20 Hz stimulation were 19.73 ± 1.83 ms, 23.89 ± 2.97 ms and 25.47 ± 1.16 ms.



As well as for the decay time constant, with higher stimulation frequencies these values were significantly increased, being 23.89 ± 2.86 ms, $39.77 \text{ ms} \pm 4.09$ ms and 48.7 ± 5.75 ms at 50 Hz; 24.86 ± 1.99 ms, 49.03 ± 4.03 ms and 68.42 ± 9.49

at 100 Hz and 24.68 ± 2.51 , 45.89 ± 5.49 and 65.16 ± 9.99 ms after 2-, 10- and 20-pulses trains correspondingly. At 500 Hz the half width of the last IPSC peak shortened compared to the other high frequencies used, exhibiting values of 27.5 ± 3.67 ms, 33.78 ± 3.79 ms and 47.82 ± 8.04 ms.

The full charge carried by the IPSCs was evaluated after train stimulations (Fig. 4.6C). The integral of the area of the elicited currents, considered as the area between the stimulation artifact and the following 1.5 second did not differ much as a function of the frequencies evaluated but did so as function of the number of pulses tested. On average, double pulse stimulation exhibited the following values: 46.4 ± 7.2 pC at 10 Hz, 49.2 ± 8.5 pC at 20 Hz, 48.2 ± 10 pC at 50 Hz, 52.6 ± 11 pC at 100 Hz, 44.7 ± 11 pC at 200 Hz and 40.2 ± 8.5 pC at 500 Hz. Values were ~ 5 fold increased when stimulation was with trains of 10 pulses. In this case, the charge was 229.2 ± 38.8 pC at 10 Hz, 227 ± 54.2 pC at 20 Hz, 273.9 ± 74.9 pC at 50 Hz, 269.3 ± 83.1 pC at 100 Hz, 191 ± 67.9 pC at 200 Hz and 114 ± 39.2 pC at 500 Hz. Again, an increase in the charge was found when the amount of pulses was increased. Typically, with trains of 20 pulses, the charge showed values that double those found after a 10-pulses train. The average values calculated were 478 ± 120.4 pC at 10 Hz, 433.9 ± 119.3 pC at 20 Hz, 503.3 ± 152.8 pC at 50 Hz, 476.8 ± 170.3 pC at 100 Hz, 335 ± 124.7 pC at 200 Hz and 190.7 ± 74 pC at 500 Hz.

In general, high frequency trains induced a prolongation of the synaptic inhibition onto DNLL neurons, suggesting that asynchronous release might be involved. Moreover, preliminary data showed that application of 100 μ M of EGTA-AM, the ester form of EGTA, a slow calcium buffer, reduces IPSCs kinetics after high

frequency trains (data not shown), suggesting that a build up of calcium in the presynaptic terminal might play a role in the extended inhibitory signal.

4.2.5 The application of a low affinity GABA_A receptor antagonist suggest the involvement of extrasynaptic receptors in prolonging synaptic inhibition in DNLL

Since spillover currents are generated by low neurotransmitter concentrations, they would be more sensitive to a low affinity antagonist. Therefore, if PI in DNLL neurons is due to spillover of GABA, as suggested by the dependency of the IPSCs kinetics on the stimulation strength, the application of a weak antagonist should have a more prominent effect on those receptors that are located further away from the release site, for instance, extrasynaptic receptors, and leaving the phasic response mostly unchanged. Thus, the application of a low affinity antagonist would reduce the IPSCs kinetics.

To study this hypothesis, the effect of 100 μ M 1,2,5,6-Tetrahydropyridin-4-yl) methylphosphinic acid hydrate (TPMPA), a weak GABA_A receptor antagonist, was evaluated after a 60 volts stimulation train at 500 Hz (n=4). Figure 4.7A illustrates superimposed IPSCs before and after the application of the drug and its normalized traces (inset) after a 500 Hz stimulus train at 60 volts (n=4). The reduction on the last IPSC peak amplitude ranged from 8.8 % to 67.3%. On average, the reduction was 42.31 ± 12.31 % from the initial peak (Fig. 4.7B). Although the decay time constant was also reduced showing an average τ

difference of 5.10 ± 0.73 ms, with values ranging from 3.31 ms to 6.29 ms (Fig. 4.7C), these differences were not significant.

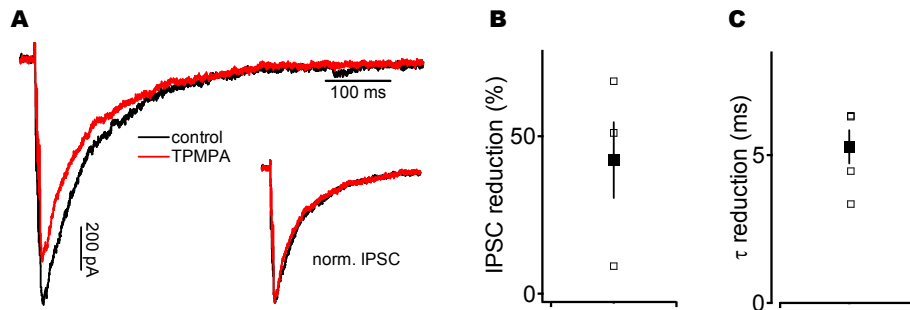


Fig. 4.7. Effect of 100 μM TPMPA on the IPSCs kinetics

A) GABAergic IPSCs recorded under control (black trace) and after 100 μM TPMPA (red trace). Inset: normalized traces. B and C) Effect of TPMPA on IPSCs peak amplitude (B) and decay time (C). C) Black square: average, open squares: single cells.

In order to achieve a larger amplitude reduction and possibly a larger and more consistent reduction in the decay time constants, 200 μM of TPMPA was applied to the bath.

Figure 4.8A illustrates the time course of the change on IPSCs amplitudes (top panel) and decay time constants (lower panel) during the wash-in of 200 μM TPMPA while stimulating the fibers with a single pulse at 60 volts. Both amplitudes and kinetics show a clear reduction. The IPSC amplitudes decreased already one minute after the drug was on the bath and it reached a plateau after 2 minutes, whereas the decrease in the decay time constant was observable after 2 minutes whereas the plateau was reached 1 minute later.

The normalized traces of evoked IPSCs after a 100 Hz stimulus train and at 60 volts under control and TPMPA conditions are depicted in Fig. 4.8B. The amplitude exhibited a reduction of ~ 83% (not shown). The decay time decreased from 50.42 ms in control to 18.36 ms during drug application.

Also TPMPA rescued the IPSCs from depression by releasing the receptors from saturation after a 100 Hz train at 60 volts as seen in Fig. 4.8C. The steady state depression was 15.97 ± 2.98 % for control and 66.07 ± 26.28 % when TPMPA was bathed (Fig. 4.8D, student t-test, $p < 0.05$, $n = 10$).

The IPSCs amplitude reduction was evaluated at 3 different stimulation strengths: 30, 60 and 90 volts (Fig. 4.8E). The reduction found for the last peak of the train at each condition was 21.16 ± 20.98 %, 38.92 ± 18.3 % and 40.65 ± 12.28 % in that order (filled circles, lower panel). In particular, the average amplitudes were 130 ± 35.6 pA and 120 ± 54.52 pA at 30 volts, 466.3 ± 113.2 pA and 245 ± 83.15 pA at 60 volts and 890 ± 225 pA and 480.3 ± 109.17 pA at 90 volts in control and TPMPA conditions respectively (top panel, student t-test, $p < 0.05$ at 90 volts, $n = 8$). On the other hand, the effective reduction on the 1st peak of the train was larger in all cases, being the values 19.9 ± 27.26 %, 69.18 ± 7.51 % and 60.16 ± 7.73 % for 30, 60 and 90 volts correspondingly (lower panel, open circles, $n = 8$, 10 and 12 respectively).

The decay time constants calculated for the last IPSC on the train were also significantly reduced at 90 volts as well as at 60 volts, exhibiting the following values: 81.71 ± 16.74 ms and 63.14 ± 13.33 ms at 60 volts and 94.79 ± 13.8 ms and 79.8 ± 9.25 ms at 90 volts in control and in TPMPA respectively (Fig. 4.8F,

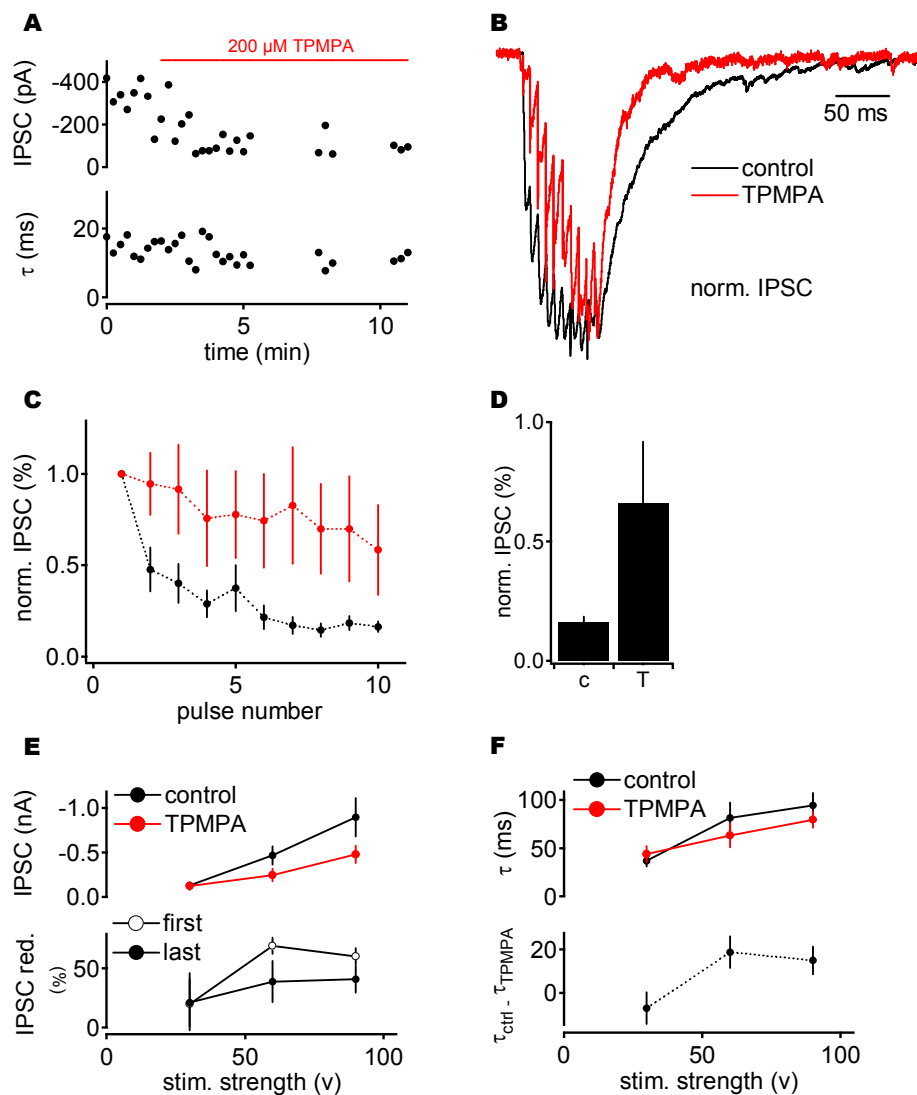


Fig. 4.8. Effect of 200 μ M TPMPA on the kinetics of the last IPSC after stimulation train.

A) Time course of the effect of 200 μ M TPMPA on the IPSC peak amplitude (top panel) and decay time (lower panel). B) Normalized IPSCs after a 10-pulses train at 100 Hz and 60 volts for a representative neuron. C) IPSCs depression curve after a 10-pulses train at 100 Hz under control (black) and TPMPA (red) conditions. D) Effect of TPMPA on the steady state depression of curves plotted on (C) for control (c) and after TPMPA (T). E) Top panel: peak amplitude of the last IPSC of a train for control (black) and after TPMPA (red) at 3 voltages tested (30, 60 and 90 V). Lower panel: percent of IPSC reduction after TPMPA for the 1st (open circles) and the last peak (filled circles) of a train at the 3 voltages tested. F) Top panel: effect of TPMPA on the decay time of the last IPSC of a train (black: control, red: after TPMPA). Lower panel: effective reduction of the decay time after TPMPA.

top panel; student t-test, $p < 0.05$, $n = 8$). The effective reduction found was ~ 18 ms at 60 volts and ~ 15 ms at 90 volts (lower panel). In contrast, at 30 volts the differences between control and TPMPA on the IPSCs kinetics were not significant. In particular, the values were 37.03 ± 6.79 ms and 43.89 ± 9.64 ms for control and drug respectively. IPSCs amplitudes at 10 Hz and 500 Hz exhibited a significant reduction when stimulated at 60 or 90 volts. In particular, at 10 Hz the reduction was found to be 42.58 ± 21.15 % and 52.21 ± 13.08 % whereas at 500 Hz these values were 41.95 ± 12.65 % and 45.09 ± 15.06 % (student t-test, $p > 0.05$). On the other hand, even though no significant changes were observed on the decay time constants, at 500 Hz time there was a reduction of ~ 5 ms when stimulation strength was 90 volts (not shown).

The effect of TPMPA on the IPSCs kinetics was also assessed after a single pulse stimulation of the fibers. In Figure 4.9A, the IPSCs before and after the wash-in of the drug for a representative cell is depicted. In this particular case, the initial amplitude was 415.5 pA whereas the amplitude after the drug took effect was 99.7 pA. The inset shows the normalized IPSCs of the same cell in which it is noticeable a reduction on the decay time constant of the evoked current after application of TPMPA. The values for the decay were 13.2 ms under control conditions and 10.6 ms after the drug application, leading to a reduction of ~ 3 ms.

The mean amplitude found after single stimulation at 60 volts was 524.35 ± 90.7 pA for control and 316.3 ± 95.32 pA under TPMPA conditions (Fig. 4.9B, student t-test $p < 0.01$). On average, the reduction of the initial amplitude after single pulse stimulation at 60 volts was 45.29 ± 11.37 %.

All cells tested exhibited this reduction in the amplitude except for one (n=9). Interestingly, only this cell showed no decrease in the decay time constant in contrast to all other 8 neurons (Fig. 4.9C). On average, the decay time was found to be 30.45 ± 2.28 ms in control condition and 25.6 ± 2.46 ms after the drug application (student t-test $p < 0.05$) and the mean reduction at this voltage was 5.02 ± 1.96 ms.

Figure 4.9D illustrates the values of IPSCs amplitudes (top panel) and decay time constants (lower panel) under control and TPMPA conditions obtained at the 3 different voltages tested (30, 60 and 90 volts). At 30 volts neither the amplitude

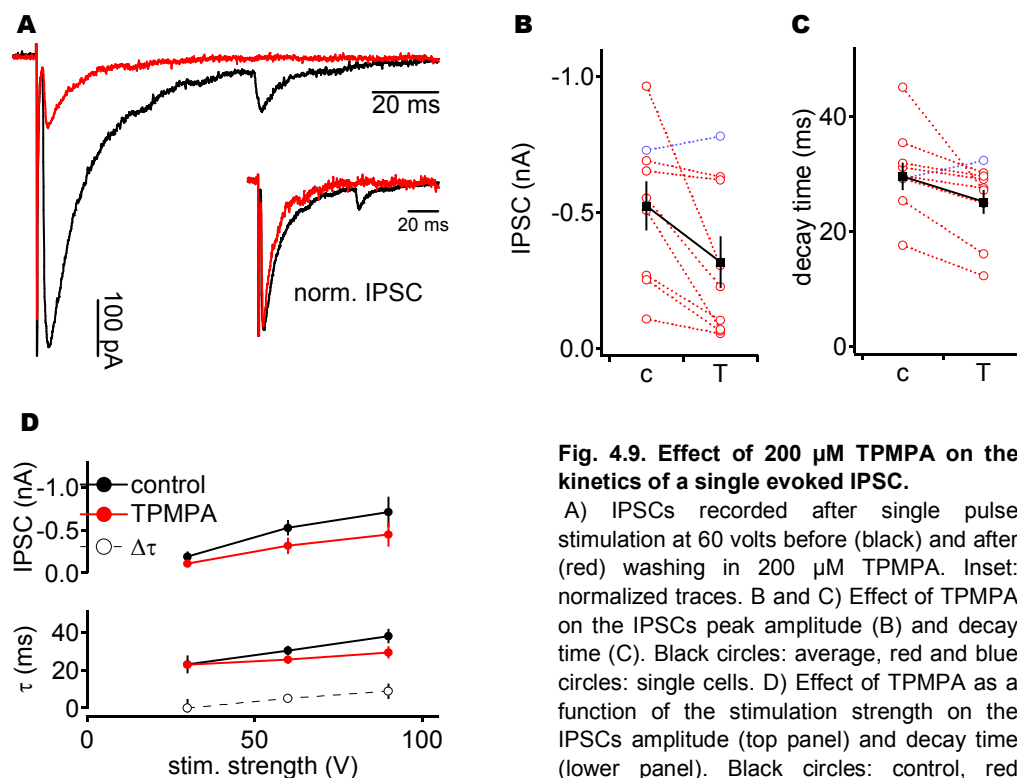


Fig. 4.9. Effect of 200 μ M TPMPA on the kinetics of a single evoked IPSC.

A) IPSCs recorded after single pulse stimulation at 60 volts before (black) and after (red) washing in 200 μ M TPMPA. Inset: normalized traces. B and C) Effect of TPMPA on the IPSCs peak amplitude (B) and decay time (C). Black circles: average, red and blue circles: single cells. D) Effect of TPMPA as a function of the stimulation strength on the IPSCs amplitude (top panel) and decay time (lower panel). Black circles: control, red circles: after TPMPA, open circles: effective reduction.

nor the decay time showed significant changes exhibiting an average peak amplitude of 187.7 ± 60.88 pA and 106.53 ± 19.35 pA and decay times of 23.11 ± 4.7 ms and 22.9 ± 1.07 ms under control and TPMPA conditions respectively. On the other hand, at 90 volts the IPSC amplitude decreased from 710.25 ± 179 pA in control to 447.7 ± 142.72 pA in TPMPA (student t-test $p < 0.05$), representing a reduction of 31.13 ± 12.98 %. Also a significant decrease in the IPSC kinetic was found at this stimulation strength, with values of 38.18 ± 3.82 ms and 29.49 ± 3.29 ms respectively (student t-test $p < 0.05$), leading to an effective reduction of 8.84 ± 4.11 ms.

Neither the amplitudes nor the decay times of the mIPSCs were changed after bath application of TPMPA (data not shown).

To confirm that the results obtained after application of TPMPA were not a merely effect of a lower occupancy of the receptors but due to the intrinsic effects of a low affinity antagonist, a high affinity GABA_A antagonist, SR95531, was used at a concentration such to induce a partial reduction on the IPSCs amplitude and its effect on the IPSCs kinetics was evaluated.

The drug was initially tested at a concentration of 200 nM, but since the recorded IPSCs were fully blocked at this concentration ($n=2$), further experiments were carried on with a concentration of 50 nM. In the example plotted in Fig. 4.10A, the evoked IPSC was reduced from 2.63 nA to 532.3 pA. The inset of this figure shows the normalized traces. In general, at this concentration only ~ 30 % of the peak amplitude was reduced ($n=3$). In addition, these data were pooled with that one obtained after application of 20 μ M of SR95531 (a concentration at which a

full blockade is reached, as shown above) when the reduction on the evoked currents was not larger than 50 % (n=5) since no significant differences were found between the two groups. On average, the amplitude reduction was 34.09 ± 16.48 % (Fig. 4.10B, n=8).

The kinetics showed no significant differences between control and drug conditions. In particular, the mean decay time constant under control condition was 16.72 ± 1.5 ms whereas after application of the antagonist this value was 19.32 ± 2.7 ms (Fig. 4.10C).

Taken together, the results described above suggest that spillover contributes to the long lasting inhibition observed.

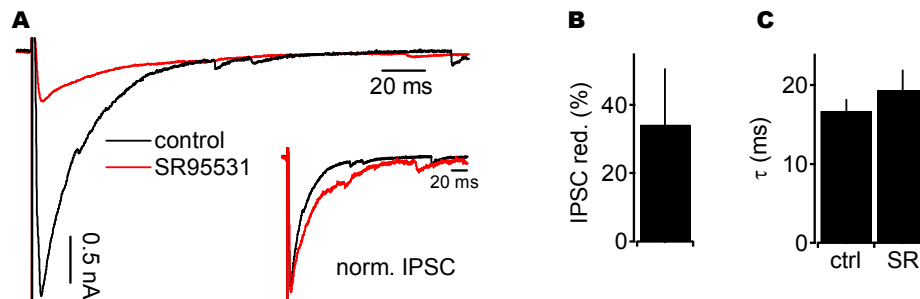


Fig. 4.10. Effect of a low concentration of a high affinity GABA_A antagonist on the IPSCs kinetics.

A) Single pulse evoked IPSCs before (black) and after (red) washing in 50 μM SR95531 for a representative neuron. Inset: normalized traces. B) Percent of reduction induced by the GABA_A receptor blocker. C) Effect of 50 μM SR95531 on IPSCs decay time.

4.2.6 Blocking GABA clearance prolonged the IPSC kinetics

To investigate the contribution of neurotransmitter transporters to GABA clearance, the effect of a selective GABA uptake blocker was tested. If transmitter

spillover contributes to the extended kinetics in DNLL neurons, then diminishing GABA clearance by blocking GAT-1, a GABA transporter, with 10 μM 1-[2-[[[(Diphenylmethylene)-imino]oxy]ethyl]-1,2,5,6-tetrahydro-3-pyridine-carboxylic-acid hydrochloride (NO711) should prolong IPSC decay.

Figure 4.11A illustrates the response to a 60 volts single pulse before and after the application of the drug for a given cell. In this particular case, the amplitude decreased from 2.47 nA in control condition to 451.16 pA after NO711 was washed in. On the other hand, the decay time constants were 16.47 ms and 22.43 ms respectively. Surprisingly, IPSCs amplitudes diminished at all voltages tested, as shown in Figure 4.11B. Average amplitudes significantly decreased from 672.1 ± 74.83 pA at 30 volts (n=2), from $1.55 \text{ nA} \pm 343.6$ pA to $442.84 \text{ pA} \pm 87.68$ pA at 60 volts (n=5) and from $2.4 \text{ nA} \pm 251.5$ pA to 839 ± 53.1 pA at 90 volts (n=3) (student t-test, $p < 0.05$). As expected, the decay time constants were increased from 14.26 ± 4.04 ms to 25.42 ± 11.07 at 30 volts, from 17.83 ± 2.84 ms to 23.86 ± 1.8 ms at 60 volts and from 22.75 ± 4.5 ms to 23.99 ± 3.18 ms at 90 volts (student t-test, $p < 0.05$ at 60 volts).

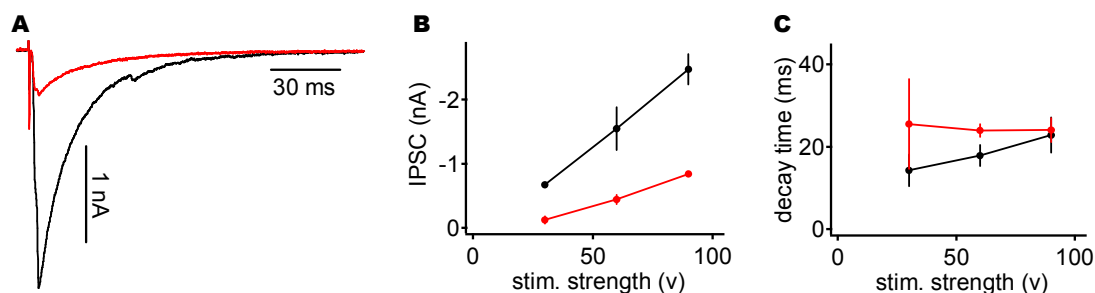


Fig. 4.11. Effect of NO711 on the IPSCs kinetics

A) Representative IPSCs traces before (black) and after (red) wash in 10 μM NO711. B and C) Effect of NO711 on IPSCs amplitude (B) and decay time (C). Black circles: control, red circles: NO711.

It could be possible that at this concentration NO711 induces receptor saturation and this could explain the observed reduction on the IPSCs amplitudes. Therefore, a lower concentration of the drug was tested. In this case, 2 μM of NNC711 (the same type of compound as NO711 but from Tocris Bioscience) was assessed.

The application of NNC711 induced to an increase of the decay time of single-pulse evoked IPSC after being bathed for 10 minutes, reaching a plateau 2.5 minutes later (Fig. 4.12A, lower panel). On the other hand, the blocker had a minimal effect on the IPSC amplitude (top panel). In the example depicted in Figure 4.12B, the IPSCs amplitude increased from 1.63 nA to 1.94 nA after application of NNC711 while stimulating the fibers with a single pulse at 60 volts. Nevertheless, the decay time constant exhibited an increase of ~ 6 ms, being in control 17.46 ms and 23.25 ms with the blocker. The inset illustrates the normalized traces for this representative cell.

In general, the amplitude of single evoked IPSCs showed no significant differences between the two conditions, being the values of the change 17.06 ± 45.3 % at 30 volts, 10.71 ± 8.67 % at 60 volts and 7.77 ± 12.5 % at 90 volts (Fig. 4.12C, top panel). In contrast, the decay time was increased by 6.76 ± 3.56 ms, 7.13 ± 1.59 ms and 7.61 ± 1.48 ms at 30, 60 and 90 volts respectively (Fig. 3.12C, lower panel, $p < 0.05$ at 30 and $p < 0.01$ at 60 and 90 volts, $n=9$).

IPSCs evoked after a 10-pulses stimulation train exhibited no significant differences on the depression curves after application of NNC711 either at 10 or 100 HZ as shown in Figure 4.12D. The achieved steady states after 60 volts

stimulation were $69.2 \pm 6.9\%$ and $71.8 \pm 6.7\%$ at 10 Hz and $26.29 \pm 5.98\%$ and $16.11 \pm 1.8\%$ at 100 Hz for control and NNC711, in that order ($n=6$ at 10 Hz, $n=7$ at 100 Hz).

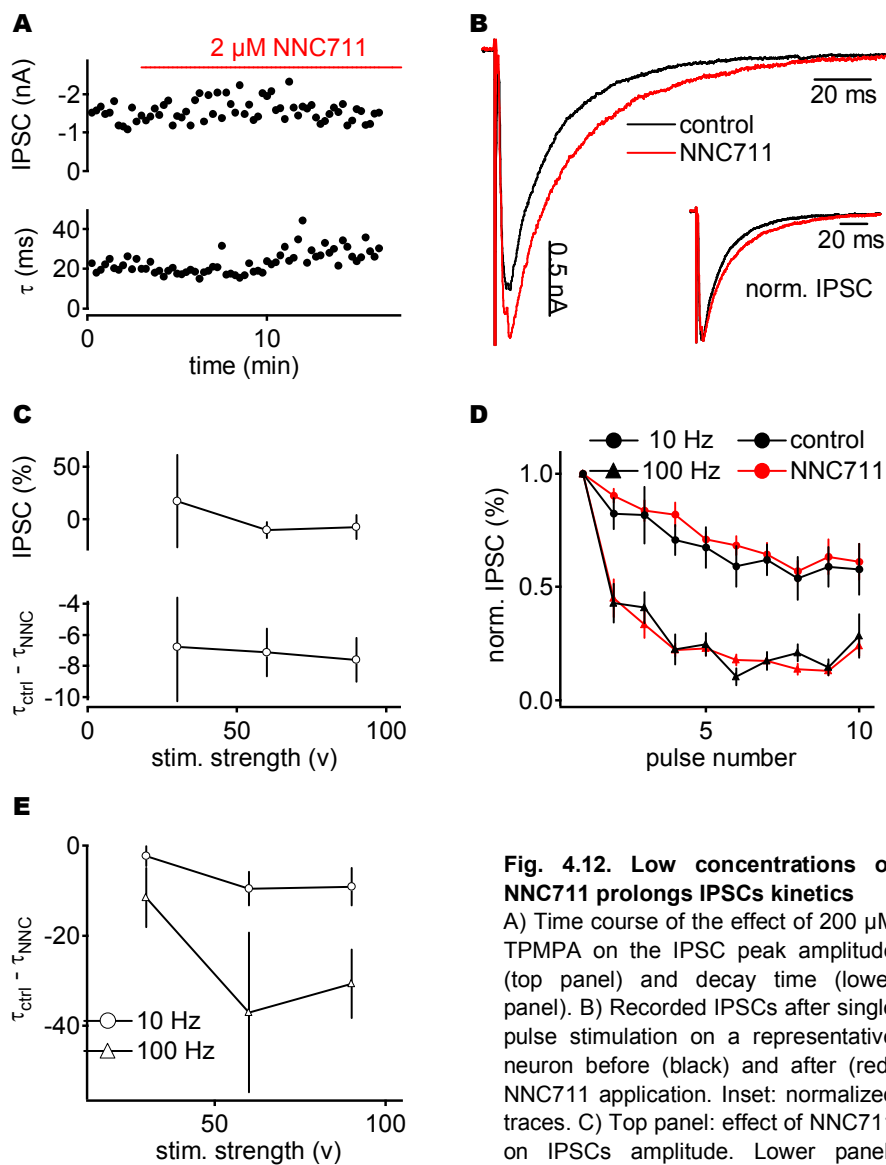


Fig. 4.12. Low concentrations of NNC711 prolongs IPSCs kinetics

A) Time course of the effect of 200 μ M TPMPA on the IPSC peak amplitude (top panel) and decay time (lower panel). B) Recorded IPSCs after single pulse stimulation on a representative neuron before (black) and after (red) NNC711 application. Inset: normalized traces. C) Top panel: effect of NNC711 on IPSCs amplitude. Lower panel: effective increase on IPSCs decay time

after application of NNC711. D) Depression curves after a 10-pulses train at 10 Hz (circles) and 100 Hz (triangles) before (black) and after (red) application of NNC711. E) Effective increase on IPSCs decay time of the last peak of a 10-pulses train at 10 Hz (circles) and 100 Hz (triangles).

Figure 4.12E shows the effective change in the decay time constants for 10 Hz and 100 Hz at the three voltages tested. At the 10 Hz the increase on τ was 2.33 ± 2.4 ms at 30 volts, 9.56 ± 4 ms at 60 volts (n=7) and 9.1 ± 4.39 ms at 90 volts (n=5). Similarly, at 100 Hz the observed increase was 11.58 ± 6.84 ms, 37.03 ± 17.88 ms (n=6) and 30.68 ± 7.7 ms (n=4) at 30, 60 and 90 volts respectively (student t-test, $p < 0.05$ at 60 and 90 volts at 10 and 100 Hz).

At 500 Hz decay time constants also exhibited a significant increase after application of NNC711. Typically, this increase was 5.39 ± 2.02 ms at 30 volts, 17.91 ± 6.11 ms (n=6) at 60 volts and 12.69 ± 4.76 (n=4) at 90 volts (student t-test, $p < 0.05$).

The sensitivity of mIPSC to transport block was also evaluated by measuring its decay time constants. No significant differences were found on the kinetics of the mIPSCs between the two conditions for the two cells tested (one after NO711 application and the other one under the effect of NNC711). On average, the decay time of the mIPSCs was 13.5 ± 0.2 ms under control conditions whereas after the drug application this value was 15.9 ± 0.5 ms (not shown).

NNC711 induced, as expected, a prolongation of IPSC decay time at high stimulus voltages, suggesting not only that GABA clearance is an important mechanism to limit long lasting IPSCs but more importantly, that synaptic crosstalk plays a substantial role in extending synaptic inhibition in the DNLL.

4.2.7 Reducing release probability decreased the IPSCs kinetics

Reducing release probability would not only reduce the number of released vesicles per site but also the number of active sites, thus spillover would also be reduced, as fewer ligand molecules are available to diffuse to extrasynaptic receptors.

This hypothesis was tested by changing the extracellular $\text{Ca}^{2+} / \text{Mg}^{2+}$ ratio to 1 mM $\text{Ca}^{2+} / 2$ mM Mg^{2+} . The lower calcium concentration induced to a decrease in the IPSCs amplitude as illustrated in Figure 4.13A. In this particular case, the amplitude of evoked IPSCs after single pulse stimulation at 60 volts was 397.81 pA in control conditions which was reduced to 315.31 pA after the calcium exchange. The decay time constant was also reduced from 25.14 ms to 14.17 ms.

In general, IPSCs evoked after one stimulation pulse were reduced from 1.18 ± 0.30 nA to 512.76 ± 69.9 pA at 60 volts and from 1.43 ± 0.22 nA to 977.14 ± 80.9 pA at 90 volts (Fig. 4.13B, student t-test, $p < 0.05$ at 60 and 90 volts ($n=6$)). On the other hand, at 30 volts ($n=5$) the average amplitudes were 183.22 ± 45.82 pA in control and 228.79 ± 86.04 pA at low calcium.

On average, the decay time constants were 13.78 ± 1.25 ms and 13.85 ± 1.75 ms at 30 volts, 17.27 ± 1.58 ms and 15.1 ± 1.42 ms at 60 volts and 19.34 ± 1.42 ms and 16.75 ± 1.18 ms at 90 volts, in control and low calcium concentration respectively (Fig. 4.13C; student t-test, $p < 0.05$ for 60 and 90 volts).

Figure 4.13D shows the percentage of reduction on the decay time constants after stimulation trains of different frequencies at 90 volts. These values were

19.02 ± 4.9 % at 10 Hz, 27.69 ± 5.96 % at 100 Hz and 21.55 ± 3.72 % at 500 Hz (n=6, student t-test, p<0.05). Even though differences in the kinetics were found at all three frequencies evaluated, no changes on the amplitudes of the last IPSC evoked from a train were observed.

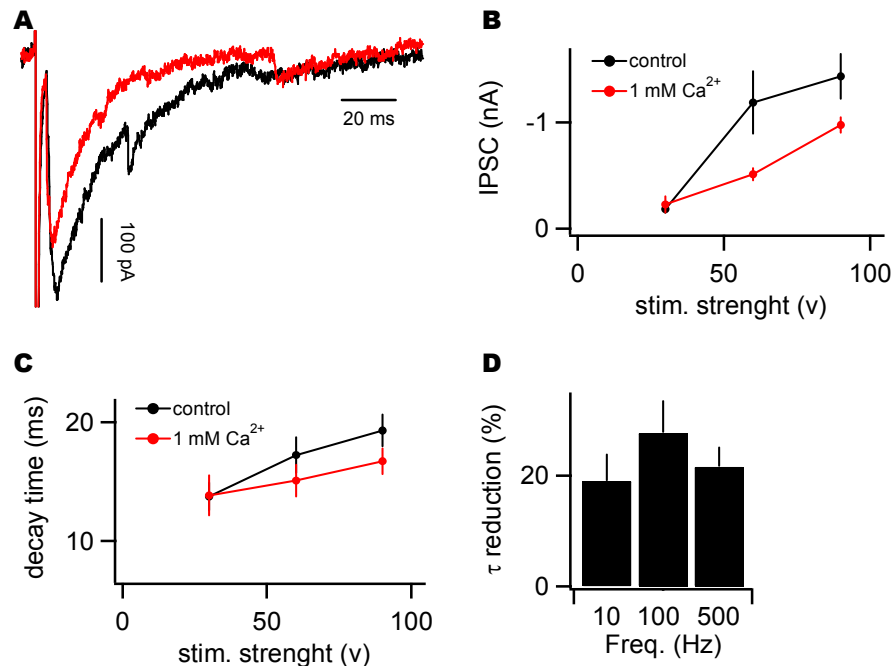


Fig. 4.13. Reducing the extracellular calcium reduces the IPSCs kinetics.

A) Recorded IPSCs after a single pulse stimulation before (black) and after (red) application of 1 mM Calcium. B) Effect of reducing extracellular calcium concentration on IPSCs amplitude. C) Effect on IPSCs decay time after reducing calcium in the bath. Black circles: control, red circles: in 1 mM calcium (B and C). D) Effective reduction on the IPSCs decay time as a function of the stimulation frequency of a train.

At lower stimulation intensities no significant differences between control and treatment were found on the kinetics or on the IPSCs amplitudes.

In order to induce a larger reduction on IPSCs amplitudes, a lower calcium concentration was tested.

Lowering the calcium concentration to 0.5 mM led to a reduction in the IPSCs amplitude and decay time constants of evoked IPSCs. Figure 4.14A shows the time course of the effect produced by the calcium concentration exchange on the amplitude and kinetics of an IPSC after single pulse stimulation at 60 volts. The amplitude started to decrease ~ 3 minutes after starting the solution exchange and it reached a plateau after ~ 8 minutes. Figure 4.14B illustrates the normalized traces of the recorded IPSCs under control and low calcium concentrations when stimulated with a single pulse at 60 volts, exhibiting decay time constants of 13.06 ms and 7.92 ms in each condition respectively.

On average, IPSC amplitudes decreased from 1.26 ± 0.24 nA to 193.02 ± 24.8 pA ($n=7$) when the calcium in the bath was reduced (Fig. 3.14C). The percentage of amplitude reduction was found to be 63.69 ± 11.84 % at 30 volts ($n=5$), 81.85 ± 3.36 % at 60 volts ($n=7$) and 83.05 ± 2.77 % at 90 volts ($n=7$) (Fig. 4.14D, top panel; student t-test, $p<0.05$ at 60 and 90 volts). Similarly, the amount of reduction on the IPSCs decay time was found to be 2.74 ± 2.38 ms, 4.12 ± 1.55 ms and 5.92 ± 1.12 ms at 30, 60 and 90 volts correspondingly (Fig. 4.14D, lower panel; student t-test, $p<0.05$).

Lowering the concentration of the extracellular calcium had an important effect on the depression curves, as observed in Figure 4.14E. The steady state reached at 60 volts after a 10-pulse stimulation at 100 Hz was 9.45 ± 3.19 % in control and 77.36 ± 16.65 % at 0.5 mM calcium ($n=5$). A similar observation was made at the other voltages tested as well as for the 10 Hz trains. In particular at this frequency, at 60 volts the depression at the steady state was 59.96 ± 15 % and

93.84 ± 17.68 % with 10 Hz trains in control and at lower calcium concentration (n=4).

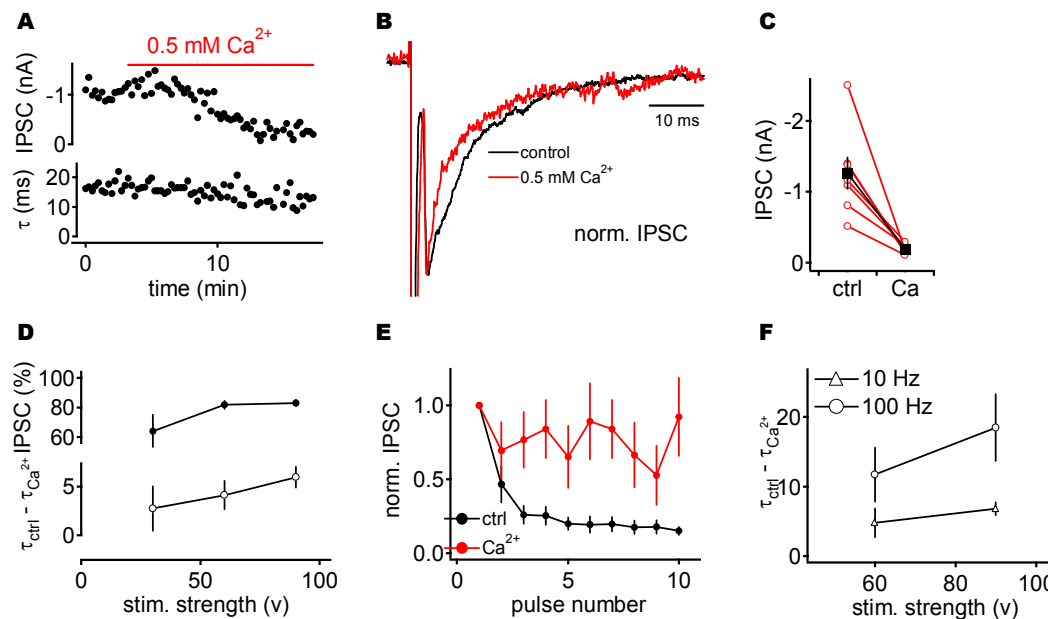


Fig. 4.14. The reduction on extracellular calcium reduces GABA spillover

A) Time course of the IPSC amplitude (top panel) and decay time (lower panel) reduction after application of 0.5 mM calcium. B) Normalized IPSC traces before (black) and after (red) wash in of 0.5 mM calcium. C) Average (black squares) and single cells (red open circles) IPSC reduction after application of a low calcium extracellular solution. D) Effective IPSC amplitude (top panel) and decay time (lower panel) reduction in 0.5 mM calcium over the voltage range tested. E) Depression curves for 10-pulses trains at 100 Hz before (black circles) and after (red circles) application of 0.5 mM calcium. F) Effective IPSC reduction after a 10-pulses train at 10 Hz (triangles) and 100 Hz (circles) at 3 voltages tested after reducing calcium concentration in the medium.

In Fig. 4.14F the differences in decay time constants before and after the concentration exchange for two voltages tested (60 and 90 volts) at 10 and 100 Hz is illustrated. On average, at 10 Hz the kinetics were 4.79 ± 2.17 ms and 6.82 ± 1.06 ms faster when stimulating at 60 and 90 volts respectively. In the same way, at 100 Hz these values were 11.7 ± 4.02 ms and 18.43 ms. At 500 Hz the

decay time constants were decreased 14.82 ± 4.69 ms at 60 volts and 12.08 ± 3.35 ms at 90 volts.

The blockade of specific calcium channels would also lead to a reduction in release probability. This was assessed by applying $10 \mu\text{M}$ of cadmium which blocks high voltage activated (HVA) channels. In the example represented in Figure 4.15A, the amplitude started to diminish after ~ 5 minutes of bath application of CdCl_2 , reaching a plateau ~ 2 minutes later. In this particular case, IPSCs decreased from 470.31 pA to 113.14 pA (Fig. 4.15 B). On the other hand, the kinetics started experiencing a slight decrease from 19.41 to 17.67 ms (Fig. 4.15B) after ~ 7 minutes (Fig. 4.15A). In general, the average IPSCs' amplitude recorded under the same conditions (1 pulse at 60 volts) was reduced from 1.32 ± 0.37 nA to 308 ± 66.04 pA (Fig. 4.15C, student t-test, $p < 0.05$, $n = 11$) and decay time constants was decreased from 23.87 ± 2.18 ms to 21.81 ± 1.84 ms (Fig. 4.15D, student t-test, $p < 0.05$, $n = 11$). At 30 volts both amplitude and decay time constant showed a significant reduction, from 1.22 ± 0.58 nA to 250 ± 58.15 pA and from 21.86 ± 2.76 ms to 19.37 ± 2.32 ms (student t-test, $p < 0.05$, $n = 7$). Also the decrease in the amplitude was significant when stimulating at 90 volts (2.04 ± 0.48 nA in control and 706.9 ± 144.4 pA in cadmium, student t-test $p < 0.05$, $n = 8$), but decay time constants showed no significant differences (27.92 ± 3.09 ms in control and 25.63 ± 2.05 ms ms).

Moreover, the depression curves for a 10-pulse stimulation train were also affected by the application of the salt, showing a smaller depression of IPSCs amplitude over the train than under control conditions. Figure 4.15E shows the average depression curves for a train of 100 Hz at 60 volts. On average, the

steady state was 15.62 ± 4.83 % in control, in contrast to 41.98 ± 8.98 % when cadmium was bath applied (Fig. 4.15 F, student t-test, $p < 0.05$, $n = 7$).

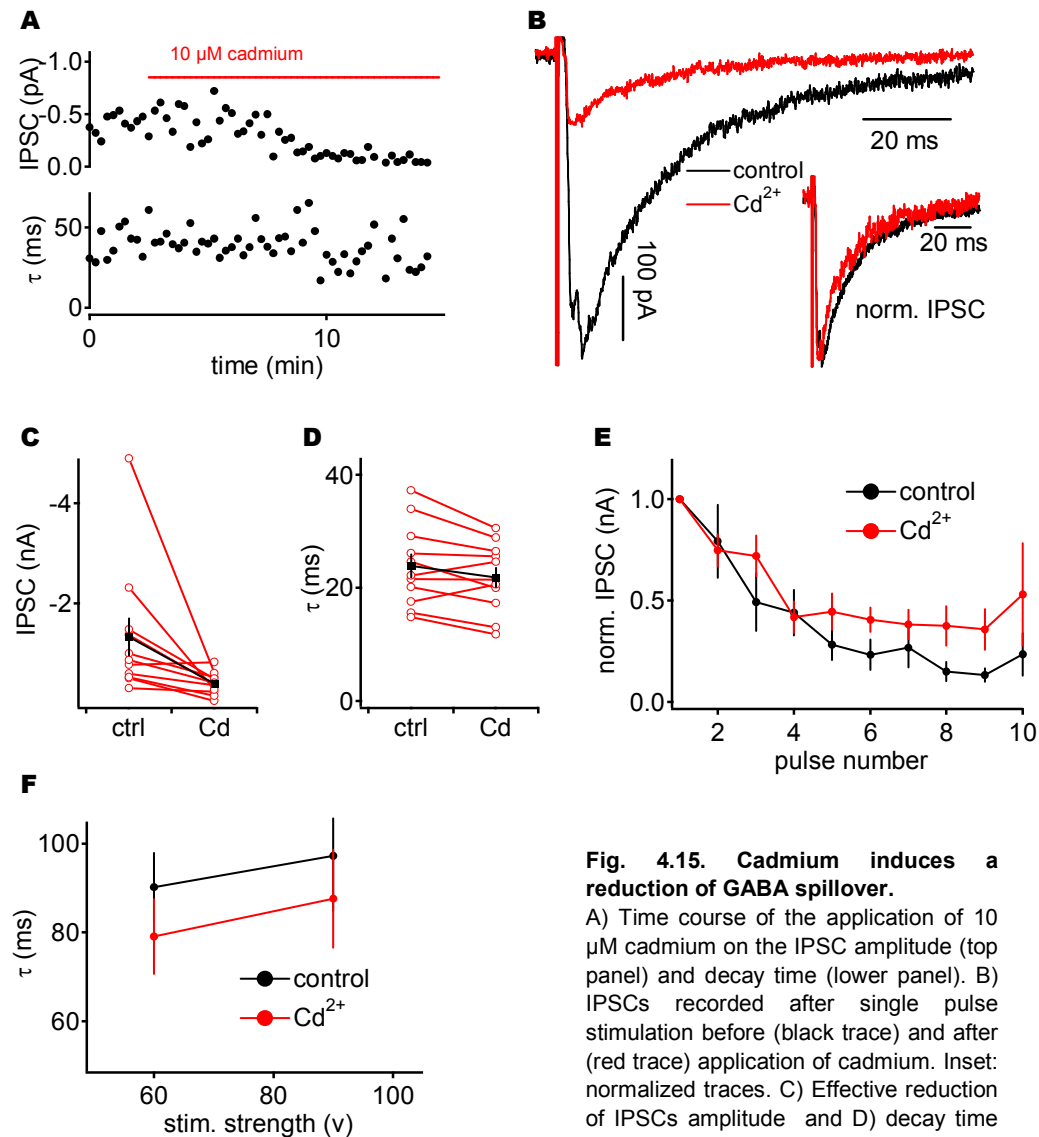


Fig. 4.15. Cadmium induces a reduction of GABA spillover.

A) Time course of the application of 10 μ M cadmium on the IPSC amplitude (top panel) and decay time (lower panel). B) IPSCs recorded after single pulse stimulation before (black trace) and after (red trace) application of cadmium. Inset: normalized traces. C) Effective reduction of IPSCs amplitude and D) decay time after application of cadmium. Black

squares: average, red open circles: single cells. E) Depression curves after a 10-pulses train at 100 Hz before (black circles) and after (red circles) cadmium was applied to the bath. F) Decay time of the last IPSC of a train at 100 Hz at different voltages tested before (black circles) and after (red circles) application of cadmium.

The application of cadmium led to a significant diminution on the amplitude of the last peak of a stimulation train at 60 volts in all frequencies tested, being at 10 Hz 61.4 ± 7.99 % (n=7), at 100 Hz 33.34 ± 15.97 % (n=7) and at 500 Hz 48.69 ± 14.12 % (data not shown, student t-test, $p < 0.05$, n=5). On the other hand, the decay time constants showed significant differences only at 100 Hz, with values of 90.2 ± 7.92 ms and 79.04 ± 8.6 ms at 60 (n=7) and 97.23 ± 12.65 ms and 87.6 ± 11.2 ms at 90 volts (n=5) in control and with cadmium, respectively (Fig. 4.15F, student t-test, $p < 0.05$).

Low calcium concentrations reduced IPSCs amplitudes and decays by reducing the amount of active sites and/or the number of vesicles being released. Therefore, the total amount of GABA in the synaptic cleft was decreased, inducing a reduction of crosstalk between synapses.

The different results observed after application of cadmium in comparison to those obtained after lowering calcium concentration might suggest the involvement of not only HVA types but also intermediate and low voltage activated channels.

4.2.8 Glycinergic inputs onto DNLL neurons

DNLL neurons receive not only GABA- but also glycinergic inputs. The characteristics of glycinergic IPSC kinetics and its contribution to persistent inhibition were assessed.

Figure 4.16A illustrates the time course of the change in amplitude (top panel) and decay time constant (lower panel) for a representative cell after single-pulse

evoked IPSCs during the bath application of SR95531 to an extracellular solution lacking strychnine. The mixed GABA- and glycinergic IPSCs had an initial amplitude of ~ 1 nA which started to decrease 1 minute after the GABA_A receptor blocker was applied and reached a plateau 1 minute later. The decay time constant was initially ~ 24 ms, reaching a plateau 2 minutes after washing in SR95531 with a value of ~ 8 ms. The representative recorded traces from before and after the application of the drug are shown in Figure 4.16B for this given cell. The decay time differences in these two conditions are better visualized in the normalized traces that are depicted as an inset in this figure. On average, at 60 volts the reduction on the IPSCs amplitude was 68.44 ± 8.34 % and 58.22 ± 8.41 % on the IPSCs kinetics (Fig. 4.16C, n=8).

Even though the average IPSC amplitudes is not a realistic measure as values such as the amplitudes have a large variability from cell to cell, the averages depicted in Fig. 4.16D are to illustrate the independence of glycinergic IPSC with the stimulation strength, in contrast to GABAergic IPSCs. The mixed current exhibited a slight voltage dependent increase on the IPSCs amplitude as shown in Figure 4.16D, whereas the currents recorded after SR95531 took effect were typically independent (n=8). Similarly, the decay time constant also showed a positive voltage dependence while the pure glycinergic IPSCs had no dependency on the stimulation strength (Fig. 4.16E, n=8).

Figure 4.16F illustrates an example of a typical sustained type cell showing a bipolar distribution of its processes and a fuseiform soma, recovered after recording mixed and isolated glycinergic IPSCs.

The voltage dependence response of isolated glycinergic IPSCs was tested by stimulating the fibers with a 2 pulse protocol at a frequency of 10 Hz and different voltage strengths ranging from 0 to 100 in 5 volts steps (Fig 4.17A). The IPSCs amplitudes showed a step like increase with the increase on the stimulation

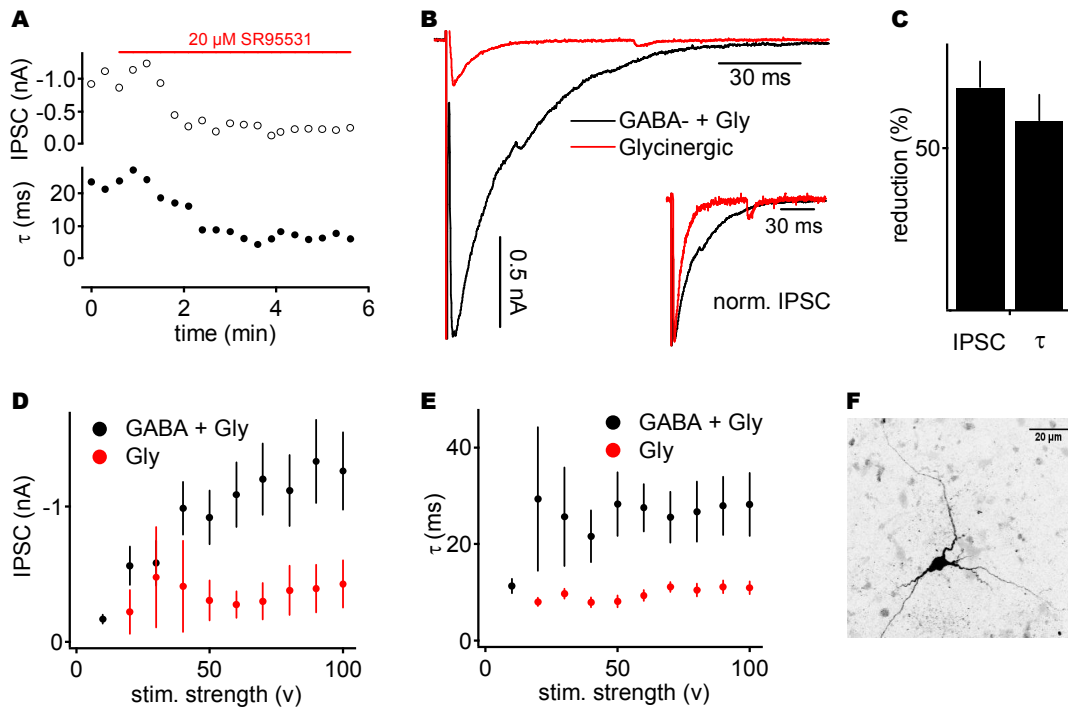


Fig. 4.16. DNLL neurons receive both GABA- and glycinergic inputs.

A) Time course of the change in mixed Glycinergic and GABAergic IPSCs amplitude (top panel) and decay time (lower panel) before and during application of SR95531. B) Recorded mixed (black trace) and pure glycinergic (red trace) IPSCs for a representative neuron. Inset: normalized traces. C) Effective reduction on IPSCs amplitude and decay time after application of SR95531. D) Voltage dependency of the peak amplitude of mixed (black circles) and pure glycinergic (red circles) IPSCs. E) Mixed (black circles) and glycinergic (red circles) IPSCs decay time as a function of the stimulus strength. F) Maximal projection of a representative DNLL neuron after recording glycinergic IPSCs with Alexa 468 containing internal solution.

strength as shown for the representative neuron depicted in the inset of Figure 4.17A. Each step observed in the recorded IPSCs represents the recruitment of an additional connected fiber. In particular, the threshold for this cell was found to be at 20 volts with an IPSC amplitude of ~ 30 pA while its maximum was found to

be ~ 1 nA. On average, the threshold was ~ 30 volts; however, the threshold for two cells was ~ 60 volts.

In general, glycinergic IPSCs exhibited a step like increase of the amplitude, with some cells exhibiting only 1 or 2 steps. In this representative example, 2 steps were apparent (inset). When 500 nM strychnine was applied to the bath the IPSCs were blocked by 82.98 ± 5.34 % (n=3, Fig. 4.17B).

The paired pulse ratio showed no obvious facilitation or depression of the 2nd peak at 10 Hz and at the different voltages tested, showing values of 1.1 ± 0.3 , 0.8 ± 0.2 and 0.9 ± 0.2 at 10 Hz at threshold, 60 and 100 volts, respectively (p<0.05).

The decay time constants of the first (filled circles) and second (open circles) of evoked glycinergic IPSCs showed no voltage dependency, exhibiting values ~ 10 ms (n=6 for 2-pulses trains and n=7 for single pulses, Fig. 4.17C, lower panel) in both cases. The same results can be observed when stimulating at 20 and 100 Hz or with a single pulse (data not shown). The rise time (top panel) was also independent of the stimulation strength with values of ~ 0.6 ms.

As for the decay time constant, the half width did not showed a dependency on the stimulation strength at none of the frequencies tested (10, 20 and 100 Hz) as well as for the single pulse stimulation. As an example, Figure 4.17D illustrates the half width as a function of the stimulation intensity for a paired pulse at 10 Hz. Typically, the half width was ~ 10 ms through all the voltage range evaluated.

In Figure 4.17E the voltage dependency of the charge after a single pulse stimulation (open circles) and a 2-pulses train at 10 Hz IPSCs is depicted. For single pulses the charge seemed to remain unchanged along the voltage range tested. In particular, at 60 volts the charge was 6.5 ± 1.7 pC. Paired pulses stimulations at 10, 20 and 100 Hz at 60 volts led to an apparent step-like increase over the stimulation strength evaluated with values of 14.8 ± 7.92 pC, 12.61 ± 8.21 pC and 8.93 ± 6.8 pC respectively.

Figure 4.17F shows a representative example of the glycinergic mIPSCs recorded for the same cell depicted in A. The frequency distribution of the amplitudes for the miniature IPSC (mIPSC) for the cell in Figure 4.17A is depicted in Figure 4.17F (lower panel). For the illustrated example 100 mIPSCs were found with amplitude values ranging from 8.3 pA to 115.9 pA and a median value for the amplitudes distribution of 24.10 pA (gaussian fit in Fig. 4.17F, lower panel in red). On average, from a total of 147 mIPSCs out of 5 neurons, amplitudes ranged from 10.3 pA to 237 pA and with a average decay time of 10.96 ± 0.84 ms and a rise time was ~ 1 ms (Fig. 4.17F, top panel inset).

Figure 4.18A illustrates superimposed traces of evoked glycinergic IPSCs after stimulating the fibers of the Commissure at 60 volts with a 10-pulses train at different frequencies for a given cell. The top panel shows the superimposed traces of the evoked response after a 10 Hz train; the middle panel exhibits the response to 100 Hz whereas in the lower panel the response to 500 Hz stimulation is depicted.

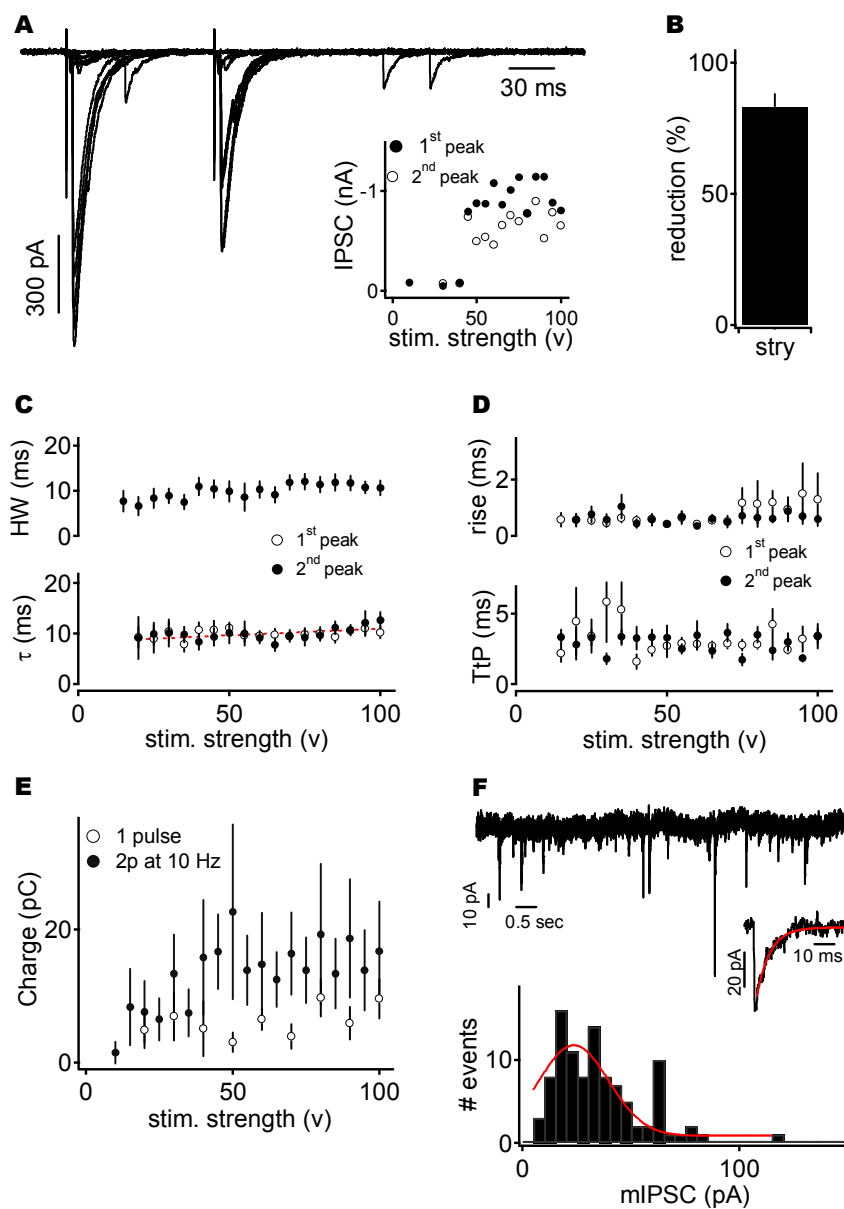


Fig. 4.17. Dependency of glycinergic IPSCs kinetics on stimulation strength.

A) Glycinergic IPSCs recording after 10 Hz paired stimulation at different stimulus strength for a given cell. Inset: IPSC amplitudes as a function of the stimulus strength. Black circles: 1st peak, open circles: 2nd peak. B) IPSC amplitude reduction after application of 500 nM Strychnine. C) Voltage dependency of Glycinergic IPSCs half width (top panel) and decay time (lower panel). D) Rise time (top panel) and time to peak (lower panel) as a function of the stimulus intensity. E) Voltage dependency of the integral of the charge after single (open circle) and 2-pulses stimulation at 10 Hz (black circles). F) Top panel mIPSCs recorded from the same cell depicted in A. Inset: representative glycinergic mIPSC. The red line represents the exponential fit. Lower panel, mIPSC amplitude distribution for the cell depicted in A.

The depression curves constructed for 10 pulses trains show no main differences between the amplitudes of evoked IPSCs at 10 (Fig. 4.18B, n=6) or 20 Hz (not shown). The calculated steady state reached (average for the last 3 peaks) in both cases did not differ from the initial amplitude. On the other hand, at higher frequencies a more significant depression was achieved earlier in the train.

Typically, at 100 Hz the reduction found at the steady state was ~ 40 %, reaching 50 % at the 5th pulse. Trains of 200 Hz led to a steady state reduction of ~ 18 %, being ~ 60 % of the depression found at the 2nd peak. The steady state of depression is depicted in Figure 4.18C, summarizing the results described above.

The decay time constants as a function of the stimulation frequency are depicted in Figure 4.18D. In general, when the trains consisted of 2 pulses, the decay times were ~ 10 ms at all frequencies tested (the minimal value was found to be 10.89 ± 0.85 ms at 10 Hz, whereas the maximal was 14.14 ± 0.81 ms at 200 Hz).

In contrast, when the stimulation trains consisted of larger amount of pulses (10 or 20) differences were observed between low (10 and 20 Hz) and high frequencies (100, 200 and 500 Hz), even though these differences were only significant when comparing 10 and 20 Hz with 100 Hz (student t-test, $p < 0.05$; the lack of significance at 200 and 500 Hz might be due to the lesser amount of data points (n=4)).

Within one frequency, the differences in decay time constants resulting after stimulation trains of 2, 10 or 20 pulses were not significant except at 100 Hz (student t-test, $p < 0.05$). In particular at this frequency, the decay time constants

were 13.34 ± 0.8 ms, 25.3 ± 4.2 and 42.7 ± 5.87 ms after a 2-, 10- and 20-pulse train respectively.

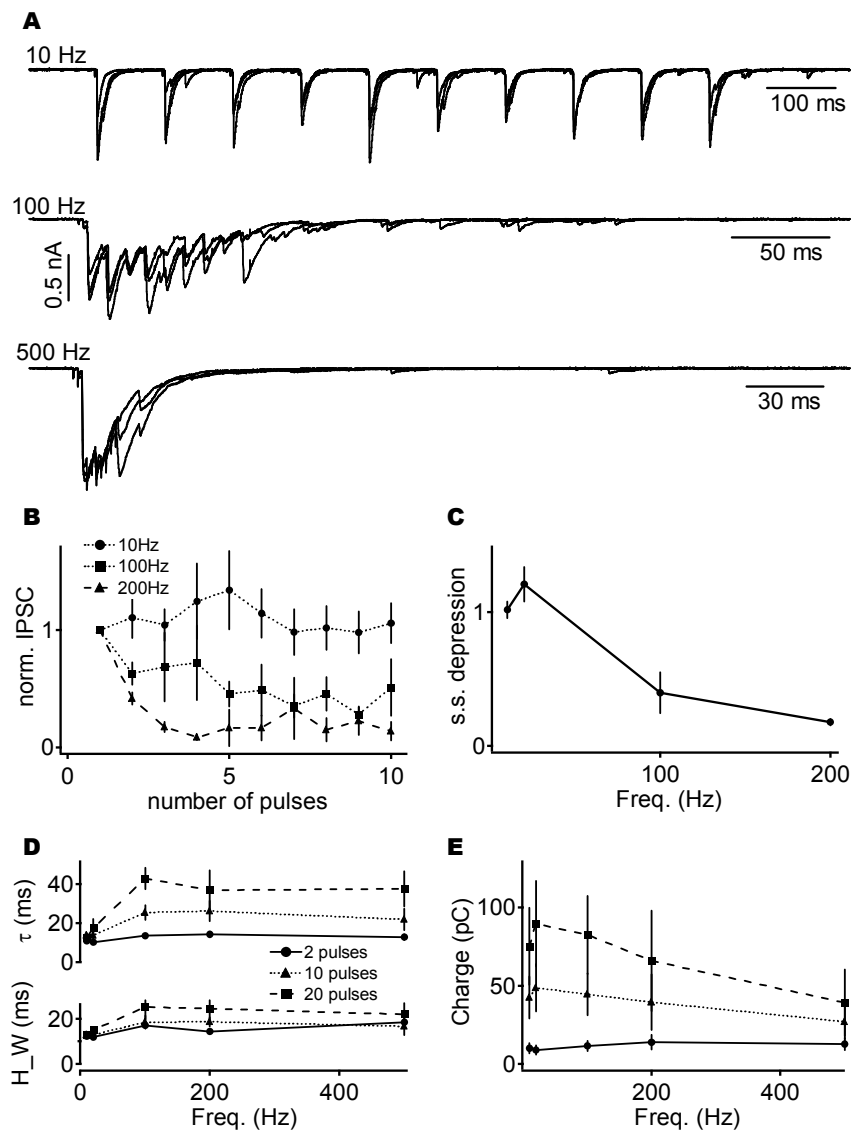


Fig. 4.18: Frequency dependency of glycinergic IPSCs

A) Overlay of 3 traces of recorded IPSCs after 10-pulses trains at 10 Hz (top panel), 100 Hz (middle panel) and 500 Hz (lower panel) at 60 volts. B) Depression curve for 3 different frequencies tested. C) Steady state depression for all the frequencies tested. D) Frequency dependency of IPSCs decay time (top panel) and half width (lower panel) for stimulation trains of different number of pulses. E) Frequency dependency of the full charge after trains of different number of pulses.

The half width of the last pulse of the train showed the same trend as for the decay time constants (Fig. 4.18E). In particular, the calculated half width showed no differences when stimulating at low frequencies with different number of pulses, presenting values ~ 12 and 13 ms at 10 Hz and ~ 12 and 15 ms at 20 Hz for 2 and 20 pulses respectively. At higher frequencies (100 , 200 and 500 Hz), differences were found when stimulating with 20 pulses, even though these values did not differ between the frequencies. Typically, with 2 pulses the elicited half width was 17.1 ± 1.93 ms at 100 Hz, 14.42 ± 0.63 ms at 200 Hz and 18.6 ± 3.7 at 500 Hz. On the other hand, these values were ~ 18 ms after 10 pulses and ~ 25 ms after 20 pulses for the 3 frequencies.

On average, the effective charge carried by the evoked IPSCs was evaluated after the different stimulation trains tested (Fig. 4.18F). The integral of the area of the elicited currents showed no main differences as a function of the frequencies evaluated but as function of the number of pulses tested as seen for the GABAergic IPSCs. For instance, with trains of 2 pulses, the charge ranged between 9.95 ± 3.86 pC at 10 Hz and 14.06 ± 5.47 pC at 200 Hz whereas after a 10 -pulse train values were ~ 2 to 4 times larger, ranging between 27.11 ± 11.6 pC at 500 Hz and 48.8 ± 15.63 pC at 20 Hz. The effective charge found after 20 -pulses trains doubled that one found at 10 pulses, with values ranging from 39.19 ± 21.76 pC at 500 Hz to 89.5 ± 28.02 pC at 20 Hz.

5. DISCUSSION

In this study, the cellular mechanisms underlying persistent inhibition in the DNLL were studied. As a first approach, the presence of long lasting spike suppression in the Mongolian gerbil was assessed *in vivo*. This long lasting inhibition was then further investigated in acute brain slices both in current and voltage clamp conditions, determining its GABAergic nature and identifying the contralateral nucleus as its source. Moreover, spillover onto extrasynaptic receptors, and possibly onto neighboring synapses as well, was found to explain, at least partially, the extended time course of the IPSCs. Additionally, asynchronous release of the neurotransmitter also played a substantial role in prolonging synaptic inhibition in response to high frequency stimulation trains. Thus, pre- and post-synaptic factors were found to be the mechanisms contributing to PI in the DNLL of the Mongolian gerbil.

5.1 Persistent inhibition in the DNLL of the Mongolian gerbil

In general, the DNLL neurons present a BF distribution representing the entire audiogram of an animal as it has been shown for different species (Markovitz and Pollak, 1993; Covey, 1993; Burger and Pollak, 2001; Bajo et al., 1998; Aitkin et al., 1970). This work focused on high frequency EI neurons as these cues are processed through the IID circuitry. The DNLL possesses a considerable number of EI cells in other animals (rats: Bajo et al., 1998; Kelly et al., 1998; and bats: Covey, 1993; Markovitz and Pollak, 1994), therefore it is not surprising that more

than half of the encountered neurons were excited by the contralateral side and inhibited by ipsilateral stimulation.

The results obtained in the present study not only confirm the existence of PI in the Mongolian gerbil as it was described by other members of the lab (T. Zahn (PhD thesis dissertation, 2003) and M. Pecka (Diploma thesis dissertation, 2004)), but also offer a more accurate value of the effective duration of spike suppression. Zahn and Pecka conducted experiments in which they assessed the presence of PI by using a 3-pulses protocol with a first binaural tone favoring the inhibitory ear and two trailing sounds delivered only to the excitatory ear, as first described by Yang and Pollak (1994). With this approach, the elicited spike suppression was quantified as the minimal interpulse separation between the first and the subsequent stimulation pulse at which DNLL neurons were able to fire action potentials. Since the interpulse intervals were predefined, their measure of PI might have not been an accurate estimate.

In contrast, and similarly to what other authors have done (Yang and Pollak, 1994b), the stimulation protocol used in this study allowed a more precise measure of the duration of PI as the excitatory sound stimulation was presented for a prolonged duration (200 ms) and therefore the effective suppression evoked by stimulation of the inhibitory ear could be calculated.

The results presented here show that binaural sounds with negative IIDs suppress action potential firing induced by contralateral excitation in the DNLL of the gerbil. As in bats (Pollak, 1997; Yang and Pollak, 1994; Burger and Pollak,

2001), this suppression can last for several tens of milliseconds beyond the end of the inhibitory signal (Pecka et al., 2007).

Moreover, the finding that PI is also present in the Mongolian Gerbil contributes the hypothesis that it might be a common feature in mammals.

5.2 DNLL cell types and their physiological properties *in vitro*

A multiplicity of neuronal types has been recognized in DNLL based on their somatic and dendritic morphology in the rat (Bajo et al. 1993, Wu and Kelly, 1995; Tanaka et al., 1985), mouse (Iwahori, 1986), cat (Adams, 1979; Shneiderman et al., 1988) and big brown bat (Covey, 1993) using retrograde labeling, Golgi immunogold or Nissl staining techniques. Accordingly, the data presented here revealed that at least two types of morphologically distinct neurons, elongated and rounded, can be found in DNLL of the gerbil. These cells also exhibited different physiological characteristics, with essential differences not only in their firing properties but also in their response to hyperpolarizing current injections. This is in line with what it has being described for DNLL cells recorded *in vivo*, where sustained and onset neurons were identified on the basis of their firing properties in response to auditory stimulation (Siveke et al., 2006; Bajo et al., 1998; Yang et al., 1996; Kelly et al., 1998).

However, Wu and Kelly (1995a,b) argue that despite the morphological diversity, biocytin-labeled neurons were indistinguishable based on their physiological properties using intracellular recordings. Nevertheless, some degree of divergence in the firing properties can be observed among the cells they

recorded from, with some neurons exhibiting only few spikes (in some cases only one or two spikes) in response to suprathreshold current injections and some others showing a “chopper-like” response. On the other hand, Wu and colleagues (Wu and Kelly, 1995a,b; Fu et al., 1997) found that many DNLL neurons often exhibit a slowly developing sag in the membrane potential during hyperpolarizing current injections as shown here for neurons with sustained firing. Furthermore, they suggest that this hyperpolarizing sag corresponds to an inward rectifying current, I_H , which might enhance the extent of excitation on these cells, thereby making the DNLL a powerful inhibitory source (Fu et al., 1997). Presumably, most neurons that Wu and colleagues recorded from were sustained type cells. Together, this might suggest that these two physiological characteristics (persistent firing and I_H currents) might be intrinsic properties of a specific type of DNLL neuron (sustained type).

On the other hand, the results presented here together with other morphological and *in vivo* evidences (Iwahori, 1986; Adams, 1979; Shneiderman et al., 1988; Siveke et al., 2006; Bajo et al., 1998; Yang et al., 1996) suggest that at least two types of neurons with particular cellular characteristics are present in the DNLL. The discrepancy between Wu’s work and the data presented here may arise from the different species used. Wu and colleagues studied the physiological properties of DNLL neurons in rats which are specialized for high frequency hearing and thus, may present anatomical and/or physiological differences. It should also be considered that both studies were conducted with different technical approaches as they performed intracellular recordings with sharp electrodes whereas this work has been done in whole cell patch-clamp

configuration and that the recording solutions used were also different. It can also not be ruled out that differences might be due to a differential sampling of neurons within the DNLL.

More work would be necessary to clearly determine the relationship between the morphology and the *in vitro* physiology of the different cell types among the DNLL and to determine their specific contribution to the sound localization pathways.

5.3 The source of PI in the DNLL

Several anatomical studies have revealed that most DNLL neurons are GABAergic (Adams and Mugnaini, 1984; Glendenning and Baker, 1988; Shneiderman et al., 1988; Vater et al., 1992). Most of these GABAergic neurons give rise to a prominent projection to the contralateral DNLL through the commissure of Probst (Adams, 1979; Bajo et al., 1993; Ito et al., 1989; Kudo, 1981; Merchán et al., 1994; Oliver and Shneiderman, 1989; Iwahori, 1986).

The contribution of this GABAergic inhibition to binaural processing has been examined both in the DNLL (Yang and Pollak, 1994; Burger and Pollak, 2001) and the IC (Li and Kelly, 1992; Kidd and Kelly, 1996; Moore et al., 1998; Bauer et al., 2000). Moreover, it has been shown that local injections of kynurenic acid, an excitatory amino-acid antagonist, into the DNLL partially releases the neurons in the opposite DNLL from binaural suppression (Kidd and Kelly, 1996), suggesting that the source of inhibition is the contralateral nucleus. In addition, Pollak and colleagues found that the inhibition evoked by ipsilateral stimulation is potent and prevents DNLL neurons from responding to contralateral signals for a period of

time following the inhibitory signal (Yang and Pollak, 1994, 1998; Burger and Pollak, 2001). Moreover, the reversible inactivation of the DNLL revealed the role of its GABAergic inhibition in processing multiple sounds in the IC of the bats (Burger and Pollak, 2001), suggesting that the DNLL might contribute to the precedence effect.

Kelly and Kidd (2000) proposed that PI might be mediated by persistently active neurons in the opposite DNLL. However, no extended firing among DNLL neurons has been observed (Covey, 1993; Bajo et al., 1998; Siveke et al., 2006). The results presented here show that the stimulation of the commissure of Probst is sufficient to suppress spike firing, discarding the hypothesis centered on persistently active LSO neurons that, in turn, induce DNLL cells to exert an extended inhibition to its contralateral counterpart (Kelly and Kidd, 2000).

Moreover, the kinetics of the evoked GABAergic IPSCs described here resembled the time course of PI observed during auditory stimulation. The stimulation of the Commissure of Probst generated IPSCs with slow kinetics that could explain the observations found *in vivo*, implying that intrinsic properties are underlying this inhibition. Similarly, Chen et al. (1999) described comparable values for the half duration of the inhibitory postsynaptic potentials (IPSPs) evoked after commissural stimulation in rats of 10-16 days of age which were dependent on the stimulation strength as well as on the number of pulses.

So far, the results presented here imply that PI might be generated by intrinsic properties at the level of synaptic information transfer of principal neurons in the DNLL rather than by network properties. Moreover, the evidence provided

suggests that the inhibition is mediated by GABA_A receptors and that the source of this inhibition is the contralateral nucleus.

5.4 Spillover prolongs synaptic inhibition in the DNLL

GABA escaping the synaptic cleft can reach receptors located extrasynaptically or on neighboring synaptic terminals (Semyanov et al., 2003; Isaacson et al., 1993; Mitchell and Silver, 2000; Scanziani, 2000). The amount of GABA that a given receptor will be exposed to will depend on its location relative to the release site, diffusional barriers and the proximity of the neurotransmitter transporters (Overstreet et al., 2000; Barbour and Häusser, 1997; Kullman, 2000). The release of multiple vesicles at one single release site or the evoked release from several terminals promotes GABA spillover and activation of both synaptic and extrasynaptic receptors. Thus, during intense synaptic activity the extracellular concentration of GABA rises, increasing spillover. This phenomenon has been described in the hippocampus (Isaacson et al., 1993; Scanziani, 2000; Overstreet and Westbrook, 2003; Alle and Geiger, 2007; Semyanov et al., 2003) and cerebellum (Rossi and Hamann, 1998; Mitchell and Silver, 2000b).

Moreover, some morphological characteristics of the synapses are thought to favor neurotransmitter diffusion to neighboring synapses, as for example closely packed synapses. In the mossy fiber-unipolar brush cell synapse, several release sites are clustered within $< 1\mu\text{M}$ and they exhibit long lasting synaptic currents (Rossi et al. 1995, Slater et al. 1997). These anatomical properties facilitate the

activation of receptors that are not located at the postsynaptic density, hence reducing synaptic independence.

There is evidence suggesting that DNLL morphology might be a good substrate for transmitter spillover, as several authors have described that GABAergic synapses are densely distributed on both the soma and dendrites of DNLL neurons (Iwahori, 1986; Adams and Mugnaini, 1984; Oliver and Shneiderman, 1989). In addition to this morphological aspect of the DNLL, the physiological data described in here support the hypothesis that transmitter spillover might be occurring and, thus, prolonging synaptic inhibition.

The dependency of the decay time constants of the evoked IPSCs on the stimulation strength suggest not only that more fibers might be recruited at higher intensities, but also that the released neurotransmitter might spill out from the synaptic cleft and activate receptors in neighboring synapses. The linearity of the amplitude increase as a function of the stimulus intensity is in line with this hypothesis. Even though at higher stimulation strength more fibers might be recruited, no shift in the IPSC latencies was observed and therefore, the recruitment of out of phase inputs cannot explain the slower kinetics.

Furthermore, the kinetics of the evoked GABAergic currents in the DNLL was not only extended with the strength of the stimulation after single pulse and trains, but they also exhibited frequency dependence. Although this observation could also imply the involvement of an asynchronous release component (explained later), this is in agreement with what it has been described in other synapses in which spillover is present. Mitchel and Silver (2000a) found that the degree of glutamate

spillover onto inhibitory synaptic terminals in the cerebellum was dependent on the frequency and duration of stimulation of the mossy fibers. This is expectable as more GABA is released during intense activity and therefore, more neurotransmitter would spill out and reach the extrasynaptic space and possibly neighboring synapses as well. Similar observations have been made in pyramidal neurons of the CA3 region in the hippocampus where glutamate spillover can be induced by brief tetanic stimulation of the mossy fiber input (Scanziani, 2000; Vogt and Nicoll, 1999).

Although transmitter spillover seems to contribute to the extended inhibition in the DNLL, we cannot rule out the possibility that calcium in the presynaptic terminal would build up after high frequency trains. Therefore, asynchronous release of GABA might also be contributing to extending the inhibition in the DNLL under conditions of intense synaptic activity. Even though asynchronous release seems to occur in this preparation after brief tetanic stimulation, it is unlikely that asynchronous release could contribute to the extended decay time constants of single evoked IPSCs since the delayed release of vesicles requires residual calcium accumulation that could only be reached after a minimum of 10 stimulation pulses (Lu and Trussell, 2000; Jensen et al., 2000). The contribution of this release modality will be discussed below.

Spillover currents are generated by low concentrations of neurotransmitter, therefore this component of the synaptic currents is more sensitive to low affinity antagonists (Diamond, 2001; Carter and Regehr, 2000; Overstreet and Westbrook, 2003; Szapiro and Barbour, 2007). It has been shown that the application of TPMPA, a low affinity GABA_A competitor (Jones et al., 2001;

Barberis et al., 2005; Szabadics et al., 2007), decreases the time constants of the IPSCs suggesting that receptors located further away from the release site might be affected in a more prominent manner than those sitting directly at the postsynaptic site (Szabadics et al., 2007). In agreement with the literature, the results described here indicate that after application of TPMPA, the GABAergic IPSCs had faster kinetics than under control conditions. Moreover, the application of a lower concentration of TPMPA (100 μ M) induced almost the same reduction on the kinetics of the IPSCs whereas the amplitudes were less reduced compared to higher concentrations of TPMPA. Since there is a concentration gradient of GABA, (higher at the release site and lower at extrasynaptic areas), TPMPA would have a larger effect further away from the active synapse, indicating that the neurotransmitter spillover might be one of the possible mechanisms extending synaptic inhibition in the DNLL. In contrast, the application of a full antagonist of GABA_A (SR95531) at a concentration that induced only a partial block of the evoked currents elicited no dramatic change in the kinetics of the IPSCs. Together, these data suggest that the prolongation of synaptic inhibition in the DNLL is, at least partially, induced by low concentrations of GABA that spills out of the synaptic cleft.

Previous studies have shown that lowering release probability reduces the level of interaction of transmitter released from neighboring release sites and that this can accelerate the decay of synaptic currents at GABAergic (Roepstorff and Lambert, 1994; Overstreet and Westbrook, 2003) and glutamatergic (Trussell et al., 1993; Otis and Trussell, 1996; Silver et al., 1996; Diamond and Jahr, 1995; Isaacson and Walmsley, 1995; DiGregorio et al., 2002) synapses.

Reducing release probability by lowering the external calcium concentration to 0.5 mM prevented the prolongation of synaptic inhibition in DNLL neurons, suggesting that pooling of transmitter released from multiple sites was required to reach sufficient concentrations for receptor activation (Arnth-Jensen et al., 2002; Overstreet and Westbrook, 2003).

Furthermore, when the extracellular concentration of calcium was 1 mM the kinetics of the IPSCs resembled the one observed at 0.5 mM, whereas the amplitudes were reduced to a lesser extent. The reduction in vesicle release reduced the overall concentration of GABA in the synaptic cleft and, therefore, diminished the receptor activation, with a larger effect observed at the extrasynaptic sites due to the neurotransmitter concentration gradient. These results indicate that the reduction on release probability induced a reduction of synaptic crosstalk.

Most of the presynaptic entry of calcium that triggers neurotransmitter release is thought to occur through high voltage-activated (HVA) channels (Llinás, 1982). These HVA channels exhibit a high sensitivity to block by Cd^{2+} (Randall and Tsien, 1995). Accordingly, the bath application of cadmium induced a reduction of the IPSCs decay, even though it was to a lesser extent than when reducing the calcium concentration extracellularly. This could suggest that other channel types might also be involved in transmitter release in the DNLL. It has been shown that in the giant mossy fiber synapse in the CA3 region of the hippocampus the R-type calcium channel ($\text{Ca}_v 2.3$) is excluded from the active zones but present outside them. This type of channel is less effective in releasing neurotransmitter than the N- and P/Q-types (HVA channels), but is effective in generating effects

that are dependent on the total calcium influx (Dietrich et al., 2003). Whether types other than the HVA receptors are also involved in the release machinery in the DNLL remains unknown and should be investigated by application of specific channel blockers.

Transmitter uptake by transporters is one of the limiting factors for synaptic spillover. In general, a fast clearance of the neurotransmitter from the synaptic cleft promotes synapse specificity by limiting spillover between release sites. One plausible explanation for crosstalk between neighboring synapses is saturation of the buffering capacity of the neurotransmitter uptakers in order to accumulate GABA extrasynaptically (Scanziani, 2000). Therefore, enhancing spillover by blocking the uptake would slow down the kinetics of synaptic currents (Hartzell et al., 1975). In general, as a result of inhibiting transmitter uptake, the role for transmitter clearance in preventing crosstalk can be unmasked (Isaacson et al., 1993; Overstreet and Westbrook, 2003; Alle and Geiger, 2007; Mitchell and Silver, 2000; Szapiro and Barbour, 2007).

Interestingly, in the DNLL spillover could be observed even without inhibiting GABA clearance. In the DNLL, the saturation of the transporters was evident even with no uptake blockers in the bath. This suggests two possibilities: the transporters might be present in low concentrations and/or GABA is released in large quantities after high activity levels.

Blocking GAT-1 activity by application of NNC711 resulted in the prolongation of synaptic inhibition whereas the decay time of the mIPSCs, which reflects the spontaneous release of a single vesicle at one release site, was unchanged. This

indicates that transporters do not influence synaptic responses at individual release sites (Isaacson et al., 1993; Overstreet and Westbrook, 2003). Furthermore, the sensitivity to transport block seems to require that multiple sites are releasing GABA simultaneously.

In the DNLL high frequency stimulation of the Commissure of Probst seemed not to have induced receptor desensitization, as it is often observed when large amounts of neurotransmitter are being released (Pugh and Raman, 2005; Bianchi and Macdonald, 2002), even after transport block. This observation could suggest that the GABA_A receptors present in these neurons not only have a high affinity for the transmitter, as they can be activated by low concentrations, but also that specific subunits of these receptors might be present which desensitize at a slow rate. However, further experiments designed to block receptor desensitization should be carried out to confirm this hypothesis.

A variety of GABA_A receptors are thought to be activated by ambient GABA in different neuronal populations (Nusser and Mody, 2002; Overstreet and Westbrook, 2001; Stell and Mody, 2002). The detection of these low GABA concentrations in the extracellular space that persist in the presence of GABA uptake might involve high affinity receptors that are not sensitive to desensitization (Rossi and Hamann, 1998). The entering of GABA_A receptors into a desensitization state is an important feature for shaping the time course of the inhibition (Jones and Westbrook, 1995; Haas and Macdonald, 1999).

As suggested above, it could be proposed that low concentrations of GABA are acting on high affinity receptors in DNLL principal neurons. Nevertheless, it is

noticeable the effect of the low affinity antagonist (TPMPA) in reducing the IPSCs decay. Thus, it can not be ruled out that large amounts of transmitter are being released, regardless of the affinity of the GABA_A receptors.

Together with the receptors affinity for the neurotransmitter and the extent of their desensitization (Stell and Mody, 2002; Mtchedlishvili and Kapur, 2006), their different location in relation to the release site is an important feature that differentiates receptors mediating phasic and tonic activation. Some extrasynaptic GABAergic receptors, with high affinity for GABA, are also characterized by slow desensitization (Banks and Pearce, 2000). It has been shown that the α_6 and δ subunits confer on cerebellar granule cells an extraordinarily high affinity for GABA and a robustness against desensitization (Rossi and Hamann, 1998; Saxena and Macdonald, 1996). Moreover, the presence of the δ subunit results in the expression of the receptor in the extrasynaptic or presynaptic membrane (Nusser et al., 1998; Wei et al., 2003). The expression profile of GABA_A receptor subunits in the DNLL is not yet known and, therefore, we cannot speculate as to whether the presence of a certain receptor subtype might be responsible for the sensitivity to GABA. For instance, the receptor localization and clustering as well as specific properties of the transmitter transporters might also contribute to the generation of spillover and the detection of low concentrations of GABA.

Further studies focusing on establishing the precise identity and localization of these molecules in DNLL sustained-type neurons will help to understand the mechanisms responsible for mediating spillover currents in this nucleus.

5.5 Asynchronous release in DNLL principal neurons contributes to PI at high frequency activity levels

The entry of Ca^{2+} into the presynaptic terminal triggers and modulates neurotransmitter release. The buildup of Ca^{2+} that may occur during high frequency activity can generate the asynchronous release of the transmitter (Barret and Stevens, 1972; Goda and Stevens, 1994; Lu and Trussell, 2000). This type of release has been described both in glutamatergic (Goda and Stevens, 1994; Atluri and Regehr, 1998; Diamond and Jahr, 1995; Otsu et al., 2004) and GABAergic (Lu and Trussell, 2000; Hefft and Jonas, 2005) synapses. In the auditory system, asynchronous release has been described in the nucleus magnocellularis of the chick (Lu and Trussell, 2000), where asynchronous release is involved in high frequency synaptic transmission.

In the DNLL, the contribution of asynchronous release to the prolongation of synaptic inhibition was observed after stimulation of the Commissure of Probst with high frequency trains. This release component, measured as the decay time of the evoked IPSCs, was dependent on the number of pulses composing the train. It has been shown that the delayed release of vesicles requires the accumulation of residual calcium in the presynaptic terminal and that this accumulation can be reached after a minimum of 10 pulses (Lu and Trussell, 2000; Jensen et al., 2000). The reduction in the extracellular calcium concentration induced not only a robust depression on the IPSCs amplitudes but also a significant reduction on the decay time of the last IPSC evoked after a stimulus train. These results suggest that asynchronous release contributes to the overall decay of synaptic inhibition in the DNLL.

Moreover, the depression of synchronous release after high frequency stimulation was coupled to the appearance of asynchronous release, as suggested by the increase on the decay time of the last IPSC of a train and the lack of change of the integral of the overall charge. This coupling between depression of synchronous release and generation of asynchronous release has been observed in other synapses (del Castillo and Katz, 1954; Lu and Trussell, 2000; Otsu et al., 2004).

The coupling between synaptic vesicles and calcium channels determines the extent of synchrony of transmitter release. A measure of how tight the calcium sensor and the calcium source are coupled can be achieved by using calcium chelators (Hefft and Jonas, 2005; Adler et al., 1991). Preliminary experiments showed that bath application of EGTA-AM, a low calcium buffer, prevented asynchronous release of GABA in the DNLL. This suggests that a long lasting presynaptic calcium transient may drive the non-phasic release in these neurons, thus the coupling between the calcium sensor and its source might not be tight. In other words, sensor and source might be located further away from each other.

The degree of asynchronous release may be limited by the decay of the calcium transient in the presynaptic terminal. A slow calcium decay would imply the presence a buffer with a high affinity for calcium which is less efficient in facilitating release and therefore, permitting the delayed release of the transmitter (Goda and Stevens, 1994).

Asynchronous release in *sustained* neurons in the DNLL may be the result of the interplay of different mechanisms. In general, the proximity of the vesicles to the

calcium source together with the affinity of the calcium sensor may play a key role for releasing neurotransmitter in a non-phasic fashion (Südhof, 2002; Hui et al., 2005). Candidate molecules for the calcium sensor that could generate asynchronous release are high affinity synaptotagmins, such as synaptotagmin 5, 6, 7, 9 and 10 (Südhof, 2002; Hui et al., 2005) that could sense low calcium concentrations such as those that can trigger delayed release.

It has been shown that the calcium sensors for synchronous and asynchronous release operate in an independent manner (Lu and Trussell, 2000; Otsu et al., 2004; Sun et al., 2007). Synaptotagmin 1, present in both excitatory and inhibitory cortical neurons can trigger synchronous release independently of asynchronous release (Maximov and Südhof, 2005; Nishiki and Augustine, 2004). Moreover, a recent study on the Calyx of Held synapse by Südhof and collaborators (Sun et al., 2007) demonstrated that synchronous and asynchronous release act on the same vesicle pools but through different pathways involving different types of Synaptotagmins. Nevertheless, the molecular identity of the calcium sensors in the DNLL is yet to be investigated.

5.6 Glycinergic inputs onto DNLL neurons

Several anatomical and physiological studies have shown that DNLL neurons also receive glycinergic inputs from the ipsilateral LSO (Glendenning et al., 1992; Yang and Pollak, 1994; Shneiderman et al., 1999). Moreover, it has been reported that not all DNLL cells are equally innervated by the glycinergic projection of the ipsilateral LSO (Shneiderman et al., 1999). This may explain

why in this study only few glycinergic input fibers were recruited during stimulation. The results described here imply that at least a subset of DNLL neurons receive both GABAergic and glycinergic inputs. Whether all cells within the nucleus co-express both types of receptors remains unknown.

Interestingly, in the DNLL of the gerbil glycinergic IPSCs exhibit faster kinetics than GABAergic currents. This is in agreement with previous studies, where they showed *in vivo* that glycinergic inhibition in the DNLL has shorter latency and shorter duration than that elicited by the GABAergic inputs (Yang and Pollak, 1994a; Yang and Pollak, 1994b; Wu and Kelly, 1995).

As has already been suggested by Pollak and his colleagues, glycinergic input seems not to play a major role in PI as it does not contribute significantly to the extended synaptic inhibition (Yang and Pollak, 1994a). The results presented here where GABAergic and glycinergic IPSCs were recorded simultaneously confirmed that the contribution of the latter to the overall kinetics is minimal with respect to PI.

6. CONCLUSIONS

The mechanisms that produce precedence are thought to be responsible for enhancing the ability to localize sounds in echoic environments. Previous studies on PE have been mainly focused on physiological mechanisms in the IC of rabbits and cats (Yin, 1994; Fitzpatrick et al., 1995; Litovski and Delgutte, 2002; Tollin et al., 2004). Moreover, Pollak and colleagues suggested that the circuitry linking the DNLL with the IC in bats is important for processing signals which generate IIDs that change over time, as those that can be generated by multiple sources that emanate from different locations (Pollak et al., 2002; Burger et al., 2001; Yang et al., 1994; Yang et al., 1998). They proposed that during the period of PI in the DNLL, EI cells in the IC may be temporarily released from inhibition, allowing these cells to respond to trailing sounds. However, the mechanisms generating PI in DNLL neurons remained unclear until now.

The work presented here provides strong evidence for the role of the DNLL in echo suppression. These results indicate that PI is due to intrinsic characteristics of DNLL neurons and explores the mechanisms underlying it.

Summarizing, the three main findings of this work are:

1. *in vivo* data provides evidences of PI in the gerbil, suggesting that this might be a common feature in mammals.
2. *in vitro* data unveils the cellular nature of PI, discarding hypotheses that suggest a network based long lasting inhibition.

3. Moreover, *in vitro* data provides information about the mechanisms underlying PI, suggesting that pre- and postsynaptic cellular properties are involved in the prolongation of synaptic inhibition in the DNLL.

Synaptic transmission relies on the interplay of many tightly regulated processes that together determine the timing, magnitude and kinetics of the postsynaptic responses. Thus, spillover of neurotransmitter could reduce synaptic transmission reliability by reducing synaptic independence. However, the effect of spillover does not seem to be disadvantageous at all synapses. Spillover has been proven to be important for amplification, increasing the postsynaptic response in the avian endbulb of Held (Trussell et al., 1993) and the cerebellar mossy fiber-granule cell synapse (DiGregorio et al., 2002).

In the DNLL, spillover and asynchronous release of GABA are important to prolong synaptic inhibition. Both cellular mechanisms have proven to occur at physiological temperature *in vitro*, suggesting that these pre- and post-synaptic mechanisms for generating long lasting inhibition may also occur in the brain *in vivo*. Moreover, spillover seems to be of extreme relevance for activating distant or extrasynaptic receptors hence, extending the transmission of information between neurons without an extra cost to the release machinery.

It has been shown that the innervation of the DNLL to the IC has a significant role in binaural processing since it creates new properties in EI neurons in the IC that are not present in the LSO or the DNLL. One of these properties is the change in the responsiveness of IC neurons to binaural stimuli. This appears to be an

important mechanism to enhance the ability of an animal to localize a sound source in an echoic environment (Yang and Pollak, 1994).

GABA spillover in the DNLL, together with asynchronous release, may ensure the faithful localization of a sound source in a reverberant environment by, on one hand, prolonging the inhibition at a level of a single cell and, on the other hand, regulating the number of neurons that will remain inhibited. The signal dispersion provided by GABA spillover releases more IC neurons from inhibition and therefore, makes it able to respond to sounds coming from different areas in space.

7. REFERENCES

- Adams JC (1979) Ascending projections to the inferior colliculus. *J Comp Neurol* 183: 519-538.
- Adams JC, Mugnaini E (1984) Dorsal nucleus of the lateral lemniscus: a nucleus of GABAergic projection neurons. *Brain Res Bull* 13: 585-590.
- Adler EM, Augustine GJ, Duffy SN, Charlton MP (1991) Alien intracellular calcium chelators attenuate neurotransmitter release at the squid giant synapse. *J Neurosci* 11: 1496-1507.
- Aitkin LM, Anderson DJ, Brugge JF (1970) Tonotopic organization and discharge characteristics of single neurons in nuclei of the lateral lemniscus of the cat. *J Neurophysiol* 33: 421-440.
- Alle H, Geiger JR (2007) GABAergic spill-over transmission onto hippocampal mossy fiber boutons. *J Neurosci* 27: 942-950.
- Allen GI, Eccles J, Nicoll RA, Oshima T, Rubia FJ (1977) The ionic mechanisms concerned in generating the i.p.s.ps of hippocampal pyramidal cells. *Proc R Soc Lond B Biol Sci* 198: 363-384.
- Atluri PP, Regehr WG (1998) Delayed release of neurotransmitter from cerebellar granule cells. *J Neurosci* 18: 8214-8227.
- Awatramani GB, Price GD, Trussell LO (2005) Modulation of transmitter release by presynaptic resting potential and background calcium levels. *Neuron* 48: 109-121.
- Bajo VM, Merchán MA, López DE, Rouiller EM (1993) Neuronal morphology and efferent projections of the dorsal nucleus of the lateral lemniscus in the rat. *J Comp Neurol* 334: 241-262.
- Bajo VM, Villa AE, de Ribaupierre F, Rouiller EM (1999) Discharge properties of single neurons in the dorsal nucleus of the lateral lemniscus of the rat. *Brain Res Bull* 47: 595-610.
- Banks MI, Pearce RA (2000) Kinetic differences between synaptic and extrasynaptic GABA(A) receptors in CA1 pyramidal cells. *J Neurosci* 20: 937-948.
- Barbour B, Keller BU, Llano I, Marty A (1994) Prolonged presence of glutamate during excitatory synaptic transmission to cerebellar Purkinje cells. *Neuron* 12: 1331-1343.
- Barbour B, Hausser M (1997) Intersynaptic diffusion of neurotransmitter. *Trends Neurosci* 20: 377-384.

-
- Barnard EA, Skolnick P, Olsen RW, Mohler H, Sieghart W, Biggio G, Braestrup C, Bateson AN, Langer SZ (1998) International Union of Pharmacology. XV. Subtypes of gamma-aminobutyric acidA receptors: classification on the basis of subunit structure and receptor function. *Pharmacol Rev* 50: 291-313.
- Barrett EF, Stevens CF (1972) The kinetics of transmitter release at the frog neuromuscular junction. *J Physiol* 227: 691-708.
- Bauer EE, Klug A, Pollak GD (2000) Features of contralaterally evoked inhibition in the inferior colliculus. *Hear Res* 141: 80-96.
- Brand A, Behrend O, Marquardt T, McAlpine D, Grothe B (2002) Precise inhibition is essential for microsecond interaural time difference coding. *Nature* 417: 543-547.
- Bianchi MT, Macdonald RL (2002) Slow phases of GABA(A) receptor desensitization: structural determinants and possible relevance for synaptic function. *J Physiol* 544: 3-18.
- Blauert J (1997) Spatial hearing with multiple sound sources and in enclosed spaces. In: *Spatial hearing: the psychophysics of human sound localization* (revised edition) pp. 201–287. Cambridge, MA: MIT
- Boudreau JC, Tsuchitani C (1968) Binaural interaction in the cat superior olive S segment. *J Neurophysiol* 31: 442-454.
- Brugge JF, Anderson DJ, Aitkin LM (1970) Responses of neurons in the dorsal nucleus of the lateral lemniscus of cat to binaural tonal stimulation. *J Neurophysiol* 33: 441-458.
- Brunso-Bechtold JK, Thompson GC, Masterton RB (1981) HRP study of the organization of auditory afferents ascending to central nucleus of inferior colliculus in cat. *J Comp Neurol* 197: 705-722.
- Burger RM, Pollak GD (2001) Reversible inactivation of the dorsal nucleus of the lateral lemniscus reveals its role in the processing of multiple sound sources in the inferior colliculus of bats. *J Neurosci* 21: 4830-4843.
- Caird D and Klinke R (1983) Processing of binaural stimuli by cat superior olivary complex neurons. *Exp. Brain Res.* 52: 385-399.
- Cant NB and Casseday JH (1986) Projections from the anteroventral cochlear nucleus to the lateral and medial superior olivary nuclei. *J. Comp. Neurol.* 247: 63-77.
- Carter AG, Regehr WG (2000) Prolonged synaptic currents and glutamate spillover at the parallel fiber to stellate cell synapse. *J Neurosci* 20: 4423-4434.
- Chen L, Kelly JB, Wu SH (1999) The commissure of probst as a source of GABAergic inhibition. *Hear Res* 138: 106-114.

-
- Chuhma N, Koyano K, Ohmori H (2001) Synchronisation of neurotransmitter release during postnatal development in a calyceal presynaptic terminal of rat. *J Physiol* 530: 93-104.
- Covey E, Vater M, Casseday JH (1991) Binaural properties of single units in the superior olivary complex of the mustached bat. *J Neurophysiol* 66: 1080-1094.
- Covey E (1993) Response properties of single units in the dorsal nucleus of the lateral lemniscus and paralemniscal zone of an echolocating bat. *J Neurophysiol* 69: 842-859.
- Del Castillo J, Katz B (1954) Statistical factors involved in neuromuscular facilitation and depression. *J Physiol* 124: 574-585.
- Diamond JS, Jahr CE (1995) Asynchronous release of synaptic vesicles determines the time course of the AMPA receptor-mediated EPSC. *Neuron* 15: 1097-1107.
- Diamond JS (2001) Neuronal glutamate transporters limit activation of NMDA receptors by neurotransmitter spillover on CA1 pyramidal cells. *J Neurosci* 21: 8328-8338.
- Dietrich D, Kirschstein T, Kukley M, Pereverzev A, von der BC, Schneider T, Beck H (2003) Functional specialization of presynaptic Cav2.3 Ca²⁺ channels. *Neuron* 39: 483-496.
- DiGregorio DA, Nusser Z, Silver RA (2002) Spillover of glutamate onto synaptic AMPA receptors enhances fast transmission at a cerebellar synapse. *Neuron* 35: 521-533.
- Dodge FA, Jr., Rahamimoff R (1967) Co-operative action a calcium ions in transmitter release at the neuromuscular junction. *J Physiol* 193: 419-432.
- Erulkar SD (1972) Comparative aspects of spatial localization of sound. *Physiol Rev* 52: 237-360.
- Fitzpatrick DC, Kuwada S, Batra R, Trahiotis C (1995) Neural responses to simple simulated echoes in the auditory brain stem of the unanesthetized rabbit. *J Neurophysiol* 74: 2469-2486.
- Fitzpatrick DC, Kuwada S (2001) Tuning to interaural time differences across frequency. *J Neurosci* 21: 4844-4851.
- Fu XW, Brezden BL, Wu SH (1997) Hyperpolarization-activated inward current in neurons of the rat's dorsal nucleus of the lateral lemniscus in vitro. *J Neurophysiol* 78: 2235-2245.
- Gahwiler BH, Brown DA (1985) GABAB-receptor-activated K⁺ current in voltage-clamped CA3 pyramidal cells in hippocampal cultures. *Proc Natl Acad Sci U S A* 82: 1558-1562.

-
- Glendenning KK, Brunso-Bechtold JK, Thompson GC, Masterton RB (1981) Ascending auditory afferents to the nuclei of the lateral lemniscus. *J Comp Neurol* 197: 673-703.
- Glendenning KK, Baker BN (1988) Neuroanatomical distribution of receptors for three potential inhibitory neurotransmitters in the brainstem auditory nuclei of the cat. *J Comp Neurol* 275: 288-308.
- Glendenning KK, Hutson KA, Nudo RJ, Masterton RB (1985) Acoustic chiasm II. Anatomical basis of binaurality in lateral superior olive of cat. *J Comp Neurol* 232: 261-285.
- Goda Y, Stevens CF (1994) Two components of transmitter release at a central synapse. *Proc Natl Acad Sci U S A* 91: 12942-12946.
- Goldberg JM, Brown PB (1969) Response of binaural neurons of dog superior olivary complex to dichotic tonal stimuli: some physiological mechanisms of sound localization. *J Neurophysiol* 32: 613-636.
- Goldberg JM, Brown PB (1968) Functional organization of the dog superior olivary complex: an anatomical and electrophysiological study. *J Neurophysiol* 31: 639-656.
- Grothe B, Sanes DH (1994) Synaptic inhibition influences the temporal coding properties of medial superior olivary neurons: an in vitro study. *J Neurosci* 14: 1701-1709.
- Grothe B, Park TJ (1998) Sensitivity to interaural time differences in the medial superior olive of a small mammal, the Mexican free-tailed bat. *J Neurosci* 18: 6608-6622.
- Haas KF, Macdonald RL (1999) GABAA receptor subunit gamma2 and delta subtypes confer unique kinetic properties on recombinant GABAA receptor currents in mouse fibroblasts. *J Physiol* 514 (Pt 1): 27-45.
- Heffner RS, Heffner HE (1988) Sound localization and use of binaural cues by the gerbil (*Meriones unguiculatus*). *Behav Neurosci* 102: 422-428.
- Hefft S, Jonas P (2005) Asynchronous GABA release generates long-lasting inhibition at a hippocampal interneuron-principal neuron synapse. *Nat Neurosci* 8: 1319-1328.
- Henkel CK, Brunso-Bechtold JK (1993) Laterality of superior olive projections to the inferior colliculus in adult and developing ferret. *J Comp Neurol* 331: 458-468.
- Henkel CK, Fuentes-Santamaria V, Alvarado JC, Brunso-Bechtold JK (2003) Quantitative measurement of afferent layers in the ferret inferior colliculus: DNLL projections to sublayers. *Hear Res* 177: 32-42.
- Hui E, Bai J, Wang P, Sugimori M, Llinas RR, Chapman ER (2005) Three distinct kinetic groupings of the synaptotagmin family: candidate sensors for rapid and delayed exocytosis. *Proc Natl Acad Sci U S A* 102: 5210-5214.

-
- Isaacson JS, Solis JM, Nicoll RA (1993) Local and diffuse synaptic actions of GABA in the hippocampus. *Neuron* 10: 165-175.
- Isaacson JS, Walmsley B (1995) Counting quanta: direct measurements of transmitter release at a central synapse. *Neuron* 15: 875-884.
- Ito Y, Lim DK, Nabeshima T, Ho IK (1989) Effects of picrotoxin treatment on GABAA receptor supramolecular complexes in rat brain. *J Neurochem* 52: 1064-1070.
- Iwahori N (1986) A Golgi study on the dorsal nucleus of the lateral lemniscus in the mouse. *Neurosci Res* 3: 196-212.
- Jensen K, Lambert JD, Jensen MS (2000) Tetanus-induced asynchronous GABA release in cultured hippocampal neurons. *Brain Res* 880: 198-201.
- Jones MV, Westbrook GL (1995) Desensitized states prolong GABAA channel responses to brief agonist pulses. *Neuron* 15: 181-191.
- Jones MV, Jonas P, Sahara Y, Westbrook GL (2001) Microscopic kinetics and energetics distinguish GABA(A) receptor agonists from antagonists. *Biophys J* 81: 2660-2670.
- Joris PX, Yin TC (1998) Envelope coding in the lateral superior olive. III. Comparison with afferent pathways. *J Neurophysiol* 79: 253-269.
- Keller CH, Takahashi TT (1996) Responses to simulated echoes by neurons in the barn owl's auditory space map. *J Comp Physiol [A]* 178: 499-512.
- Kelly JB (1974) Localization of paired sound sources in the rat: small time differences. *J Acoust Soc Am* 55: 1277-1284.
- Kelly JB, Liscum A, van Adel B, Ito M (1998) Projections from the superior olive and lateral lemniscus to tonotopic regions of the rat's inferior colliculus. *Hear Res* 116: 43-54.
- Kelly JB, Buckthought AD, Kidd SA (1998) Monaural and binaural response properties of single neurons in the rat's dorsal nucleus of the lateral lemniscus. *Hear Res* 122: 25-40.
- Kelly JB, Kidd SA (2000) NMDA and AMPA receptors in the dorsal nucleus of the lateral lemniscus shape binaural responses in rat inferior colliculus. *J Neurophysiol* 83: 1403-1414.
- Kidd SA, Kelly JB (1996) Contribution of the dorsal nucleus of the lateral lemniscus to binaural responses in the inferior colliculus of the rat: interaural time delays. *J Neurosci* 16: 7390-7397.
- Klug A, Park TJ, Pollak G (1995) Glycine and GABA influence binaural processing in the inferior colliculus of the mustache bat. *J Neurophysiol* 74: 1701-1713.

-
- Kudo M (1981) Projections of the nuclei of the lateral lemniscus in the cat: an autoradiographic study. *Brain Res* 221: 57-69.
- Kullmann DM (2000) Spillover and synaptic cross talk mediated by glutamate and GABA in the mammalian brain. *Prog Brain Res* 125: 339-351.
- Kuwada S, Fitzpatrick DC, Batra R, Ostapoff EM (2006) Sensitivity to interaural time differences in the dorsal nucleus of the lateral lemniscus of the unanesthetized rabbit: comparison with other structures. *J Neurophysiol* 95: 1309-1322.
- Li L, Kelly JB (1992) Inhibitory influence of the dorsal nucleus of the lateral lemniscus on binaural responses in the rat's inferior colliculus. *J Neurosci* 12: 4530-4539.
- Litovsky RY, Yin TC (1998) Physiological studies of the precedence effect in the inferior colliculus of the cat. II. Neural mechanisms. *J Neurophysiol* 80: 1302-1316.
- Litovsky RY, Colburn HS, Yost WA, Guzman SJ (1999) The precedence effect. *J Acoust Soc Am* 106: 1633-1654.
- Litovsky RY, Delgutte B (2002) Neural Correlates of the Precedence Effect in the Inferior Colliculus: Effect of Localization Cues. *J Neurophysiol* 87: 976-994.
- Llinas R, Sugimori M, Silver RB (1995) The concept of calcium concentration microdomains in synaptic transmission. *Neuropharmacology* 34: 1443-1451.
- Llinas RR (1982) Calcium in synaptic transmission. *Sci Am* 247: 56-65.
- Lohmann C, Friauf E (1996) Distribution of the calcium-binding proteins parvalbumin and calretinin in the auditory brainstem of adult and developing rats. *J Comp Neurol* 367: 90-109.
- Loskota, P Lomax and M. A. Verity (1974) *A Stereotaxic Atlas of the Mongolian Gerbil Brain (Meriones unguiculatus)*, W. J Ann Arbor Science Publishers Inc..
- Lu T, Trussell LO (2000) Inhibitory transmission mediated by asynchronous transmitter release. *Neuron* 26: 683-694.
- Magnusson AK, Kapfer C, Grothe B, Koch U (2005) Maturation of glycinergic inhibition in the gerbil medial superior olive after hearing onset. *J Physiol* 568: 497-512.
- Markovitz NS, Pollak GD (1993) The dorsal nucleus of the lateral lemniscus in the mustache bat: monaural properties. *Hear Res* 71: 51-63.
- Markovitz NS, Pollak GD (1994) Binaural processing in the dorsal nucleus of the lateral lemniscus. *Hear Res* 73: 121-140.
- Maximov A, Sudhof TC (2005) Autonomous function of synaptotagmin 1 in triggering synchronous release independent of asynchronous release. *Neuron* 48: 547-554.

-
- Meinrenken CJ, Borst JG, Sakmann B (2003) Local routes revisited: the space and time dependence of the Ca²⁺ signal for phasic transmitter release at the rat calyx of Held. *J Physiol* 547: 665-689.
- Merchan MA, Saldana E, Plaza I (1994) Dorsal nucleus of the lateral lemniscus in the rat: concentric organization and tonotopic projection to the inferior colliculus. *J Comp Neurol* 342: 259-278.
- Mitchell SJ, Silver RA, b (2000) GABA spillover from single inhibitory axons suppresses low-frequency excitatory transmission at the cerebellar glomerulus. *J Neurosci* 20: 8651-8658.
- Mitchell SJ, Silver RA (2000) Glutamate spillover suppresses inhibition by activating presynaptic mGluRs. *Nature* 404: 498-502.
- Moore JK, Moore RY (1987) Glutamic acid decarboxylase-like immunoreactivity in brainstem auditory nuclei of the rat. *J Comp Neurol* 260: 157-174.
- Moore MJ, Caspary DM (1983) Strychnine blocks binaural inhibition in lateral superior olivary neurons. *J Neurosci* 3: 237-247.
- Moushegian G, Rupert A, Whitcomb MA (1964) Brain-stem neuronal response patterns to monoaural and binaural tones. *J Neurophysiol* 27: 1174-1191.
- Mtchedlishvili Z, Kapur J (2006) High-affinity, slowly desensitizing GABAA receptors mediate tonic inhibition in hippocampal dentate granule cells. *Mol Pharmacol* 69: 564-575.
- Newberry NR, Nicoll RA (1985) Comparison of the action of baclofen with gamma-aminobutyric acid on rat hippocampal pyramidal cells in vitro. *J Physiol* 360: 161-185.
- Nishiki T, Augustine GJ (2004) Synaptotagmin I synchronizes transmitter release in mouse hippocampal neurons. *J Neurosci* 24: 6127-6132.
- Nusser Z, Hajos N, Somogyi P, Mody I (1998) Increased number of synaptic GABA(A) receptors underlies potentiation at hippocampal inhibitory synapses. *Nature* 395: 172-177.
- Nusser Z, Mody I (2002) Selective modulation of tonic and phasic inhibitions in dentate gyrus granule cells. *J Neurophysiol* 87: 2624-2628.
- Oliver DL, Shneiderman A (1989) An EM study of the dorsal nucleus of the lateral lemniscus: inhibitory, commissural, synaptic connections between ascending auditory pathways. *J Neurosci* 9: 967-982.
- Oliver DL (2000) Ascending efferent projections of the superior olivary complex. *Microsc Res Tech* 51: 355-363.
- Olsen RW, Tobin AJ (1990) Molecular biology of GABAA receptors. *FASEB J* 4: 1469-1480.

-
- Otis TS, Trussell LO (1996) Inhibition of transmitter release shortens the duration of the excitatory synaptic current at a calyceal synapse. *J Neurophysiol* 76: 3584-3588.
- Otsu Y, Shahrezaei V, Li B, Raymond LA, Delaney KR, Murphy TH (2004) Competition between phasic and asynchronous release for recovered synaptic vesicles at developing hippocampal autaptic synapses. *J Neurosci* 24: 420-433.
- Overstreet LS, Jones MV, Westbrook GL (2000) Slow desensitization regulates the availability of synaptic GABA(A) receptors. *J Neurosci* 20: 7914-7921.
- Overstreet LS, Westbrook GL (2001) Paradoxical reduction of synaptic inhibition by vigabatrin. *J Neurophysiol* 86: 596-603.
- Overstreet LS, Westbrook GL (2003) Synapse density regulates independence at unitary inhibitory synapses. *J Neurosci* 23: 2618-2626.
- Park TJ, Grothe B, Pollak GD, Schuller G, Koch U (1996) Neural delays shape selectivity to interaural intensity differences in the lateral superior olive. *J Neurosci* 16: 6554-6566.
- Park TJ, Monsivais P, Pollak G (1997) Processing of interaural intensity differences in the LSO: Role of interaural threshold differences. *J Neurophysiol* 77: 2863-2878.
- Park TJ (1998) IID sensitivity differs between two principal centers in the interaural intensity difference pathway: the LSO and the IC. *J Neurophysiol* 79: 2416-2431.
- Park and Pollak (1994) Receptive fields in the inferior colliculus of the mustache bat are shaped by GABAergic inhibition. *J Neurophysiol* 72:1080-1102.
- Pecka M, Zahn TP, Saunier-Rebori B, Siveke I, Felmy F, Wiegrebe L, Klug A, Pollak GD, Grothe B (2007) Inhibiting the inhibition: a neuronal network for sound localization in reverberant environments. *J Neurosci* 27: 1782-1790.
- Pollak GD (1997) Roles of GABAergic inhibition for the binaural processing of multiple sound sources in the inferior colliculus. *Ann Otol Rhinol Laryngol Suppl* 168: 44-54.
- Pollak GD, Burger RM, Park TJ, Klug A, Bauer EE (2002) Roles of inhibition for transforming binaural properties in the brainstem auditory system. *Hear Res* 168: 60-78.
- Pollak GD, Burger RM, Klug A (2003) Dissecting the circuitry of the auditory system. *Trends Neurosci* 26: 33-39.
- Pugh JR, Raman IM (2005) GABAA receptor kinetics in the cerebellar nuclei: evidence for detection of transmitter from distant release sites. *Biophys J* 88: 1740-1754.
- Randall A, Tsien RW (1995) Pharmacological dissection of multiple types of Ca²⁺ channel currents in rat cerebellar granule neurons. *J Neurosci* 15: 2995-3012.

-
- Rayleigh, L. J. W. S. 3. B. R. On our perception of sound direction. 13[1907], 214-232. *Philos Mag.* RefType:Generic
- Roberts RC, Ribak CE (1987) GABAergic neurons and axon terminals in the brainstem auditory nuclei of the gerbil. *J Comp Neurol* 258: 267-280
- Roepstorff A, Lambert JD (1994) Factors contributing to the decay of the stimulus-evoked IPSC in rat hippocampal CA1 neurons. *J Neurophysiol* 72: 2911-2926.
- Rose JE, Gross NB, Geisler CD, Hind JE (1966) Some neural mechanisms in the inferior colliculus of the cat which may be relevant to localization of a sound source. *J Neurophysiol* 29: 288-314.
- Rossi DJ, Alford S, Mugnaini E, Slater NT (1995) Properties of transmission at a giant glutamatergic synapse in cerebellum: the mossy fiber-unipolar brush cell synapse. *J Neurophysiol* 74: 24-42.
- Rossi DJ, Hamann M (1998) Spillover-mediated transmission at inhibitory synapses promoted by high affinity alpha6 subunit GABA(A) receptors and glomerular geometry. *Neuron* 20: 783-795.
- Ryan (1976) Hearing sensitivity of the mongolian gerbil, *Meriones unguiculatus*. *J Acoust Soc Am* 59: 1222-1226
- Sanes DH, Rubel EW (1988) The ontogeny of inhibition and excitation in the gerbil lateral superior olive. *J Neurosci* 8: 682-700.
- Saxena NC, Macdonald RL (1996) Properties of putative cerebellar gamma-aminobutyric acid A receptor isoforms. *Mol Pharmacol* 49: 567-579.
- Scanziani M (2000) GABA spillover activates postsynaptic GABA(B) receptors to control rhythmic hippocampal activity. *Neuron* 25: 673-681.
- Scheuss V, Taschenberger H, Neher E (2007) Kinetics of both synchronous and asynchronous quantal release during trains of action-potential evoked EPSCs at the rat calyx of Held. *J Physiol.*
- Schneggenburger R, Neher E (2005) Presynaptic calcium and control of vesicle fusion. *Curr Opin Neurobiol* 15: 266-274.
- Schuller G, Radtke-Schuller S, Betz MA (1986) A stereotaxic method for small animals using experimentally determined reference profiles. *J Neurosci Methods* 18: 339-350.
- Semyanov A, Walker MC, Kullmann DM (2003) GABA uptake regulates cortical excitability via cell type-specific tonic inhibition. *Nat Neurosci* 6: 484-490.
- Shneiderman A, Oliver DL, Henkel CK (1988) Connections of the dorsal nucleus of the lateral lemniscus: an inhibitory parallel pathway in the ascending auditory system? *J Comp Neurol* 276: 188-208.

- Shneiderman A, Oliver DL (1989) EM autoradiographic study of the projections from the dorsal nucleus of the lateral lemniscus: a possible source of inhibitory inputs to the inferior colliculus. *J Comp Neurol* 286: 28-47.
- Silver RA, Cull-Candy SG, Takahashi T (1996) Non-NMDA glutamate receptor occupancy and open probability at a rat cerebellar synapse with single and multiple release sites. *J Physiol* 494 (Pt 1): 231-250.
- Siveke I, Pecka M, Seidl AH, Baudoux S, Grothe B (2006) Binaural Response Properties of Low Frequency Neurons in the Gerbil Dorsal Nucleus of the Lateral Lemniscus. *J Neurophysiol*.
- Slater NT, Rossi DJ, Kinney GA (1997) Physiology of transmission at a giant glutamatergic synapse in cerebellum. *Prog Brain Res* 114: 151-163.
- Smith AJ, Owens S, Forsythe ID (2000) Characterisation of inhibitory and excitatory postsynaptic currents of the rat medial superior olive. *J Physiol* 529 Pt 3: 681-698.
- Smith AJ, Simpson PB (2003) Methodological approaches for the study of GABA(A) receptor pharmacology and functional responses. *Anal Bioanal Chem* 377: 843-851.
- Stell BM, Mody I (2002) Receptors with Different Affinities Mediate Phasic and Tonic GABAA Conductances in Hippocampal Neurons. *J Neurosci* 22: 223RC.
- Sudhof TC (2002) Synaptotagmins: why so many? *J Biol Chem* 277: 7629-7632.
- Sun J, Pang ZP, Qin D, Fahim AT, Adachi R, Sudhof TC (2007) A dual-Ca²⁺-sensor model for neurotransmitter release in a central synapse. *Nature* 450: 676-682.
- Szabadics J, Tamas G, Soltesz I (2007) Different transmitter transients underlie presynaptic cell type specificity of GABAA,slow and GABAA,fast. *Proc Natl Acad Sci U S A* 104: 14831-14836.
- Szapiro G, Barbour B (2007) Multiple climbing fibers signal to molecular layer interneurons exclusively via glutamate spillover. *Nat Neurosci* 10: 735-742.
- Takahashi M, Kovalchuk Y, Attwell D (1995) Pre- and postsynaptic determinants of EPSC waveform at cerebellar climbing fiber and parallel fiber to Purkinje cell synapses. *J Neurosci* 15: 5693-5702.
- Tanaka K, Otani K, Tokunaga A, Sugita S (1985) The organization of neurons in the nucleus of the lateral lemniscus projecting to the superior and inferior colliculi in the rat. *Brain Res* 341: 252-260.
- Thompson SP (1882) On the function of the two ears in the perception of space. *Philos Mag* 13: 406-416.
- Tollin DJ, Yin TC (2002) The coding of spatial location by single units in the lateral superior olive of the cat. I. Spatial receptive fields in azimuth. *J Neurosci* 22: 1454-1467.

- Tollin DJ, Populin LC, Yin TC (2004) Neural correlates of the precedence effect in the inferior colliculus of behaving cats. *J Neurophysiol* 92: 3286-3297.
- Trussell LO, Zhang S, Raman IM (1993) Desensitization of AMPA receptors upon multiquantal neurotransmitter release. *Neuron* 10: 1185-1196.
- Tsuchitani C (1988a) The inhibition of cat lateral superior olive unit excitatory responses to binaural tone-bursts. I. The transient chopper response. *J Neurophysiol* 59: 164-183.
- Tsuchitani C (1988b) The inhibition of cat lateral superior olive unit excitatory responses to binaural tone-bursts. II. The sustained discharges. *J Neurophysiol* 59: 184-211.
- Vater M, Kossl M, Horn AK (1992) GAD- and GABA-immunoreactivity in the ascending auditory pathway of horseshoe and mustached bats. *J Comp Neurol* 325: 183-206.
- Vogt KE, Nicoll RA (1999) Glutamate and gamma-aminobutyric acid mediate a heterosynaptic depression at mossy fiber synapses in the hippocampus. *Proc Natl Acad Sci U S A* 96: 1118-1122.
- Watanabe T, Liao TT, Katsuki Y (1968) Neuronal response patterns in the superior olivary complex of the cat to sound stimulation. *Jpn J Physiol* 18:267-287
- Wei W, Zhang N, Peng Z, Houser CR, Mody I (2003) Perisynaptic localization of delta subunit-containing GABA(A) receptors and their activation by GABA spillover in the mouse dentate gyrus. *J Neurosci* 23: 10650-10661.
- Whiting PJ, Bonnert TP, McKernan RM, Farrar S, le Bourdelles B, Heavens RP, Smith DW, Hewson L, Rigby MR, Sirinathsinghji DJ, Thompson SA, Wafford KA (1999) Molecular and functional diversity of the expanding GABA-A receptor gene family. *Ann N Y Acad Sci* 868: 645-653.
- Wu SH, Kelly JB (1995a) In vitro brain slice studies of the rat's dorsal nucleus of the lateral lemniscus. I. Membrane and synaptic response properties. *J Neurophysiol* 73: 780-793
- Wu SH, Kelly JB (1995b) In vitro brain slice studies of the rat's dorsal nucleus of the lateral lemniscus. II. Physiological properties of biocytin-labeled neurons. *J Neurophysiol* 73: 780-793
- Wu SH, Kelly JB (1995c) Inhibition in the superior olivary complex: pharmacological evidence from mouse brain slice. *J Neurophysiol* 73: 256-269.
- Wu SH, Kelly JB (1996) In vitro brain slice studies of the rat's dorsal nucleus of the lateral lemniscus. III. synaptic pharmacology. *J Neurophysiol* 75: 1271-1282.
- Yang L, Pollak GD (1994) The roles of GABAergic and glycinergic inhibition on binaural processing in the dorsal nucleus of the lateral lemniscus of the mustache bat. *J Neurophysiol* 71: 1999-2013.

- Yang L, Pollak GD (1994) GABA and glycine have different effects on monaural response properties in the dorsal nucleus of the lateral lemniscus of the mustache bat. *J Neurophysiol* 71: 2014-2024.
- Yang L, Liu Q, Pollak GD (1996) Afferent connections to the dorsal nucleus of the lateral lemniscus of the mustache bat: evidence for two functional subdivisions. *J Comp Neurol* 373: 575-592.
- Yang L, Pollak GD (1997) Differential response properties to amplitude modulated signals in the dorsal nucleus of the lateral lemniscus of the mustache bat and the roles of GABAergic inhibition. *J Neurophysiol* 77: 324-340.
- Yin TC, Chan JC (1990) Interaural time sensitivity in medial superior olive of cat. *J Neurophysiol* 64: 465-488.
- Yin TC (1994) Physiological correlates of the precedence effect and summing localization in the inferior colliculus of the cat. *J Neurosci* 14: 5170-5186.
- Zahn TP (2003) Neural architecture for echo suppression during sound source localization based on spiking neural cell models. from http://www.bibliothek.tu-ilmenau.de/elektr_medien/dissertationen/2003/Zahn_Thomas/ Retrieved January 16, 2007.
- Zurek PM (1987) The precedence effect. In: *Directional hearing* (Yost WA, Gourevitch G, eds) pp. 85–105. New York: Springer.

LIST OF ABBREVIATIONS

AP	action potential
AVCN	anteroventral cochlear nucleus
BF	best frequency
CN	cochlear nucleus
DNLL	dorsal nucleus of the lateral lemniscus
EE	excitatory/excitatory
EI	excitatory/inhibitory
EPSC	excitatory post-synaptic currents
GABA	gamma-aminobutyric acid
IC	inferior colliculus
IID	interaural intensity differences
INLL	intermediate nucleus of the lateral lemniscus
IPSC	inhibitory post-synaptic currents
IPSP	inhibitory post-synaptic potentials
ISD	interstimulus delay
ITD	interaural time difference
LSO	lateral superior olive
mIPSC	miniature inhibitory post-synaptic currents
MNTB	medial nucleus of the trapezoid body
MSO	medial superior olive
nMag	nucleus magnoceullaris
PE	precedence effect
PI	persistent inhibition
SOC	superior olive complex
SPL	sound pressure level
VNLL	ventral nucleus of the lateral lemniscus

CURRICULUM VITAE

Bernadette Saunier Rebori

Department of Neurobiology, Biozentrum, Ludwig Maximilians Universität

Großhadernerstr. 2, 82152, Munich, Germany

Phone: +49 2180 74369 Email: saunier@zi.biologie.uni-muenchen.de

PERSONAL INFORMATION

Date of birth: March 16th, 1976 in Buenos Aires, Argentina

Nationality: Argentinean citizenship

ACADEMIC EDUCATION

Licenciatura en Ciencias Biológicas / M.Sc. (1995-2002)

Faculty of Exact and Natural Sciences, University of Buenos Aires, Buenos Aires, Argentina

PUBLICATIONS

B.T. Saunier-Rebori, B. Grothe, A. Klug and F. Felmy: Synaptic properties contributing to the time course of persistent inhibition in DNLL. (*in preparation for submission*)

M. Pecka*, T. Zahn*, **B.T. Saunier Rebori***, I. Siveke, F. Felmy, L. Wiegrebe, A. Klug, G. Pollak, B. Grothe: Inhibiting the inhibition – a neuronal network for localization in reverberant environments. (2007) *J Neurosci.* 27(7):1782-90

(*) Authors contributed equally to this work.

B.T. Saunier Rebori and J.H. Pazo: Inhibition of the jaw opening reflex and single neurons in the trigeminal subnucleus caudalis by activation of striatal D₂ dopamine receptors. (2006) *Neuropharmacology* 51(2):263-71

PROFESIONAL EXPERIENCE

Feb 2004 – today Neurobiology, Dept. Biology II, Biozentrum, LMU

Jan 2003 – Jan 2004 Neurobiology, Biozentrum, Basel, Switzerland

Mar 2000 – Jan 2003 Neurophysiology, Dept. of Physiology and Biophysics,
School of Medicine, Univ. Buenos Aires

Feb 1994 – June 1996 Experimental Leukemia Lab, Academy of Medicine,
Buenos Aires.

PUBLISHED ABSTRACTS

B. Saunier Rebori, B. Grothe, A. Klug and F. Felmy: Pre- and post-synaptic mechanisms promote persistent inhibition in the DNLL. *Society for Neuroscience Abstracts, 2007, USA*

B. Saunier Rebori, B. Grothe, A. Klug and F. Felmy: GABA spillover and asynchronous release contribute to persistent inhibition in the DNLL. *7th Meeting of the German Neuroscience Society 2007, Germany.*

B. Saunier Rebori, B. Grothe, G. Neuweiler, and A. Klug: The neural substrate for persistent inhibition in the DNLL. *Society for Neuroscience Abstracts, 2006, USA.*

J.E. Belforte, **B. Saunier Rebori**, J.H. Pazo: Pharmacological modulation of striatal analgesic effects. *SAFE 2003; XXXV, Argentina.*

B. T. Saunier Rebori, J.E. Belforte and J.H. Pazo: JOR (jaw-opening reflex) inhibition and evoked neuronal response by striatal D₂ dopaminergic receptors activation. *4th Workshop on Neuroscience, 2002, Argentina.*

J.E. Belforte, **B. Saunier Rebori**, J.H. Pazo: Analgesic effect mediated by striatal dopaminergic receptors. *SAIC 2000; 60: III-XXII, Argentina.*

J.E. Belforte, **B. Saunier Rebori**, J.H. Pazo: Circling behavior induced by stimulation of subthalamic 5HT receptors. *SAFE 2000, XXXII, Argentina.*

LANGUAGE PROFICIENCY

Spanish: mother tongue

English: fluent

French: intermediate level

German: beginner level

REFERENCES

Prof. Benedikt Grothe

Biozentrum, Ludwig Maximilians Universität

Tel: +49 2180 74361

grothe@zi.biologie.uni-muenchen.de

Dr. Gustavo Murer

Laboratorio de Redes Neuronales, Dept. Fisiología y Biofísica

Facultad de Medicina, Universidad de Buenos Aires

Paraguay 2155 - 7° piso (C1121ABG), Ciudad de Buenos Aires, Argentina

murer@fmed.uba.ar